

**Micron precision calibration
methods for alignment sensors
in particle accelerators**

ANDREAS HERTY

**A thesis submitted in partial fulfilment of the
requirements of Nottingham Trent University
for the degree of Master of Philosophy**

March 2009

Copyright statement:

This work is the intellectual property of the author. You may copy up to 5% of this work for private study, or personal, non-commercial research. Any re-use of the information contained within this document should be fully referenced, quoting the author, title, university, degree level and pagination. Queries or requests for any other use, or if a more substantial copy is required, should be directed in the owner of the Intellectual Property Rights.

Abstract

Herty, A., 2009. Micron precision calibration methods for alignment sensors in particle accelerators. Master of Philosophy thesis. School of Architecture, Design and the Built Environment, Nottingham Trent University.

Large Hadron Collider (LHC) at CERN, the European Organization for Nuclear Research, has, on each side of its four experiments, a set of three magnets, called low-beta magnets. These magnets provide the final-focus for the beams that collide head on in the experiments. The magnets have to be permanently monitored with micron precision as they are crucial for collisions with high luminosity in the experiments. The systems used are hydrostatic levelling systems, wire position systems and invar radial systems. The sensors have to withstand a highly radioactive environment, strong magnetic fields and cannot be returned for check and calibration to the manufacturer once exposed to radiation. In order to validate the sensors before their installation in the tunnel, to check them within their measurement system and for check and calibration after use, a series of tests have been put in place.

The different methods that are devised and implemented by the author allow for checking of the manufacturer's calibration, variations during warm-up and stability checks. In addition to these standard checks, the installation in the low-beta monitoring system of the LHC needed additional investigation into parameters of the behaviour of the sensor as for example the repeatability of installation, interchangeability and radiation tolerance. Several in-situ check methods have been introduced by the author to complete the checks made in the laboratory.

The sensor checks and calibrations show the reliability of the sensors in laboratory conditions for linearity, warm-up and stability. Additional mechanical constants of the sensors have been successfully calibrated. Radiation and magnetic field tests showed the acceptability of the sensors for use in the LHC.

Keywords: accelerator alignment, calibration, hydrostatic levelling sensor, wire position sensor, distance offset measurement sensor.

Contents

List of Tables	4
List of Figures	5
List of Abbreviations	7
1 Accelerator Alignment	9
1.1 CERN	9
1.2 LHC alignment - problem description	10
1.3 Aim and Objectives	15
1.4 Structure	16
2 Literature Review	17
2.1 Monitoring and Alignment	17
2.2 Particle Accelerator Alignment	18
2.2.1 Height Observations	20
2.2.2 Horizontal Alignment	21
2.3 Calibration: Sensor or System	23
2.4 Conclusion	23
3 Monitoring sensors and applications	25
3.1 Capacitive Measurements	25
3.2 Radiation related sensor design	27
3.3 Hydrostatic Levelling Sensor	27
3.4 Hydrostatic Levelling System	29
3.5 Wire Position Sensor	31
3.6 Wire Offset System	35
3.7 Distance Offset Measurement Sensor	35
3.8 Invar Radial System	36
3.9 Data Acquisition System	37
3.10 Summary	40

4	Sensor validation and calibration	41
4.1	Reception check	42
4.2	Warm-up	42
4.3	Stability	43
4.4	Linearity	46
4.5	External Reference	48
4.6	Repeatability	49
4.7	Radiation	49
4.8	Magnetic field	50
4.9	Orientation	50
4.10	Summary	52
5	Validation benches and measurements	53
5.1	Thermal expansion	53
5.2	HLS	54
5.2.1	Warm-up and stability	54
5.2.2	Linearity	59
5.2.3	Zero reference	61
5.2.4	External Reference	63
5.3	WPS	65
5.3.1	Warm-up and stability	65
5.3.2	Linearity	69
5.3.3	Assembly	72
5.3.4	External reference	73
5.3.5	Reference surfaces	75
5.3.6	Frequency check	75
5.3.7	Radiation	76
5.4	DOMS	78
5.4.1	Warm-up and Stability	78
5.4.2	Linearity	82
5.4.3	External reference and repeatability	84
5.4.4	Magnetic field	86
5.5	Summary	88
6	Conclusions and recommendations	89
6.1	Sensors	89
6.2	Checks and calibrations	91
6.3	Benches	92
6.4	Recommendations	93
6.5	Summary	95

Reference List	97
Appendix A Calibration files	103
A.1 HLS calibration file	104
A.2 WPS calibration file	107
A.3 DOMS calibration file	113
Appendix B Measurements	115
B.1 HLS repeatability	116
B.2 HLS measurement pot	117
B.3 WPS linearity measurement	118
B.4 WPS surface measurement	119
B.5 WPS frequency measurement	120
Appendix C Publications	121
C.1 Radiation induced effects on the sensors of the Hydrostatic Levelling System for the LHC low beta quadrupoles	121
C.2 Radiation induced effects on the sensors of the Hydrostatic Levelling System for the LHC low beta quadrupoles	139
C.3 Combined levelling systems for the vertical monitoring of a large physics experiment	145
C.4 Radiation induced effects on hydrostatic levelling sensors	159
C.5 The remote positioning of the LHC Inner Triplet	171
C.6 Alignment of the low-beta magnets and the experiments in the LHC .	177

List of Tables

3.1	HLS specification (FOGALE nanotech, 2006 & 2007b)	29
3.2	WPS specification (FOGALE nanotech, 2006)	32
3.3	Wire specification (FOGALE nanotech, 2006)	34
3.4	DOMS specification (FOGALE nanotech, 2007)	36
5.1	WPS assembly check measurements	73
5.2	External reference determination of WPS reference sensors	74

List of Figures

1.1	low-beta magnet radial monitoring sensor layout	12
1.2	low-beta magnet vertical and tilt sensor layout	12
1.3	low-beta magnets in the LHC tunnel	14
2.1	monitoring and alignment flow chart	18
2.2	straightness alignment systems after Ruland (1995)	19
2.3	DESY HLS after Schlösser and Herty (2002)	21
3.1	Standard capacitor (left), electrode with guard ring (right)	26
3.2	HLS (left to right: second, fourth and third generation)	29
3.3	HLS ranges	30
3.4	standard configuration	31
3.5	free-surface configuration	31
3.6	Closed and opened WPS	32
3.7	WPS coordinate system	33
3.8	Field lines after after Prochnow et al., 1999 (left) and FOGALE nanotech, 2007 (right)	35
3.9	DOMS	36
3.10	IRS	37
3.11	HLS with sensor, electronics and cable	38
3.12	layout data acquisition system	38
4.1	inclination error	51
5.1	HLS measurement on water (left) and fixed target (right)	54
5.2	HLS measurement pots	55
5.3	HLS warm-up measurement	56
5.4	HLS warm-up distribution	57
5.5	HLS stability measurement	58
5.6	HLS linearity check bench	59
5.7	recalculated polynomial residuals	61
5.8	check measurements compared to calibration function	62

5.9	HLS absolute zero reference	63
5.10	measurement pot calibration	64
5.11	HLS external reference	65
5.12	external reference calibration bench	66
5.13	WPS stability bench	68
5.14	warm-up (blue) and stability (red) measurements	69
5.15	WPS linearity bench	70
5.16	WPS linearity measurements	71
5.17	WPS assembly and offset bench layout	72
5.18	WPS offset bench fixation	74
5.19	TID and DRD set-up	77
5.20	TID results sensor	77
5.21	TID results electronics	78
5.22	DOMS stability check bench (first design)	79
5.23	DOMS stability check bench (second design)	80
5.24	DOMS stability check bench (third design)	80
5.25	DOMS warm-up	81
5.26	DOMS stability	82
5.27	DOMS linearity	84
5.28	DOMS external reference	85
5.29	DOMS external reference	86
5.30	magnetic field test installation	87
5.31	magnetic field measurements	87
6.1	automated linearity calibration bench	93

List of Abbreviations

Notation	Description
ALICE	A Large Ion Collider Experiment at CERN
ATLAS	A Toroidal LHC Apparatus
CCC	CERN Control Centre
CCD	Charge-Coupled Device
CCS	CERN Coordinate System
CEA	Commissariat à l'Énergie Atomique
CERN	European Organization for Nuclear Research
CLIC	Compact Linear Collider
CMM	Coordinate-Measuring Machine
CMS	Compact Muon Solenoid
CTF	CLIC Test Facility
DAQ	Data Acquisition
DESY	Deutsches Elektronen-Synchrotron
DOMS	Distance Offset Measurement Sensor
DRD	Dose Rate Dependence
EDM	Electronic Distance Measuring
ESRF	European Synchrotron Radiation Facility
FFTB	Final Focus Test Beam
FLASH	Freie-Elektronen-Laser Hamburg
GPS	Global Positioning System
GUI	Graphical User Interface
HERA	Hadron Elektron Ring Anlage
HLS	Hydrostatic Levelling Sensor
INB	Installation Nucléaire de Base
IP	Interaction Point
IRS	Invar Radial System

Notation	Description
ITL	Inner Triplet Line
LEP	Large Electron-Positron Collider
LHC	Large Hadron Collider
LHCb	Large Hadron Collider beauty experiment
LINAC	Linear Accelerator
MHN	Main Hydraulic Network
MSM	MultiSystMetrolog
OTL	Outer Triplet Line
PETRA	Positron-Elektron-Tandem-Ring-Anlage
PS	Proton Synchrotron
RMS	Root Mean Square
SEE	Single Event Effects
SLAC	Stanford Linear Accelerator Center
SLS	Swiss Light Source
SPS	Super Proton Synchrotron
TESLA	TeV-Energy Superconducting Linear Accelerator
TH	Taylor-Hobbsen
THN	Triplet Hydraulic Network
TID	Total Ionizing Dose
WGS-84	World Geodetic System 1984
WPM	Wire Position Monitor
WPS	Wire Position Sensor

Chapter 1

Accelerator Alignment

1.1 CERN

The European Organization for Nuclear Research (CERN) is the world's largest particle physics centre and is situated at the Franco-Swiss border near Geneva in Switzerland. This laboratory provides, for scientists from all over the world, the infrastructure to find out about fundamental questions in physics, reaching from research on the forces during creation of the universe to the creation of antimatter.

CERN was founded in 1954 as an European joint venture and has today 20 member states. The name CERN is originally from the French name *Conseil Européen pour la Recherche Nucléaire* which was the name of a provisional body founded in 1952 whose mission was the creation of a research institute for particle physics.

CERN finished the installation of a next generation, high energy physics particle accelerator called the Large Hadron Collider (LHC) in 2008. The LHC has proton beams running in opposite directions at an energy level of 14 TeV. This accelerator has a circumference of 27 km and is situated at an average of 100 m underground. The counter rotating beams have particle bunches separated from each other by approximately 7 m, which is an equivalent of 25 ns. The proton beams have a diameter of 16 μm and contain $1.1 \cdot 10^{11}$ protons (CERN, 2008). They are forced to collide in four large experiments. The experiments at these interaction points (IP) are called A Toroidal LHC Apparatus (ATLAS), Compact Muon Solenoid (CMS), A Large Ion Collider Experiment (ALICE) and Large Hadron Collider beauty experiment (LHCb) and they are installed in caverns. The large experiments ATLAS and CMS have new caverns that are slightly bigger than the caverns of LHCb and ALICE that are recycled from the Large Electron-Positron Collider (LEP). The

cavern size of the ATLAS experiment is $53\text{ m} \cdot 30\text{ m} \cdot 35\text{ m}$ (Lippitsch, 2007). As the particle bunches travel at close to the speed of light, they will complete 11245 orbits per second and provide 600 million collisions per second in the experiments (CERN, 2008). To arrive at this energy, speed and particle densities in the bunch, different particle accelerators are in use at CERN. Generation of the particles starts in a linear accelerator (LINAC), afterwards they are layered in the PS Booster complex. The Proton Synchrotron (PS) and the Super Proton Synchrotron (SPS) are older machines from the 1970s (Mainaud Durand et al., 2008), which are used for the acceleration of the particles. They are designed to bring the particle bunches close to the speed of light before injecting them into the LHC storage ring.

1.2 LHC alignment - problem description

In this section, the alignment concept for the LHC and in particular of the final-focus magnets is presented. The constraints for the alignment and the approach to monitor and reposition the magnets within the required accuracy are shown.

In a high performance environment for particle physics, the technical infrastructure of the operating laboratory has to provide the means to run the accelerator in the best conditions possible. At CERN, the survey section within the Beams Department is responsible for controlling, positioning and aligning the beam lines and detectors with respect to a layout defined by the physicists.

Overview During the installation phase of an accelerator, optical surveying methods like levelling, total station measurements and laser tracker measurements are applied in order to put the machine components in a reference frame. Once the accelerator components are connected to each other, a second survey to obtain the local best fit is carried out. For this smoothing of the machine, special techniques like wire offset measurements are carried out in order to obtain the relative shape of the machine.

In experimental areas, measurements of all detector parts during assembly are carried out. Their position in the final installation is determined to allow the physicists to track the particle collisions and reconstruct three-dimensional particle trajectories with respect to the nominal beam line. These survey measurements consist mainly of total station or photogrammetric measurements.

The final-focus magnet region, also called low-beta magnet triplet, is on both sides of each experiment. The magnets are used to reduce the diameter of the beams, to

give them their final direction in order that they collide in the experiment. The low-beta magnets are composed of a set of three quadrupole magnets (Q1, Q2 and Q3). To make the particle beams collide, very tight alignment tolerances are required (Coosemans et al., 2002). The position of one low-beta magnet triplet with respect to the other has to be maintained within ± 0.5 mm and one quadrupole inside its triplet has to be stable to a few microns. To fulfil these demands, a permanent monitoring and repositioning system has to be installed. The sensors used for those measurements allow monitoring of horizontal and vertical movements as well as rotations of the magnet. The resolution of those sensors is better than $1\ \mu\text{m}$. The jacks of the quadrupole magnets are motorized in order that the quadrupole magnets may be remotely repositioned. In addition to the low-beta magnets the monitoring system extends to one dipole (D1) as illustrated in figures 1.1 and 1.2 and a central feed box (DFBX) for electricity and cryogenics supply. The length of the assembly is approximately 50 m. Both figures, 1.1 and 1.2, show the left side installation of the monitoring system with respect to the experiment. The arrangement of the right side is symmetrical. The final alignment of these magnets is carried out using the same wire and levelling techniques as used for the standard components of the accelerator.

Global Network The complete process of aligning large machines, for example particle accelerators, is in most cases split into several steps. First, the installation of the components is carried out using a reference network linked to a coordinate frame. This frame can be linked to an absolute network like World Geodetic System 1984 (WGS-84) or to national reference networks, but in most cases it is a local coordinate system. In the case of CERN, a local coordinate network, the CERN coordinate system (CCS) has been defined (Jones, 2001). The advantage of such a network for engineering surveying is the fact that it is free of large scale deformations that can appear in national reference frames. Deformations in national reference networks can be up to several centimetres. Networks determined with Global Positioning System (GPS) measurements can provide relative point accuracy of ± 0.1 ppm to ± 1.0 ppm in a static measurement mode and with post-processing methods (Hofmann-Wellenhof et al., 1994). In the field of accelerator alignment, the use of GPS can only be for a surface network as the accelerator itself is situated underground where the GPS signal cannot be received. Transfer measurements to establish the surface network underground are necessary.

LHC alignment After the installation of the beam conducting accelerator components, like for example magnets, a first alignment of their position is carried out with respect to the CCS. The tolerances for the radial and vertical alignment are

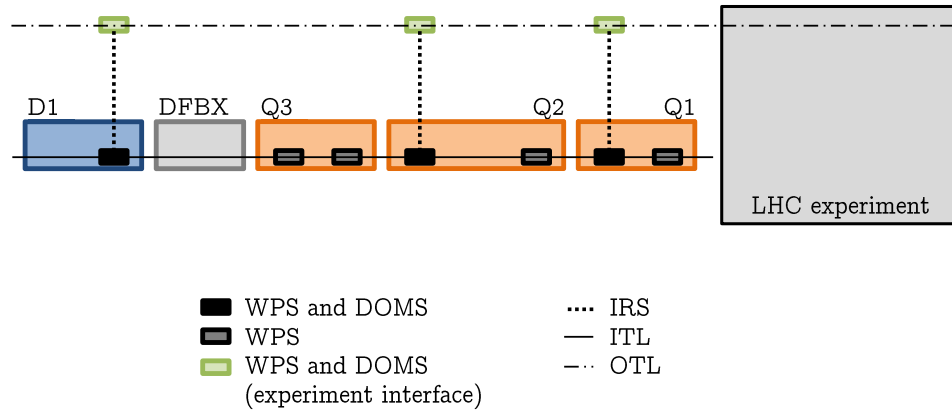


Figure 1.1: low-beta magnet radial monitoring sensor layout

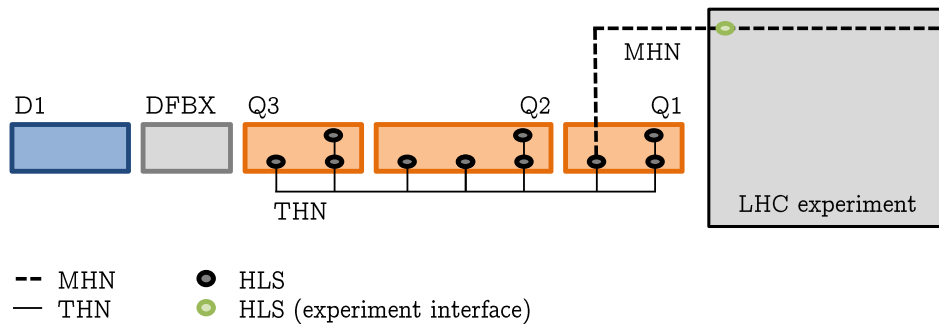


Figure 1.2: low-beta magnet vertical and tilt sensor layout

defined to be better than 0.25 mm and 0.15 mrad for the tilt of the magnet over a slot of 100 m along the machine (Quesnel, 2004).

In a second step, the alignment of the local best fit for the components is carried out. Relative wire offset measurements for radial determination and levelling for the vertical are used. The components have to be aligned to better than 0.15 mm over a distance of 150 m (Quesnel, 2004). This slot of 150 m can be placed at any position along the machine and the components included in this slot have to fulfil the alignment requirement.

LHC final-focus magnet alignment All final-focus magnets are equipped with motorized jacks that are used to allow remote repositioning. This remotely operated alignment is implemented, as the required alignment tolerances are very tight and therefore even small movements of the magnets will require a realignment. The high radiation doses that occur in this region of the LHC of up to 16 kGray (kGy) per

year make it necessary to limit working time in this region (Dimovasili et al., 2005a). In relation to the position of each jack, reference points are installed on the magnets allowing the installation of the different monitoring sensors. Those reference points are known with respect to the geometric and magnetic beam axis in the magnet. They establish the internal geometry of the magnet relative to the cryostat. The cryostat is the external housing of the magnet.

The tolerances for the low-beta magnets are described by three alignment functions in the LHC design report (Quesnel, 2004).

- alignment of Q1, Q2 and Q3 for one triplet better than 0.1 mm in long-term and to several μm in short-term stability
- alignment of one triplet with respect to the other triplet to better than 0.3 mm
- alignment of the experiment with respect to the machine to better than 0.3 mm

To allow for the required alignment of the final-focus magnets, their positions have to be known with five degrees of freedom: vertical and radial translation as well as three rotations. The monitoring system has redundant measurements in order to allow control and compensation of the system itself. The longitudinal component, parallel to the beam lines, is less critical and is therefore not monitored on-line. The relative movements of the magnets after the initial alignment have to be monitored. Realignment is performed using the monitoring data. This will be done via a visualisation system that allows the monitoring of all measurements of the magnets in real time. The remote repositioning of the magnets can be done from the CERN control centre (CCC) and does not need people to enter the radioactive environment in the area of the magnets.

Monitoring system configuration The layout of the monitoring and repositioning system of the final-focus magnets is shown in figures 1.1 and 1.2. A photo of the installation is shown in figure 1.3. At either end of the four experiments the final-focus magnets are equipped with a hydrostatic levelling system called the Triplet Hydraulic Network (THN). The hydrostatic levelling system is installed for monitoring of relative vertical displacement of the magnets, roll and tilt angles of the magnet as well as for the sag of the Q2 magnet. This magnet is longer than its neighbouring magnets Q1 and Q3 and has an additional central jack (Bestmann and Missiaen, 2006). The main part of the THN is installed on yellow pillars, see figure 1.3, that are independent from the magnets. The THN is installed horizontally having a common half-filled stainless steel tube with a diameter of 50 mm for the water and air connection of the system. This free-surface hydrostatic levelling



Figure 1.3: low-beta magnets in the LHC tunnel

sensor (HLS) system allows the minimization of temperature effects on the system (Schlösser and Herty, 2002). Silicone tubes link this network to the sensors on the magnets. For this short part of the network, a two tube system, one filled with water and one for the air link, has been chosen. The two tube solution is preferable as it allows easy replacement of the HLS. To minimize the temperature effect in this part of system, the tube has to be installed with the least possible sag (Busch (1981), Schlösser and Herty (2002)).

A wire position system monitors the movement of the magnets. It is called the inner triplet line (ITL). This is a stretched wire reference along the magnets and is designed to detect the radial and vertical movement as well as the roll and pitch angles. Two sensors are installed on each magnet. The wire stretching pillars are installed independently from the magnets.

The experiments in the LHC are linked to the final-focus magnets by interface points available in the cavern or in the survey galleries. These special survey galleries have been excavated into the rock, in the ATLAS and CMS cavern, for radial monitoring of the triplets with respect to each other (Quesnel (1997), Mainaud Durand et al. (2004)). To make the permanent, vertical link between the two final-focus magnet triplets and the experiment, the Main Hydraulic Network (MHN) is installed in all four experiments. This stainless steel tube has an inner diameter of 100 mm. The MHN network is also established as a free-surface water network.

In the survey galleries, a stretched wire, 140 m in length, is installed in each of the survey galleries to form the outer triplet line (OTL). The link between the wires installed on the ITL and the OTL is made with a distance measurement between the wires. Three invar rods on each side of the experiment, bridge the distance between

the two lines. The invar radial system (IRS) is assembled from several invar bars with targets at the extremities (Lippitsch, 2007). Each rod has been calibrated using interferometer reference measurements in the laboratory. The position of the wires with respect to those targets are determined with the Wire Position Sensors (WPS) and Distance Offset Measurement Sensors (DOMS). Both are mounted on the same support. The WPS measures the position relative to the wire while the DOMS measures the distance to the target on the invar rod.

1.3 Aim and Objectives

The motivation for this research is based on the need to provide permanent monitoring and repositioning for the final-focus magnets in the LHC and an alignment interface to the experiments (Herty and Mergelkuhl, 2008). As a part of the alignment concept and system, the sensors used for the monitoring and repositioning have to be checked in different quality aspects before their installation in the tunnel. The design of the alignment network and the use of the sensors in this context, also needs additional checks and calibrations to those provided by the manufacturer.

The aim of the author in this research project is to investigate methods for the validation of the sensors used for the LHC final-focus magnet monitoring and to evaluate the need for the introduction of additional sensor parameters due to the alignment concept.

The main objectives for the research project are classified in four categories. First, the review of the sensors and the alignment concept chosen for this project in order to identify checks and calibration needs. Second, the definition of the checks and calibrations, the methods proposed and criteria for the acceptance of the sensors. This step is followed by the design of validation and calibration benches for each type of sensor and measurement carried out, including the optimisation of each bench following the measurement results obtained. This iteration process in the bench design is parallel with the objective of statistically analysing the measurement results. In addition, possible check and calibration methods for the sensors are investigated for the case that they are already installed in the tunnel and their performance needs to be evaluated.

1.4 Structure

In this first chapter, an introduction into accelerator alignment and the particular case of the monitoring of the LHC final-focus magnets is given. The literature review in chapter 2 defines the difference between monitoring and alignment, shows different systems and methods used in other laboratories for particle accelerator alignment and discusses the advantages and disadvantages of calibrating the single sensors or a complete system. In chapter 3, the measurement principles of the three types of sensors and their corresponding monitoring and repositioning system for the LHC are introduced. The proposed checks and calibrations applied to the sensor with its parameters are presented in chapter 4. Based on the methods proposed, the check benches designed for these measurements are introduced. The measurement set-up of the sensors, the analysis of the results obtained and criteria for accepting the sensors are shown in chapter 5. Chapter 6 concludes with the techniques used, during the checks and calibrations. The sensors and benches are evaluated, analysed by rigorous methods leading to proposals for future, automated calibration systems.

Chapter 2

Literature Review

After introducing the content of the research project, the literature review gives an overview of current geodetic monitoring and alignment techniques in the field of accelerator alignment. Comparisons and examples are related to surveying applications in particle accelerators, in order to allow a detailed review of the variety of systems available in this particular field.

2.1 Monitoring and Alignment

The term monitoring describes the observation of system parameters at certain intervals to allow analysis and prediction of the system's behaviour. Monitoring does not include the action taken as a consequence of the observation. In the field of surveying, alignment can be one corrective measure that uses the observation in case the object is adjustable. The relationship between monitoring and alignment is shown in figure 2.1.

A measurement gives information about the object only at one moment. By comparing several observation epochs, one can state the evolution of an object over time. Evaluating the associated risk in relation to the importance of and time delay for detecting movements a monitoring system does not have to be operated permanently; only for highly sensitive systems, permanent monitoring systems are put in place.

In the classical, geodetic sense, alignment means the positioning of points with respect to a reference line or determination of offsets of points with respect to a reference line (Schwarz et al., 1995). This means an action takes place in order to position object points in a desired configuration. Therefore alignment is concerned

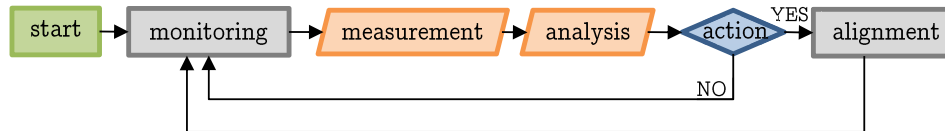


Figure 2.1: monitoring and alignment flow chart

with monitoring, but also has an active component, as the positioning of object points is the aim.

2.2 Particle Accelerator Alignment

In particle accelerators the alignment issue can often be divided into the classical approach of a radial and a vertical determination of a component and its rotation angle with respect to the beam line. As components like beam tubes, magnets and connections have only a very limited relative displacement range with respect to each other, it is important in some cases to monitor movements of the magnets in real-time.

It is not common that a whole machine is monitored permanently with geodetic sensors. This is only the case, if the ground on which the machine is built, is considered to be unstable due to environmental influences. This can be the case for example close to a river. Such permanent monitoring systems are installed at the European Synchrotron Radiation Facility (ESRF) (Roux, 1993) and at the Swiss Light Source (SLS) (Ingensand et al. (2002), Wei et al. (2002)). In most cases only very special sections of the accelerator, like the final-focus magnets and experiments, are permanently monitored.

As the demands for high precision monitoring arise with the upcoming generation of particle accelerators, many monitoring and alignment systems are installed. Examples include the low-beta magnet repositioning system in the LHC (Coosemans et al. (2002), Mainaud Durand et al. (2004)) or the final-focus monitoring of the Linear Coherent Light Source (LCLS) at Stanford Linear Accelerator Center (SLAC) (Anon., 2002). Existing systems are installed at Deutsches Elektronen-Synchrotron (DESY), linking the two sides of the Hadron Elektron Ring Anlage (HERA) machine around the experiment with an HLS system (Löffler et al., 1992) or a wire referenced monitoring system in the accelerator Freie-Elektronen-Laser Hamburg (FLASH).

Straightness Alignment Systems						
Mechanical Reference Line		Optical Reference Line			Gravity Reference	
optical detection	electrical detection	optical axis	laser beam	diffraction optics	hydrostatic level	differential tilt
differential diode	low frequency induction pick up	alignment telescope	phase sensitive detector	Fresnel pattern	portable	optical inclinometer
CCD sensor	radio frequency induction pick up	photogrammetry	light intensity measurements	Poisson pattern	mercury	electronic inclinometer
scanner	capacitive sensor	electro auto-collimation	interferometric measurements	Airy pattern	automatic	differential mercury HL

Figure 2.2: straightness alignment systems after Ruland (1995)

The installation of alignment systems depends on the shape of the magnets and infrastructure installations in the tunnel. Establishing a reference line in a mechanical or optical way, means having a straight line of sight between all network points. If permanent monitoring is not possible with these methods, photogrammetry, laser tracker or total station measurements may be used instead.

Alignment Types In his categorization, Ruland (1995) identifies three different classes of alignment systems. These classes point out the different reference systems, but do not ask for the need in the alignment. For the particle accelerator alignment a classification of radial alignment, vertical alignment, straight line alignment and inclination alignment would be more appropriate as the alignment problem can be attributed to one of these classes. Mostly the measurements are split into two-dimensional horizontal plus one-dimensional vertical measurements. In cases where only radial alignment is important the problem can be reduced to a one-dimensional radial plus a one-dimensional vertical alignment. Evaluating Ruland's (1995) classification, photogrammetric methods do not establish a reference line, but create a reference network of points, so strictly speaking they do not take part in the optical reference line classification. To complete the list, the widespread introduction of laser trackers has allowed the use of these instruments for accelerator alignment for some years.

The system used for the measurements has to be evaluated for its accuracy and reliability under the conditions on site. Refraction of the beam or mirror effects on reflective surfaces can cause problems in the measurement if optical systems are used. Mechanical reference lines, for example wires and hydrostatic systems, can be affected by temperature gradients, ventilation and pressure differences as well as by vibrations from surrounding infrastructure. Radiation means that not every system

is suitable due to radiation influences on the sensor or because of materials that are not radiation tolerant. Electro-magnetic influences have to be studied as well.

2.2.1 Height Observations

For permanent height observation, hydrostatic levelling systems are in use. Different concepts have been studied and implemented in the last decade. In the following paragraphs an overview of the different approaches is shown.

DESY The system was developed during studies for the TeV-Energy Superconducting Linear Accelerator (TESLA) project and is now used for monitoring parts of existing accelerators like the Positron-Elektron-Tandem-Ring-Anlage (PETRA). The measurement is carried out with an ultrasonic sensor installed in the bottom of the measurement pot. The resolution is at $3\ \mu\text{m}$ (Schlösser, 2004). The system presented by Schlösser and Herty allows an in-situ calibration of the measurement. Temperature effects and sensor drifts can be compensated for by measuring to two reference surfaces (R_1 and R_2) and a measurement to the water surface (W). The layout is shown in figure 2.3. By determining a scale factor between the measured distance, $D1_m$, and the calibrated distance, $D1_c$, the measurements can be compensated for errors due to speed variation of the signal in the water and at the same time for drifts of the sensor. A link to a tooling ball interface (target) with the reference made of invar allows height measurements with optical instruments and the integration of the system in a geodetic network.

SLS The system used at the SLS is based on a capacitive measurement. The distance between the sensor's electrode and the water surface is measured by the charge present on the electrode. The system allows measurements in the range of 14 mm with a resolution of $2\ \mu\text{m}$ and an accuracy of $10\ \mu\text{m}$ (Meier et al., 2004). The measurement itself is contact-free although the calibration of the absolute reference is carried out with a touch point. This point is known from the mechanical design of the sensor and measurement pot. By changing the water height in the system and searching for the touch point, one can have an absolute reference of the sensors with respect to each other.

CERN / ESRF CERN and ESRF are using hydrostatic levelling sensors which are based on capacitive measurements. The prototypes of these sensors were developed at the ESRF (Roux, 1993). The first sensors had their electronics integrated in the sensor body, where it was sufficiently protected for the needs in the synchrotron at ESRF and at installations at LEP at CERN. For the use in the LHC, the electronics had to be separated from the sensor body to allow their use in a highly radioactive

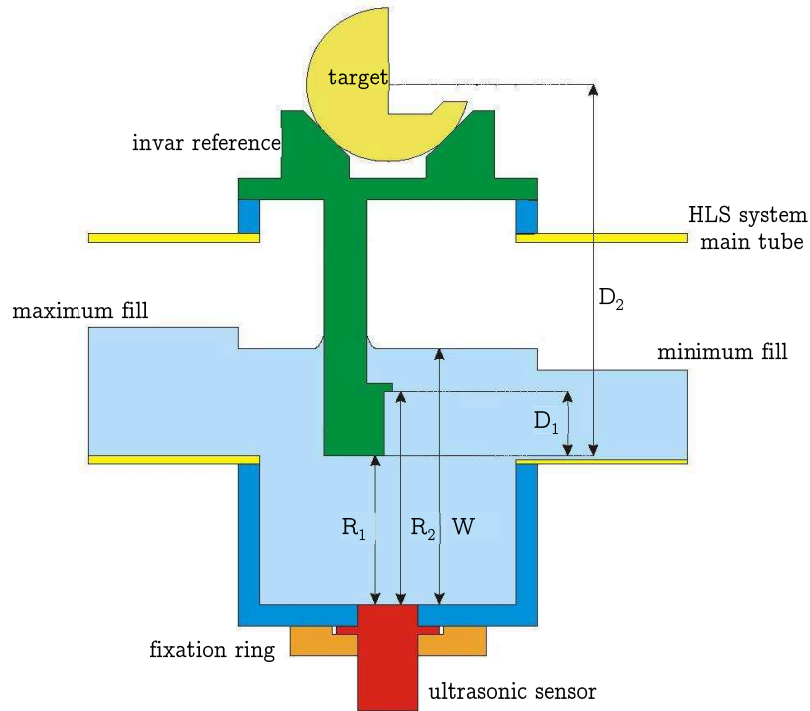


Figure 2.3: DESY HLS after Schlösser and Herty (2002)

environment. These sensors will be discussed in the following chapters as a series of tests were performed with them. A system performance analysis of the sensors at ESRF was given by Martin (2002; 2004).

Argonne National Laboratory An optical hydrostatic levelling sensor has been presented by Kivioja et al. (1997). A laser triangulation sensor is used in this case for a distance measurement to the water surface. The sensor is placed on top of the measurement pot performing the measurement from the air side. The variation of the CCD array of the sensor indicates the distance to the water level. For this system, problems have been concerned with the definition of the water surface as an optical mirror. Beams penetrating the surface, depending on the angle of refraction, caused problems during measurements.

2.2.2 Horizontal Alignment

Horizontal monitoring and alignment of components are mostly performed with optical or mechanical reference lines, if permanently installed. The references are independent from the components. In the case of mechanical references, stretched wire systems are used. They allow the determination of movements with respect to the wire. Optical references are mainly represented by a laser beam.

Mechanical and optical measurements are influenced by the temperature gradient along the measurement line, so both types of system need special protection of the system from environmental influences. In addition, mechanical systems have the mechanical distortion due to air conditioning or the thermal expansion of the stations where the wire is fixed to them. In the case of non-metallic wire it can also be subject to expansion due to humidity. For optical systems the influence of refraction can be important (Schwarz, 1997). As an example of the influence of refraction, a line of sight of $l = 150\text{ m}$ in length will be deviated from the straight line by $z = 2.8\text{ mm}$ in equation 2.1, following the approach of Schwarz et al. (1995). This is based on a temperature change of $1^\circ\text{C}/\text{m}$ perpendicular to the line of sight.

$$z = \frac{l^2}{8} \cdot -10^{-6} \cdot \frac{\partial T}{\partial y} \quad (2.1)$$

To avoid this influence on optical systems a vacuum tube can be used, but this makes it difficult to connect to reference points on the magnet. In a discussion of recent concepts for future accelerators, presented for example by Schwarz (1997), Coosemans and Mainaud (1997) or in the LCLS conceptual design report (Anon., 2002) a mechanical reference is preferred. The systems compared in the following section are wire systems that will come into operation in accelerator projects.

CERN A two-dimensional, capacitive wire sensor is used for the alignment of the LHC final-focus magnets with wire lengths of up to 140 m (Mainaud Durand et al., 2004; Mainaud Durand, 2006). The WPS allows the measurement with respect to a conductive wire. The resolution is $0.1\text{ }\mu\text{m}$ and the drift of the sensor is quoted to be better than $0.4\text{ }\mu\text{m} \pm 10\text{ }\mu\text{m}$ per month (Fogale Nanotech, 2007b). The system has been used for the LEP (Prochnow et al., 1999) and Compact Linear Collider (CLIC) studies (Becker et al., 2003; Coosemans and Mainaud, 1997).

SLAC For the alignment of the LCLS undulator section, a wire position monitor (WPM) system is used (Peters, 2005). The system uses a radio frequency pulsed wire and antennas to detect the position of the wire. The system can be used as a two-dimensional system and has two antennas per axis. The resolution is better than $0.1\text{ }\mu\text{m}$ but also the instrument drift is around this value per day. The accuracy along the sensor's range is $3\text{ }\mu\text{m}$. This system has also been used for the monitoring of four straight sections at DESY in the HERA straight sections (Peters, 2005) and in the Final Focus Test Beam (FFTB) at SLAC (Peters, 2005; Schwarz, 1990). The system has been tested and installed with a length of 60 m, but no indication on the maximum length is given.

2.3 Calibration: Sensor or System

This section focuses on the aspect of checking sensors used in a multi-sensor monitoring and alignment concept. The question as to whether it is necessary to check sensors individually or to check the system as one, must be answered. Instruments used for today's standard surveying tasks like total stations, digital levels or laser trackers are complex multi-sensor instruments. Different sensors like angular encoders, electronic distance measuring (EDM) devices or laser interferometers work together and deliver an output in coordinates.

There is interest in such a system to know about the performance of one sensor and whether it is within specification. Furthermore compensation of the sensor output can only be done when the sensor itself is calibrated. The system's performance can only be validated, if the individual error of each sensor is known.

Sensors are mostly calibrated for stability and linearity throughout a specified range. The use of a suitable sensor parameter estimation model is especially important for linearity compensation. The model can be described by polynomials of different degrees, spline functions or lookup tables, depending on the use. An in-situ calibration for each sensor integrated into the system is always preferred.

Both calibration types are important as the system's performance can only be known if the sensors have been validated before. The system itself has to be tested as well to see what influences there are that only occur when the sensors are integrated into a system.

2.4 Conclusion

In today's particle accelerators, the methods used for monitoring critical parts of the accelerator come basically back to two methods. For vertical alignment, HLS systems are implemented; for horizontal alignment, stretched wire systems are in use. The concept for monitoring depends on the time span, Δt , between two sets of observations. For most accelerator components Δt is not less than the time between two service periods of the machine. If this time span is too long and these components need permanent monitoring, suitable systems have to be installed. Permanent monitoring and alignment aspects become more and more important as for future machines the alignment requirements will be tighter than today.

Multi-sensor systems are used for monitoring components. Measurements are

mostly analysed in terms of relative movements to each other and not considered as absolute measurements. Most monitored alignment issues can be reduced to a one-dimensional horizontal plus one-dimensional vertical alignment, considering the longitudinal aspect as less critical and being sufficiently precise aligned with standard methods. Rotations of the magnet are calculated by using the relative readings of sensors to calculate a rotation angle.

With the examples of monitoring and alignment systems that have been developed in recent years, hardly any off-the-shelf products are available that can fulfil the criteria of reliability and long-term stability in a radiation environment. There is a variety of systems available, that in most cases are made for relative and short-term observations of several weeks, before resetting the sensors to a reference value.

Chapter 3

Monitoring sensors and applications

In chapter 2, the available systems on the market have been compared to each other and conclusions were drawn with respect to the different aspects of the systems. For the alignment of the LHC final-focus magnets, a complex configuration of several techniques and sensors is needed. This has been presented in section 1.2. Therefore three sensor types from FOGALE nanotech were chosen in order to have sensors fulfilling the required accuracies, resistant to the harsh environment and with a homogeneous data acquisition system (DAQ). The experience from previous sensor installations in former accelerators like LEP and CLIC Test Facility 2 (CTF2) have shown the capability of these sensors to handle the influence of radiation. The three types of sensors that will be discussed in this chapter are hydrostatic levelling sensors, wire positioning sensors and distance offset measurement sensors. Their corresponding alignment system in the final-focus magnet alignment is presented as well as the capacitive measurement principle the sensors are based on.

3.1 Capacitive Measurements

Sensors based on the capacitive principle measure, contact-free, the distance to an object. They act as parallel-plate capacitors. The capacitance, C , is measured as a function of the constants ε_0 and ε_r , the surface, S , of the electrode and the distance, h , between the two electrodes as shown in equation 3.1 (Bader and Dorn, 1993).

$$C = \frac{\varepsilon_0 \cdot \varepsilon_r \cdot S}{h} \quad (3.1)$$

The constant $\varepsilon_0 = 8.85 \cdot 10^{-12} C/Vm$ is the permittivity of free space and the dielectric constant for air is $\varepsilon_r = 1.0059$.

Permanent monitoring of the sensor's relative position with respect to an internally

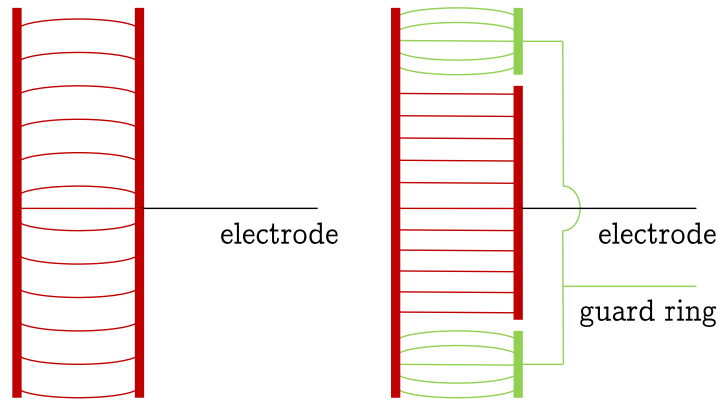


Figure 3.1: Standard capacitor (left), electrode with guard ring (right)

calibrated reference is achieved using measurements of the capacitance. A specified voltage, v_e , is applied to the electrode of the capacitor which is part of the sensor. This voltage creates an electric field between the plates. The electronics of the sensor continuously changes this field across the electrodes by applying a variable voltage. For WPS, frequencies are typically between 3 kHz and 8 kHz whereas HLS and DOMS operate at 50 kHz. The change, ΔC , of the capacitance is related to the change in the distance, Δh , between the electrode and the target as shown in equation 3.1. The output voltage of the sensor is given by equation 3.2 (Dimovasili et al., 2005a):

$$v = \left(v_o + \frac{1}{C} \cdot v_e \cdot C_{ref} \right) \cdot G \quad (3.2)$$

C_{ref} is the reference capacitance of the sensor. The specified voltage applied to the plate of the capacitor is v_e . The voltage creates the capacitance, C , during the measurement. The offset voltage, V_o is a function of the distance offset from a defined reference point. G is the gain, a scaling factor for the sensor's measurement range. The equations 3.1 and 3.2 can be unified as:

$$v = \left(v_o + \frac{h}{\varepsilon_0 \cdot \varepsilon_r \cdot S} \cdot v_e \cdot C_{ref} \right) \cdot G \quad (3.3)$$

In a field between two electrodes only the centre part can be assumed to be a homogeneous field. A homogeneous field has parallel field lines between the electrodes, which are perpendicular to the electrode. This defines the shortest distance between the electrodes and therefore the distance which has to be determined. To avoid falsification of measurements due to the heterogeneous distribution of field lines a second electrode, the guard ring, is introduced by the manufacturer. This electrode is situated around the measurement electrode and

causes the field of the measurement electrode to be more homogeneous. Comparison of the mode of operation between a standard capacitor and a sensor's electrode with guard ring is illustrated in figure 3.1. The shape of the field lines is only valid, if the electrodes are of the same size or if the passive electrode is larger.

3.2 Radiation related sensor design

An important influence on sensor design and the sensors' measurements is the radiation environment where they will operate. Every type of component that will be installed in the LHC therefore has to be tested for its response to radiation (Rausch et al., 2002). Electronic components can be very sensitive to radiation, even at low doses (Dimovasili et al., 2005a). Therefore the monitoring sensors with remote electronics and cable lengths of up to 30 m had to be evaluated. A series of tests in different irradiation facilities showed instantaneous influences, for example offsets in the measurements as well as long term influences such as the drift of the output signal (Herty et al., 2006). In section 4.7 the tests carried out are described. Publications on the test series are available in sections C.1, C.2 and C.4. As a result, a compensation model has been determined for the HLS (Dimovasili et al. (2005a), Herty et al. (2006)).

3.3 Hydrostatic Levelling Sensor

An HLS system is designed to determine the level of water within itself. In combination with other sensors and a hydraulic network, the height differences between instruments can be determined. This section gives an overview about the FOGALE nanotech HLS, its characteristics and the calibration function which comes with it.

Characteristics The tested HLS are of different types and series as shown in figure 3.2. There are three generations of sensors available at CERN (Herty et al., 2006):

- **second generation** with stainless steel housing, ceramic body and with the electrode printed on the ceramic body,
- **third generation** with stainless steel housing and body with the electrode protected behind a glass surface and
- **fourth generation** with stainless steel housing and body with the electrode printed on a ceramic surface.

Due to problems with the stability of the sensor, the development of third generation sensors has been abandoned by the manufacturer. The second generation sensors available at CERN date from their use in the LEP and are no longer produced. They come only with integrated electronics. The fourth generation is the actual one that is mainly used at CERN. It is available with remote or integrated electronics and has ranges of 5 mm or 10 mm. The specification of the sensors is given in table 3.1. These characteristics are the same for the second and fourth generation HLS.

When the sensor is exposed to humidity, condensation of water can cause falsification of the measurements. This can lead to a short-circuit of the sensor if the electrodes of the sensor and the guard ring come in contact through the water and form a short circuit. Also a deposit on the sensor from evaporation of water can limit the function of the sensor. To prevent these problems, the electrode is heated with a heating mechanism that keeps the electrode's temperature above the ambient temperature. This is sufficient to prevent condensation. Splash water on the electrode, for example during installation, has to be removed before operating the sensor.

The sensor comes with a temperature probe, PT-100 (British Standards Institution, 1996), that makes it possible to determine the temperature of the liquid used in the associated measurement pot. The temperature measurement is used to apply corrections due to thermal expansion of the measurement pot and the liquid, depending on the type of hydrostatic levelling system used. To enable the link between the sensor's measurement and a standard geodetic measurement device, for example a tooling ball or level staff, the HLS is equipped with an interface support.

Calibration function For the conversion of the sensor's voltage output to a metric distance, the HLS comes with a third or fourth order polynomial, determined by the manufacturer.

$$d = \sum_{i=0}^m a_i \cdot v^i \quad (3.4)$$

In equation 3.4, v is the voltage output of the sensor's electronics as shown in equation 3.2. The coefficients which have to be applied, a_i , are the coefficients of the polynomial to the degree m . The result is the distance, d , measured with respect to the calibrated offset. Figure 3.3 shows the three sensor ranges that are used at CERN with their different distances with respect to the electrode.

The electronics allow an adjustment of the zero point of each sensor as well as their



Figure 3.2: HLS (left to right: second, fourth and third generation)

Table 3.1: HLS specification (FOGALE nanotech, 2006 & 2007b)

working range	5 / 10 mm
signal output	0 - 10 V
resolution	0.2 μm
repeatability	$< \pm 1 \mu\text{m}$
stability zero	$\pm 0.7 \mu\text{m}/\text{month}$ $\pm 0.3 \mu\text{m}/^\circ\text{C}$
stability gain	$\pm 5 \mu\text{m}/\text{month}$ $\pm 2.5 \mu\text{m}/^\circ\text{C}$
linearity error	$\pm 0.8 \mu\text{m}$
absolute reference	$\pm 50 \mu\text{m}$
warm-up time	48 h

gain. This can be done for the sensor's measurement as well as for the temperature probe measurement.

3.4 Hydrostatic Levelling System

A hydrostatic levelling system is used to determine height differences. The system uses the property that an undisturbed liquid surface forms an equipotential surface provided that the forces applied to the system are balanced. All stations used for measuring are linked to allow a free flow of water between the stations. Balanced

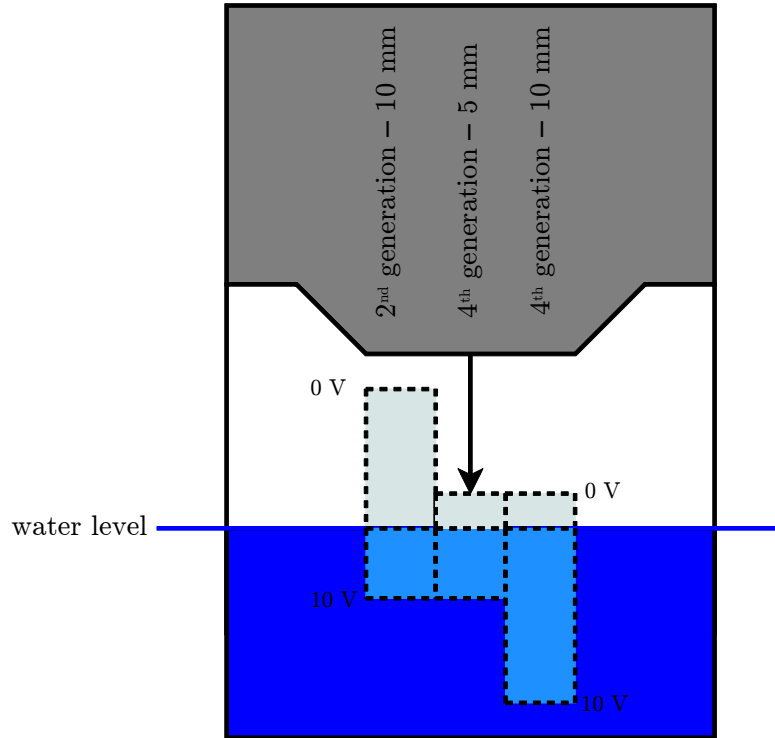


Figure 3.3: HLS ranges

conditions are achieved when the Bernoulli equation, as shown in equation 3.5, is fulfilled.

$$p + \rho \cdot g \cdot h + \frac{\rho}{2} \cdot v^2 = constant \quad (3.5)$$

with p as the atmospheric pressure over the liquid, ρ the density of the liquid, g the local acceleration due to gravity and h the height of the liquid (Meyer-Dietrich and Felshart, 1999). Assuming for a local network, that the acceleration due to gravity is the same for all stations and therefore no dynamic processes are taking place, only the density of the liquid and the atmospheric pressure influence the measurement and the acceleration term, $\rho/2 \cdot v^2$, can be eliminated.

With a system that is linked by a flexible tube having a sag, s , temperature gradients may arise, influencing the density of the liquid. As also shown in figure 3.4, an open system can have different atmospheric pressure on the liquid surfaces. Both influences significantly change the readings (Busch (1981), Schlösser and Herty (2002), Meyer-Dietrich and Felshart (1999)), so that a system in a closed circuit configuration is necessary for high precision measurements. One solution that gives the same pressure throughout the system uses an air link between the stations. A

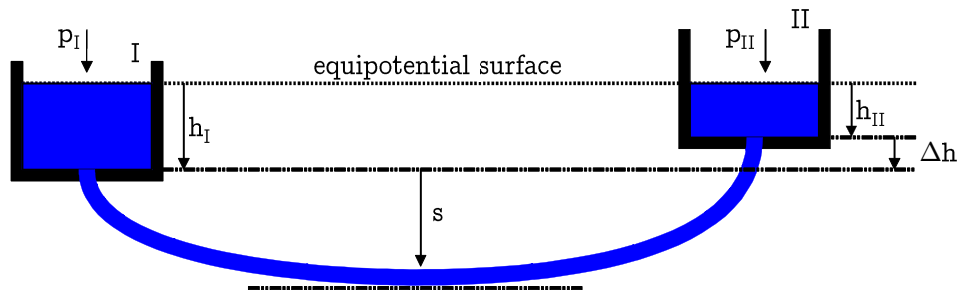


Figure 3.4: standard configuration

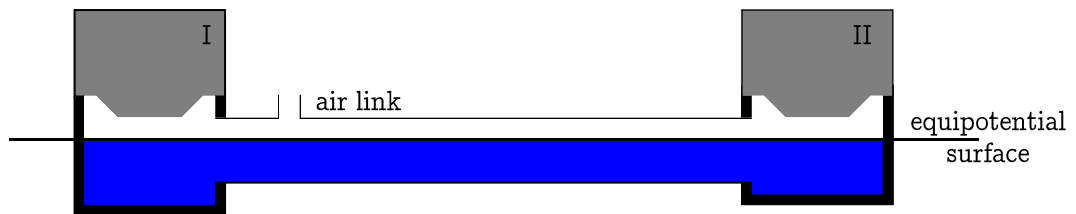


Figure 3.5: free-surface configuration

more sophisticated system provides constant air pressure and a tube sag of $s = 0$. This configuration is called a free surface system and is shown in figure 3.5.

The horizontal connecting tube and the common air link provide the same air pressure in the system. Temperature gradients are compensated, as no water columns can build up and therefore a change in the water density, and the associated change in volume, is transferred. In a free surface system the rise or fall of the liquid level is homogeneous. Elimination of temperature gradient and air pressure aspects improve the creation of a stable equipotential surface. Disadvantageous is the fact that waves can more easily be transmitted in such systems and the balancing time after perturbation is longer than in fully filled tube systems (Zhang et al., 2002).

The alignment configuration as used for the LHC final-focus magnet alignment is described in section 1.2.

3.5 Wire Position Sensor

The WPS is designed for monitoring objects with respect to a stretched wire reference line. The sensors that are available are the WPS-1D type and the WPS-2D type where the 1D and 2D indicate the number of measuring axis on the sensor. At

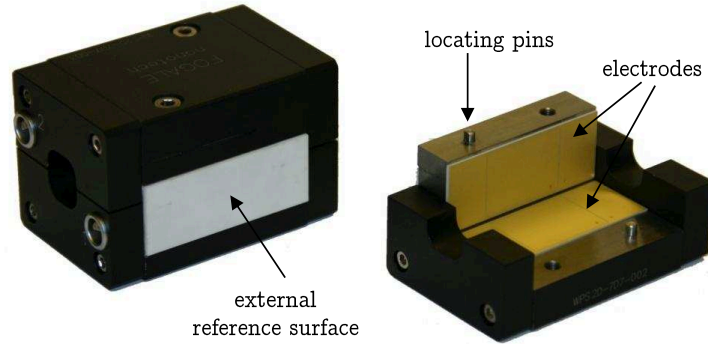


Figure 3.6: Closed and opened WPS

Table 3.2: WPS specification (FOGALE nanotech, 2006)

working range	10 mm
signal output	0 - 10 V
resolution	0.1 μm
repeatability	$< \pm 0.3 \mu\text{m}$
stability zero	$\pm 0.4 \mu\text{m}/\text{month}$ $\pm 0.5 \mu\text{m}/^\circ\text{C}$
stability gain	$\pm 10 \mu\text{m}/\text{month}$ $\pm 5 \mu\text{m}/^\circ\text{C}$
linearity error	$\pm 4 \mu\text{m}$
absolute reference	$\pm 50 \mu\text{m}$
warm-up time	5 min

CERN the WPS-2D sensors with axis measurements in radial, x , and vertical, y , are in use.

A stretched wire is the reference line for a sensor. One can assume, for horizontal monitoring, a straight reference line when looking at the wire from above. For relative vertical measurements, the form of the wire is not important, as the relative displacement of the wire will be seen correctly as long as the shape of the wire is constant over time. For modelling the wire for absolute measurements, models for the shape of the wire have to be calculated. Mainaud (1996) has evaluated models for the calculation of the wire shape in order to take into account the sag of the wire due to gravity.

Characteristics This sensor is based on the capacitive measurement principle. It has two electrodes per axis facing each other, which makes a total of four electrodes

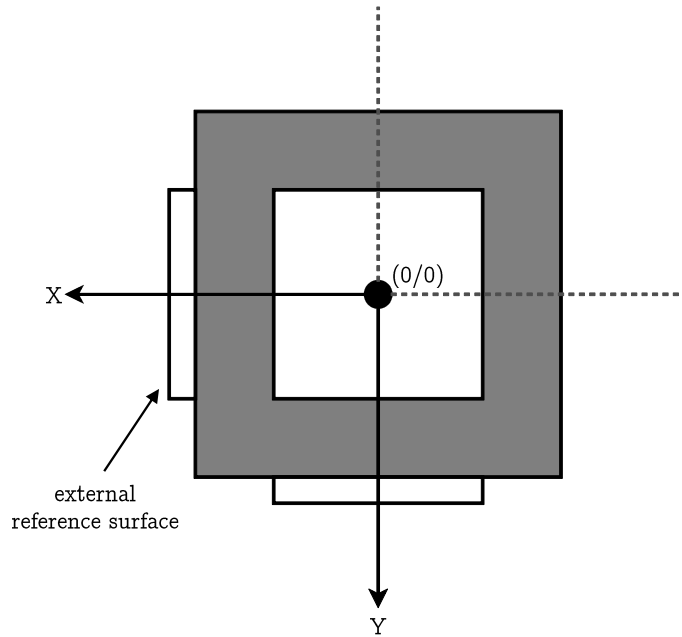


Figure 3.7: WPS coordinate system

as illustrated in figure 3.6. The sensor can be unscrewed into two parts to allow the installation of the wire. The two parts are assembled with locating pins allowing precise relative repositioning. The specifications of the sensor are given in table 3.2 (Fogale Nanotech, 2006; Fogale Nanotech, 2007b).

The sensor is calibrated to have the centre of the sensor at the position of the wire with an output voltage of $(v_x/v_y) = (5.000/5.000)$ in V. This position of the wire in the centre is defined as $(d_x/d_y) = (0.000/0.000)$ in mm and gives the sensor ± 5 mm range on each axis. The coordinate system of the sensor is defined as shown in figure 3.7 and is defined as the sensor's measurement with respect to the position of the wire in the sensor. The ceramic external reference surfaces define the orientation of the sensor. As the wire is generally assumed and controlled to be stable, the coordinate system defines movement of the sensor and the associated output, although the observer sees a movement of the wire in the opposite direction.

Calibration function For the calculation of metric coordinates, (d_x/d_y) , for the wire position, the manufacturer provides one transformation matrix per axis. Each matrix contains 36 elements for the calculation and is defined as follows (Mainaud, 1996):

$$d_x = \sum_{i=0}^5 \sum_{j=0}^5 a_{i,j} \cdot v_x^i \cdot v_y^j \quad (\text{horizontal component}) \quad (3.6)$$

Table 3.3: Wire specification (FOGALE nanotech, 2006)

material	carbon-peek
diameter	0.4 mm
weight	235 g/km
thermal expansion	-1 $\mu\text{m}/^\circ\text{C}$

$$d_y = \sum_{i=0}^5 \sum_{j=0}^5 b_{i,j} \cdot v_x^i \cdot v_y^j \quad (\text{vertical component}) \quad (3.7)$$

From the equations above the output of one sensor axis depends on the measurement of both axes. Both axes of the WPS can be adjusted in offset, which defines the centre point, and the gain independently.

Wire Basically any wire can be used for the measurement as long as it is conductive. In contrast to the HLS or DOMS, where the flat surface of the target is related to the distance to the sensor's electrode, the wire's surface is round.

A carbon-peek wire is used for the measurements. The carbon provides the necessary conductivity and the peek wires that are braided around the carbon give the tensile strength necessary to stretch the wire and avoid fuzzing of the carbon filaments. The nominal force of 15 kg that is applied to the wire is about 2/3 of the breaking force.

Electrical Field Distribution The electrical field distribution in this sensor is more difficult compared with that of the HLS or DOMS. The WPS is also equipped with a measuring surface and a guard around it. This allows a distribution of the field lines in straight lines to the wire (Fogale Nanotech, 2007b). This interpretation of the field line distribution is different from that shown by Prochnow et al. (1999). The figure shown by Prochnow et al. does have intersections as the lines are curved and the field lines do not represent the shortest distance between the two electrodes. This is shown in figure 3.8.

Frequency A WPS is characterized by a frequency that is emitted by the sensor on the wire. The sensor frequency is situated between 3 kHz and 8 kHz typically at steps of 100 Hz. The frequency does not influence the measurement values of the sensor. The frequencies have a reserved bandwidth of ± 10 Hz around the nominal frequency. If another sensor frequency gets into this range, a noisy signal is received by on one or both sensors as they start to interfere with each other. In the case that

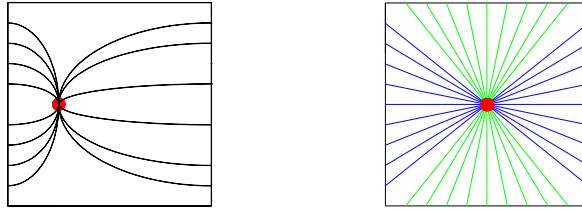


Figure 3.8: Field lines after Prochnow et al., 1999 (left) and FOGALE nanotech, 2007 (right)

the frequencies have to be readjusted; a potentiometer in the electronics is used to do this.

3.6 Wire Offset System

A wire offset system is an alignment system in the sense of ISO 9849:2000 (2000). In the ISO definition, an alignment system has two fixed points; the station of the instrument and the target. It allows measurements to be made vertically and radially with respect to the line of sight. The fixed points in a wire offset system are defined by wire stretching units that apply a known longitudinal force to the wire. The optical line of sight is replaced by a stretched wire.

Wire offset systems have two main problems that have to be balanced: weight and stability of the wire. The weight of the wire increases the wire's sag and in consequence the height difference between the sensors installed along the wire. At the same time the weight is good for stability as it makes the system less vulnerable to wind influences.

The natural frequency of a wire is dependant on the density, applied force, diameter and the length of the wire. Mainaud (1996) describes the calculation of lateral and longitudinal natural frequencies of wires.

3.7 Distance Offset Measurement Sensor

The DOMS can be considered as the same as HLS from the electrical point of view. The heating unit required to avoid condensation on the HLS is not applicable. In addition the DOMS is suitable for high frequency measurements in the kHz range.

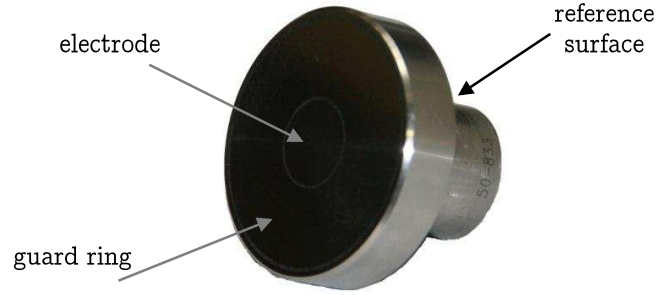


Figure 3.9: DOMS

Table 3.4: DOMS specification (FOGALE nanotech, 2007)

working range	10 mm
signal output	0 - 10 V
resolution	$\pm 0.1 \mu\text{m}$
repeatability	$< 1 \mu\text{m}$
stability	$< 1 \mu\text{m}/\text{month}$
absolute reference	$\pm 50 \mu\text{m}$

Characteristics The specifications of the sensors are given in table 3.4. The sensor's reference surface is the back of the sensor.

Calibration function For the DOMS a third to fifth order polynomial is calculated during calibration. Therefore the same determination method is valid as shown for the HLS in equation 3.4. The difference between the calibration of an HLS and DOMS is that a DOMS is only adjustable in its gain. The zero of the sensor is defined by contact to the electrodes' surfaces.

3.8 Invar Radial System

A distance offset measurement system using a DOMS is measuring the distance between the sensor's electrode and a target. In the case of LHC final-focus magnet alignment, the sensor is combined with an invar rod to form the IRS. The sensor measures in combination with the WPS the distance between the two wires by using the readings and calibrations of the WPS and DOMS, the mechanical constants of the supports and the calibrated length of the invar rod. The measurement concept is illustrated in figure 3.10

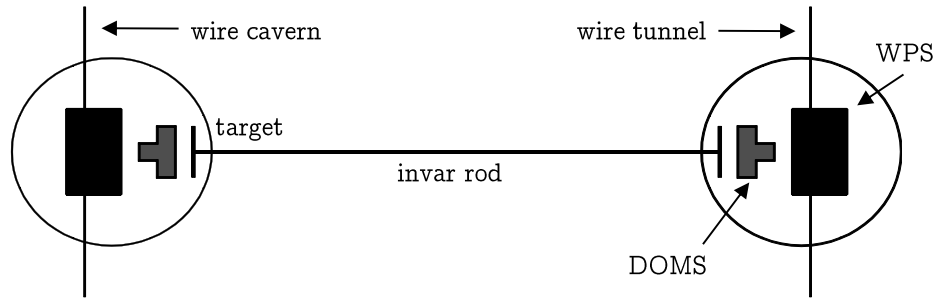


Figure 3.10: IRS

3.9 Data Acquisition System

The DAQ system for the sensors is presented in this section. The sensor unit consists of the sensor, its calibrated cable and the electronics associated with it. Figure 3.11 shows a sensor with its cable and electronics. The calibrated cables transport the primary, capacitive signal. After transformation in the electronics, a voltage output of 0 V to 10 V is provided at the electronics output. The sensors are powered with a 15 VDC supply. A connecting cable of up to several hundred metres in length connects the sensor to the multiplexing and powering unit. In the multiplexing unit, the return signal is provided for each sensor in two channels which for the:

- HLS are the distance measurement, h , and the temperature, t ,
- WPS are the radial measurements, x and the vertical measurement, y , and
- DOMS are the distance measurement, d and an unused channel.

From the multiplexing unit onwards, voltage measurements can either be directly displayed with a voltmeter or transferred via RS232/485 connection into software for visualisation and data storage. This minimum standard configuration is needed to obtain measurements from the sensor.

The connecting cable is made of a screened cable with 0.22 mm^2 wire diameter on each of the eight wires. The cable length can be of several hundred meters in the LHC. The cable is specified to have a linear resistance of $85\ \Omega$ per kilometre. According to Ohm's law represented by equation 3.8

$$V = I \cdot R \quad (3.8)$$

with I as the current, V as the potential difference between two points and R as the linear resistance, the signal loss with respect to the cable length can be determined.

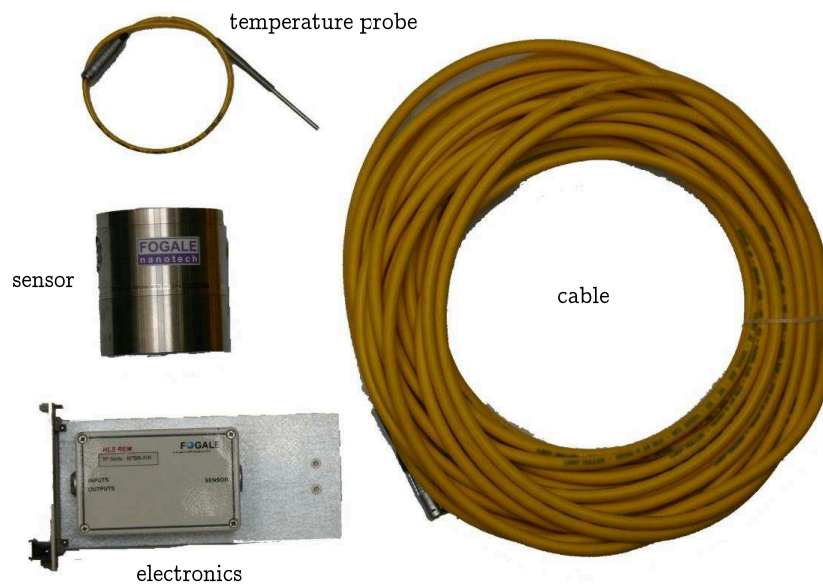


Figure 3.11: HLS with sensor, electronics and cable

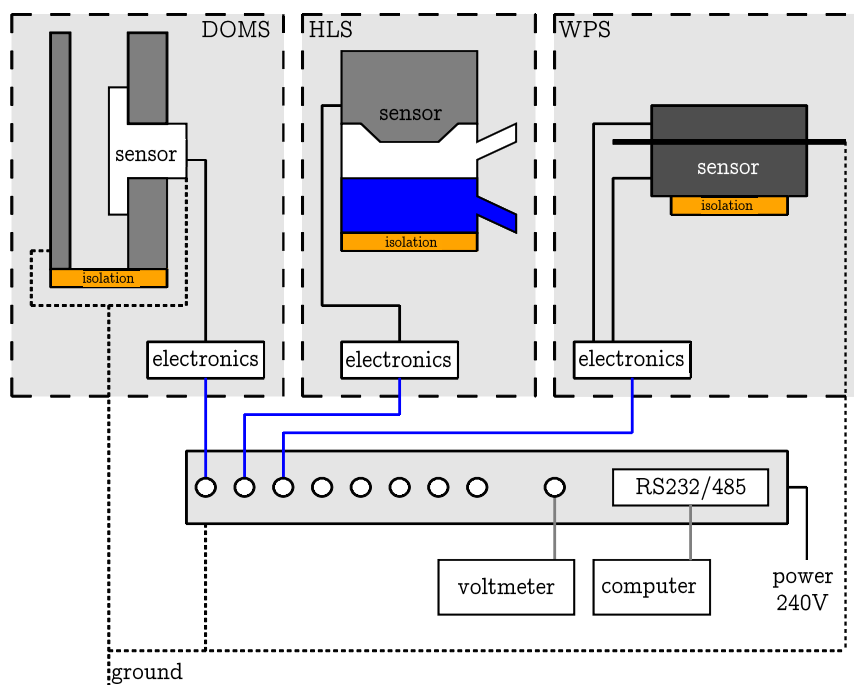


Figure 3.12: layout data acquisition system

The current I is constant and the difference ΔV is therefore only depends on the cable length. For short connecting cables the influence can be neglected.

Measurement and analysis software The first test series had been measured with software that allowed only measurements of the uncorrected voltage output. This software was written in Microsoft Visual Basic and was initially made for other testing purposes. Due to the programming language, long-term, real-time measurements were limited as the clock in the software had a drift of a few seconds per hour. Furthermore only single measurements were taken and not averaged over a period of time. As the level of electrical noise of the sensor is one of the criteria for accepting the sensor, as shown in section 4.1 the single, uncorrected measurements were only of limited use for carrying out all types of tests. In addition, the conversion of voltage output was simple for HLS and DOMS, but complicated for WPS, see equations 3.6 and 3.7, and therefore software enabling voltage and metric measurements as well as providing averaging functions had to be used.

Existing data acquisition software provided by the manufacturer is used to operate the control benches. This keeps the data processing of the measurements simple and in the configuration as designed by the manufacturer. This approach avoids the need for bug fixing and synchronizing problems in locally written data acquisition software and therefore wrong results from the sensor check measurements. The installation of the sensors for data acquisition corresponds to the layout shown in figure 3.12.

The software from FOGALE nanotech is called MultiSysMetrolog (MSM) and allows all types of tested sensors to be connected to the data acquisition rack and software. The measurements can be taken automatically using the calibration function provided. A modification of the calibration files allows the measurement of voltage output i.e. raw measurements to be taken uncorrected for temperature or other effects.

One objective was that the data acquisition and analysis of the measurements could be partially automated. This was necessary as approximately 200 sensors had to be tested. Therefore data analysis software had to be developed for each type of sensor and each type of control. The software MATLAB was used. The software grew with the needs of different tests and different DAQ modes. The final version of the check benches software was written as a script based set of functions. The implementation of a graphical user interface (GUI) was not made.

3.10 Summary

In this chapter, the three sensor types used for the LHC final-focus magnet monitoring and repositioning system have been presented. The HLS, WPS and DOMS are measuring based on the capacitive principle. The monitoring system comprises three sub-systems. An HLS system is used for vertical and tilt measurements of the magnets. A WPS system follows the movements in radial and vertical of the final-focus magnets and is redundant for vertical measurements with the HLS system. In order to link measurements from one side of the experiment to the other, wire measurements are combined with DOMS measurements used in the IRS. In total 113 HLS, 60 WPS and 24 DOMS are installed in the LHC.

Chapter 4

Sensor validation and calibration

The previous chapter presented an overview of the sensors and monitoring systems used in the LHC, the author introduces in this chapter the checks and calibrations he has carried out in order to validate the sensors.

The harsh accelerator environment with radiation and magnetic fields can perturb the long-term performance of the sensors at the μm precision level. Even drifts of the electronics within the limits indicated by the manufacturer make it necessary to check and calibrate sensors regularly. Before the initial exposure to ionizing radiation, the sensors can be returned to the manufacturer for checking, maintenance and calibration. This maintenance will later have to be carried out at CERN as the sensors can be radioactive after use in the accelerator. Shipping them to the manufacturer is therefore forbidden by law as the LHC is declared a nuclear base installation (INB) by the CERN host state authorities.

To be able to check and calibrate the sensors after the first beam injection into the LHC regularly, methods and benches have been designed and evaluated. The implementation of the benches and the associated methods is done in two steps. During the reception phase of the sensors, check methods are evaluated and manually operated benches are designed to allow the controls described in this chapter. In a second step, the results of the test series lead, where possible, to the design of automated calibration benches.

One part of the set of tests is derived from tests that are carried out by the manufacturer, like stability and linearity measurements. The test installations are conceived by the author as details about the test procedures by the manufacturer are not known. In addition, new calibrations and checks are introduced by the author to complete the knowledge about the sensor for the use in the LHC. This includes

the determination of offsets of the sensor's measurements to geodetic interfaces as for example a tooling ball support or reference surfaces. Also the interchangeability of sensors relative to each other is determined.

The environment necessary for checking and calibrating is a laboratory with controlled environmental conditions. The tests of the sensors are therefore undertaken in the calibration laboratory. The three types of sensors that are used for the LHC final-focus magnet monitoring and alignment are checked: HLS, WPS and DOMS.

4.1 Reception check

Before starting a detailed check of the sensor, a general function check has to be performed. The success of this reception check is determined by the functioning of the sensor as delivered by the manufacturer or as returned from the tunnel. The test is split in two parts: First, the components are checked visually for damage, e.g. scratches on the electrodes, broken cable connections or broken components on the electronics' circuit board. Passing this step, the functioning check is performed, using the DAQ set-up as shown in figure 3.12. The test comprises a test measurement on a fixed target with known reference parameters to be compared against the obtained measurement.

4.2 Warm-up

Using a sensor with a resolution of better than 1 μm and knowing that electronics need some time to stabilize after being powered makes this warm-up check necessary. The test determines the quantity, sense and duration of the warm-up.

During the warm-up check, the sensor will be installed for measuring to a fixed target. The measurements start when powering the sensor at the instant t_0 . The change in the sensor reading, Δx , during the warm-up period is defined as the difference between measurements at the end, t_h , and measurements at the beginning, t_0 , as shown in equation 4.1.

$$\Delta x = x(t_h) - x(t_0) \quad (4.1)$$

The end time for the measurements, t_h , is defined by the manufacturer as $h = 48$ as the time in hours after starting the measurements. The sensor has to be installed on its support sufficiently before starting the check. This negates any influence

due to mechanical constraints after fixing the sensor or insufficient equalisation of temperatures.

4.3 Stability

A stability measurement determines whether a sensor can be considered stable over time within the limits defined by the manufacturer. The stability check starts directly after the warm-up phase and takes typically a period of more than one week. The measurements give significant evidence of whether the sensor has a drift rate less or equal to the quantity indicated in the sensor specification.

The hypothesis that the sensor is stable during the measurement period is

- **true** if the condition from equation 4.2 is fulfilled,
- else it has to be considered as **false**.

$$\Delta x \leq s_o(t) \cdot \Delta t + s_o(T) \cdot \Delta T + (s_g(t) \cdot \Delta t + s_g(T) \cdot \Delta T) \cdot \frac{x_t}{x_{max}} \quad (4.2)$$

The parameters are the stability of the zero, s_o , and gain of the sensor, s_g . They depend on the measurement period of time, Δt , and the temperature variation, ΔT . The gain stability is corrected for by scaling the possible gain drift by the fraction of the measurement of the sensor, x_t , over the maximum possible measurement of the sensor, x_{max} . In equation 4.2, the definition of Δx is shown

$$\Delta x = x_t - x_0 \quad (4.3)$$

with the index t as the end time of the stability measurement and the index 0 as the start time of the measurement.

The measurements have to be performed on a fixed target. The distance of the target to the sensor is determined by the range of the sensor. Possible drifts can be separated into two parts. One is the drift of the zero reference point. This drift of the zero reference leads to a shift of the measurement range, but keeps measured distances accurate relative to each other within the measurement range.

The second part is a drift of the gain. The gain defines the range of the sensor. In this case, the scaling of the measurements change. In consequence, the range of the sensor changes as well. To illustrate the two drifts, one can imagine a third

degree polynomial, as used for example for the DOMS. The gain drift influences the parts of the polynomial where the measurement is a multiplier.

$$d = \underbrace{a_0}_{zero} + \underbrace{a_1 \cdot v + a_2 \cdot v^2 + a_3 \cdot v^3}_{gain} \quad (4.4)$$

To observe both types of drift, a stability measurement of the sensor has to be carried out in the upper range of the sensor, which means between 8 V and 10 V output voltage in the case of the FOGALE nanotech sensors. Such a measurement set up emphasises the gain drift as the influence is more important at the sensor's upper range with the gain drift acting as scaling factor.

Noise Level From these measurements, one can also determine the electronic noise of the sensor. This value has to be known to estimate the expected variation of the measurements with respect to the true signal. The electronic noise is caused by a random variation in the current or the voltage. This effect occurs in all electronics. A basic quantification, the range analysis and a determination of the standard deviation is carried out with the measurement data.

The electrical noise of the sensor limits the resolution and increases the standard deviation of sensor measurements. Noise in electrical components is normal and is caused by the components used in the electronics as well as by the cable. FOGALE nanotech states that the noise level will not exceed ± 1 mV for a sensor with a maximum cable length of 30 m.

The check is carried out by monitoring the voltage output with respect to a target and comparing single measurements over time. The noise, n , of the sensor is calculated from the raw measurement vector, x , with the measurements x_1 to x_i as shown in equation 4.5. If $n \leq 2$ mV, the noise level of the sensor can be accepted.

$$n = \max\{x\} - \min\{x\} \quad (4.5)$$

The stability test of a sensor as described in this section is for a sensor, cable and electronics measuring on a fixed target. This results in a measured capacitance that is returned to the electronics. This method can be applied for measurements that are carried out continuously on the same bench without modification.

Capacitive standards Using capacitive standards to check the sensors at regular intervals is another way to see if components in the electronics have drifted. The sensor and its cable are replaced by a capacitive standard, which is made of capacitors that are simulating the return signal of the sensor. To distinguish between

zero and gain drift two measurements in the case of the HLS and DOMS and three measurements for the WPS are made. The capacities simulate a measurement at the lower range of the sensor to measure the zero drift and a measurement at the upper range of the sensor to measure the gain drift. For the WPS, an additional measurement in the centre of the sensor is made, as the zero of the sensor is adjusted there.

The capacitive standard measurement does not allow an adjustment of the sensor. It is a relative measurement that gives information about the change in the electronics over time. The returned capacitance is transformed in the electronics to a voltage output. In equation 4.6, the calculation of the zero drift is shown

$$\Delta O_z(t) = O_z(t) - O_z(t_0) \quad (4.6)$$

with ΔO as the zero drift, z as the evaluated axis of the sensor, t as the most recent measurement and t_0 as the initial, reference measurement. Equation 4.7 shows how the gain drift, ΔG , of the electronics is calculated

$$\Delta G_z(t) = \frac{G_z(t) - O_z(t)}{G_z(t_0) - O_z(t_0)} - 1 \quad (4.7)$$

For the HLS and DOMS, the measurement of the zero and the gain determine the characteristics throughout the sensor range. For the WPS, the zero point is in the centre of the sensor's range, and in consequence two gain measurements have to be introduced. In the case of the WPS, the index z in equation 4.7 is $z-$ and $z+$ indicating the lower, $z-$, and upper, $z+$, gain range of the sensor.

The capacitive standards are determined to $\pm(1.5 \cdot 10^{-5} \cdot C + 0.0001 \text{ pF})$ with C as the capacity of the capacitor and a maximum thermal drift of $-35 \text{ ppm}/^\circ\text{C}$ (Fogale Nanotech, 2007a). Converting the capacity to metric units, the reference standard is therefore known to better than $\pm 1 \mu\text{m}$.

Conclusion The two methods for stability measurement over time differ in their approaches. While the stability bench is for monitoring drift over time in a continuous measurement, the capacitive standards allow snap-shots of the state of the sensor at different epochs.

The stability measurement on the bench makes it possible to follow the continuous evolution of the sensor. This means it can distinguish between a stability problem occurring as a single event, e.g. due to the failure of a electronic component, or as a continuous movement. Both measurement methods are necessary for the

interpretation of measurement results. From observations with both methods, drift models of the sensors can be calculated. A measurement on a mechanical reference surface is preferable, as the capacitive standards used in the reference has also to be controlled before use. The approach with capacitive standards is suitable for check measurements in-situ, when the sensor cannot be removed for tests from its installation.

4.4 Linearity

Checking the sensor's linearity is achieved by verification of the calibration parameters. This check gives an indication as to whether the polynomial supplied with the sensor is valid. At the same time it is possible to quantify drifts.

For this check, a comparison is made using a calibrated length measuring device. There are two approaches to performing this test, depending on the type of sensor used and the number of points to be measured to control the sensor. The calibration function can either be recalculated or a direct comparison of readings can be done.

Recalculation A set of measurements, over the range of the sensor, is taken in order to re-determine the sensor's calibration function, f_c , and to compare it to the function, f_m , provided by the manufacturer. The sensor's measurements vector, \vec{x} , and the reference length measurements vector, \vec{y} , with measurements at i positions throughout the sensor's range allow the determination of the coefficients of the calculated calibration function, f_c . In the case of a polynomial of degree n , the coefficients a_i with $i = 0$ to n are determined.

The hypothesis for considering a sensor's calibration function as valid is given in equation 4.8. The difference between the determined calibration function, f_c , and the manufacturer's calibration function, f_m , should be less or equal to 10 mV

$$\Delta f \leq f_c - f_m \leq 10 \text{ mV} \quad (4.8)$$

The hypothesis is

- **true** if the condition from equation 4.8 is fulfilled,
- else it has to be considered as **false**.

In the case that the hypothesis is false, a graphical and numerical comparison of the re-calculated compensation curve and the originally provided curve gives indication about changes the calibration function. If the two calibration functions

- are **parallel**, the sensor has changed its zero reference,
- have **different slopes**, the sensor has changed the gain.

The check measurements are performed with the same number of measurements as made by the manufacturer and the distribution of measuring points in the sensor's range should be the same.

Direct Comparison The re-calculation method is suitable for a limited number of measurements along one axis, especially if the control benches are operated manually. For multi-axial sensors, a comparison between the reference length and the corrected output values provide the faster solution.

This method can only verify the calibration function at the measurement points and not over the whole range of the sensor. In summary, *direct comparison* is only to be used if there is large number of measurements to be performed manually. For automated checks the *recalculation* method is preferable as information about the state of the sensor throughout the range is given and a new calibration of the sensor is available with the same measurement data.

For calibrations, the degree of the polynomial has to be chosen so that it allows for the best possible fit for the function with respect to the measured values. The more measurements taken along the sensor range, the more statistically meaningful the determination of the polynomial is. To determine the best fitting function with respect to the original set of data, the sum of the squares of the differences between the measured points used to determine the calibration function and the points computed from the function has to be as small as possible. The function is shown in equation 4.9

$$s = \sum_{i=1}^n (y_i - f(x_i))^2 \quad (4.9)$$

where y_i is the value obtained during measurement and $f(x_i)$ is the result of the polynomial function corresponding to the set of measurements (x, y) at the position i . The standard deviation of each coefficient of the function can be determined from the covariance matrix of the model.

$$\mathbf{o} = (\mathbf{A}^T \mathbf{W} \mathbf{A})^{-1} \cdot (\mathbf{A}^T \mathbf{W} \mathbf{e}) \quad (4.10)$$

with \mathbf{W} as the weight matrix, \mathbf{A} as the design matrix (Blobel and Lohrmann, 1998), \mathbf{e} as the input vector and \mathbf{o} as the output vector. The diagonal of the covariance matrix

of observations, \mathbf{W}^{-1} , has the same variance, σ^2 , for every observation, therefore $\mathbf{W}^{-1} = \sigma^2 \cdot \mathbf{I}$.

4.5 External Reference

If a movement has to be monitored relative measurements are often sufficient; for example the displacement of a WPS with respect to other sensors situated on the same wire. For referencing the measurements of the system with respect to another geodetic framework absolute referencing of the sensor is necessary. This process relates the measurement to a reference surface or tooling ball support situated on the sensor.

The determination of an external reference allows, at the same time, a determination of the differences between sensors in case there is the need to exchange them. As the three types of sensors that are tested have different shapes, individual concepts for determination have to be developed.

Measurements of interchangeability are not performed by the manufacturer individually for each sensor. The uncertainty of the absolute reference of the sensors is described in tables 3.1, 3.2 and 3.4. The envelope for the interchangeability is defined by this uncertainty.

The external references for the three sensor types are defined by the manufacturer in the following way.

For the HLS a Taylor-Hobson (TH) sphere mount is used. The external reference point of the sensor is the centre of the sphere. The measurement is referenced with respect to the measurement of the sensor.

The two axes of the WPS allow measurements from 0 V to 10 V as shown in table 3.3. The centre point is defined as the 5 V output for each axis which corresponds to a 0 mm output after applying equations 3.6 and 3.7. With respect to that point the theoretical distance to the external reference surfaces on the sensor is 23.5 mm. The determination of the external reference is not done, as it is not possible to determine the distance between the external reference surfaces of the WPS and the wire with the available instruments. Relative comparison between the sensors gives the differences between the sensors which allows compensation for differences in external referencing.

The DOMS is referenced with respect to its electrode. Contact with the electrode corresponds to a reading of 0 mm. As no referencing to geodetic instruments is directly possible, a relative comparison between the sensors is carried out.

External referencing can only be applied, if a reference point for geodetic instruments is available. For the sensors where only a reference surface is provided, relative measurements between the sensors give information about the interchangeability of the sensors with respect to each other.

4.6 Repeatability

The International Organization for Standardization (2004) has defined the repeatability of a measurement as

”precision under condition of measurement in a set of conditions including the same measurement procedure, same operator, same measuring system, same operating conditions and same location, and replicated measurements over a short period of time.”

The positioning of the sensor in a support has to be repeatable in order to allow absolute measurements to be taken. The standard deviation associated with the sensor installation method has to be known. By repeating the installation of a sensor on the test bench, a standard deviation for each sensor type can be determined.

The repeatability value for HLS and DOMS only depends on the installation of the sensor itself. Sensors are clamped or screwed into their supports. The WPS is made of two parts. The accuracy of the position of the pinned parts influences the measurement results, which means that the repeatability of a WPS has to be tested for repeatability of the assembly as well as repeatability of the installation of the sensor.

4.7 Radiation

For installation of sensors in the radiation environment of the LHC final-focus magnets, tests on the influence of radiation are carried out. Two basic tests cover different aspects on the sensor’s performance. One test is the *total dose test*, where the sensor is exposed to the quantity of radiation it will be exposed to during the lifetime of the LHC. The second test series takes a closer look at a possible *dose rate dependency* of the sensor. The electronics and the sensors are tested separately.

The two test methods described are based on the influence of radiation that will cause a degradation of the measurement signal over time. A detailed description of the tests is given by Dimovasili et al. (2005a), Dimovasili et al. (2005b) and Herty et al. (2006). The publications are available in the appendix C.1, C.2 and C.4.

Radiation linked influences on the electronics such as a single event effects (SEE) are not discussed. These effects change the state of components in the electronics which changes the functionality of the component or leads to its destruction.

4.8 Magnetic field

The second harmful influence to the sensors in particle accelerators can be the influence of magnetic fields. The magnets in the LHC are designed to have a small intensity stray field around the magnet. The experiments are designed to achieve a strong magnetic field in the detector. In the case of CMS for example, the field of the solenoid is designed to reach 4 Tesla (T). This field in the experimental areas produces a larger stray field and can influence sensors in the cavern and on the low-beta magnets.

The manufacturer states that HLS, WPS and DOMS withstand the influence of a magnetic field of 0.03 T. The electronics of the sensor are particularly at risk of damage due to the field. They are installed away from the magnets in the survey galleries or in the adjacent tunnel by-pass. Considerably more risk can be assumed for sensors and electronics installed in the cavern, e.g. for sensors with integrated electronics.

Tests in a magnetic field have to be carried out to quantify the influence of the field on the sensor, the cable and the electronics.

4.9 Orientation

Care must be taken of the orientation of the sensor with respect to its target when installing the sensor for a measurement. The limit for the inclination angle between the sensor and the target has to be less than 1° (FOGALE nanotech, 2006). To respect this value, a maximum estimation for the three sensors is calculated.

An HLS is installed on a measurement pot with an inner diameter of $d = 80$ mm. By

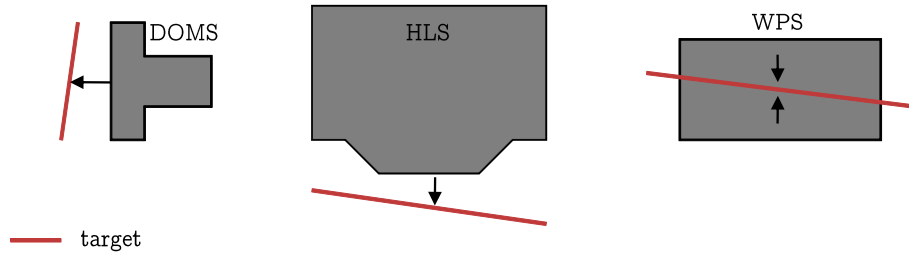


Figure 4.1: inclination error

applying the theorem of intersecting lines, the maximum allowable inclination, i_{max} between sensor surface and target is given by equation 4.11.

$$i_{max} \leq d \cdot \sin 1^\circ \quad (4.11)$$

By solving equation 4.11 with the given diameter d , i_{max} will be less or equal to 1.4 mm. The DOMS with a diameter of 40 mm has to be oriented to better than 0.7 mm, applying the same principle and using equation 4.11.

The HLS and DOMS are fixed for warm-up, stability, linearity, repeatability and external reference measurements on benches. The inclination between the target and the reference surface of the sensor can be adjusted before measurement in order not to exceed the maximum inclination i_{max} . The condition is fulfilled for the check and calibration benches.

The WPS is fixed in two different ways, depending on the test benches used. In the case of warm-up, stability and linearity check, the sensor is mounted with its two fixing screws on the an electrically isolated mount. The two fixing screws are separated by a distance $d = 45$ mm and have a play of $p = 0.1$ mm. Using equation 4.11 in reverse and assuming 0.1 mm in the worst case per fixing screw, the maximum inclination angle, α , of the sensor will be

$$\alpha = \arcsin\left(\frac{i_{max}}{d}\right) \quad (4.12)$$

with $i_{max} = 0.2$ mm as the maximum influence on the horizontal axis. The maximum possible angle for the inclination of the sensor with respect to the wire due to the fixing screw is $\alpha = 0.25^\circ$. To exclude a vertical error, the support has to be mechanically adjusted to fulfil the required accuracy. The WPS wire cannot be mechanically fixed to the sensor. The adjustment of the wire with respect to the sensors has to be taken into account. The two wire stretching units are at a distance, d , of 1000 mm. To obtain a misalignment angle of 1° the wire would have to be

rotated by 17mm with respect to the nominal position at one fixing point of the wire. A system of v-shaped bolts is used to put the wire in place to better than 20 μm on each side.

4.10 Summary

This chapter showed the descriptive approach to the sensor check, validation and calibration methods. It has been shown that some tests have to be carried out per type of sensor, as the radiation and magnetic field test. Other validations and calibrations are necessary for each sensor before its acceptance and installation.

The implementation of the validation benches and the measurement results are presented in the next chapter.

Chapter 5

Validation benches and measurements

The validation benches for the three types of sensors were implemented by the author for the performance check of the sensors. They allow checking equipment that arrived from the manufacturer as well as equipment returned from an installation. These benches are designed to perform checks and calibrations of the sensors. The manually operated prototypes of the linearity calibration benches are designed for checking the sensors and will be upgraded with an automated bench.

This chapter presents the different types of benches that were designed by the author. Advantages and disadvantages of the benches are discussed. Performance of and problems with the sensors are discussed by using the validation results of the sensors.

5.1 Thermal expansion

Thermal influences during long-term tests falsify the measurements. Temperature influences on benches cause the distance between target and sensor to change. In this section the thermal influence on the tested sensors will be discussed. Following the sensor design presented in chapter 3, the maximum distance measured between electrode and target can be 10 mm for HLS and DOMS. For WPS, the relevant distance between the external ceramic plate references and the centre of the sensor is 23.5 mm. With these distances, L , the maximum thermal expansion influence can be estimated. For the test benches stainless steel components with a thermal expansion coefficient of $\alpha = 13 \mu\text{m}\cdot\text{m}^{-1}\cdot\text{K}^{-1}$ or aluminium with $\alpha = 24 \mu\text{m}\cdot\text{m}^{-1}\cdot\text{K}^{-1}$ have been used (Gieck, 1995).

$$\Delta L = L \cdot \alpha \tag{5.1}$$

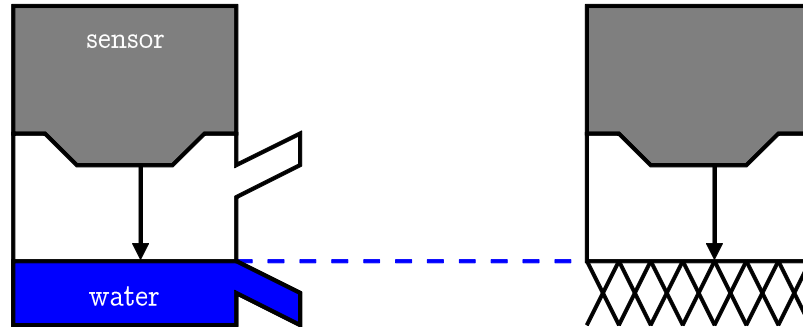


Figure 5.1: HLS measurement on water (left) and fixed target (right)

The maximum influence of the thermal expansion, ΔL , can be calculated from equation 5.1. The distance $L=0.010$ m as the maximum range of the HLS and DOMS, and calculates to a change in the distance to the target, ΔL , in the case of aluminium, of $0.24 \mu\text{m}$. Other influences on the measured distance are compensated for by the set-up. The WPS has a maximum a thermal expansion of $0.56 \mu\text{m}$ per $^{\circ}\text{C}$.

5.2 HLS

The HLS have to pass the tests described in chapter 4. The warm-up and stability check is very important for this type of sensor as the heating of the electrode, described in section 3.3, needs a warm-up period of several hours before stabilisation of the signal.

5.2.1 Warm-up and stability

The stability of the HLS can be determined in their normal working environment, a hydrostatic network. This test needs at least two sensors to be tested as evaporation of the liquid in the network causes effects that could be interpreted as drifts if only one sensor was tested. On the left side of figure 5.1 only one sensor of such a network is shown. The stability measurements for an HLS has to be calculated as the difference of the average of the raw measurements of the sensors.

$$\Delta h_i(t) = h_i(t) - \frac{1}{n} \sum_{i=1}^n h_i(t) \quad (5.2)$$

By using equation 5.2 the influence of evaporation in the system can be eliminated. In combination with a free-surface system as presented in section 3.4 the influence of a temperature gradient and barometric pressure can be excluded as well.



Figure 5.2: HLS measurement pots

After calculation of the difference $\Delta h_i(t)$ and comparing it to the reference measurement at t_0 the sensor can be as designated

- **stable**, if the difference $\Delta h_i(t)$ is less or equal to the tolerance defined in table 3.1
- **unstable**, if the difference $\Delta h_i(t)$ is larger than the defined tolerance.

over the measurement period. Tidal movements (Schlösser and Herty, 2002) can also influence a hydrostatic network and cause variation in the measurement which would have to be corrected for.

To avoid those influences the water surface is replaced by a fixed target, which is the bottom of an HLS measurement pot with reduced clearance as shown in figure 5.1 on the right side. After the warm-up period, the sensor measuring on a fixed target can be considered

- **stable**, if the change in the measurements is less than the sum of offset and gain drift indicated by the manufacturer, over the measurement period
- **unstable**, if it does not satisfy the criteria for a stable measurement

Design and manufacture The measurement pots designed, as shown in figure 5.2, are made to measure with the HLS in the sensor's range. The sensor is placed on top of the measurement pot in its normal working position and fixed with three screws integrated into the sensor.

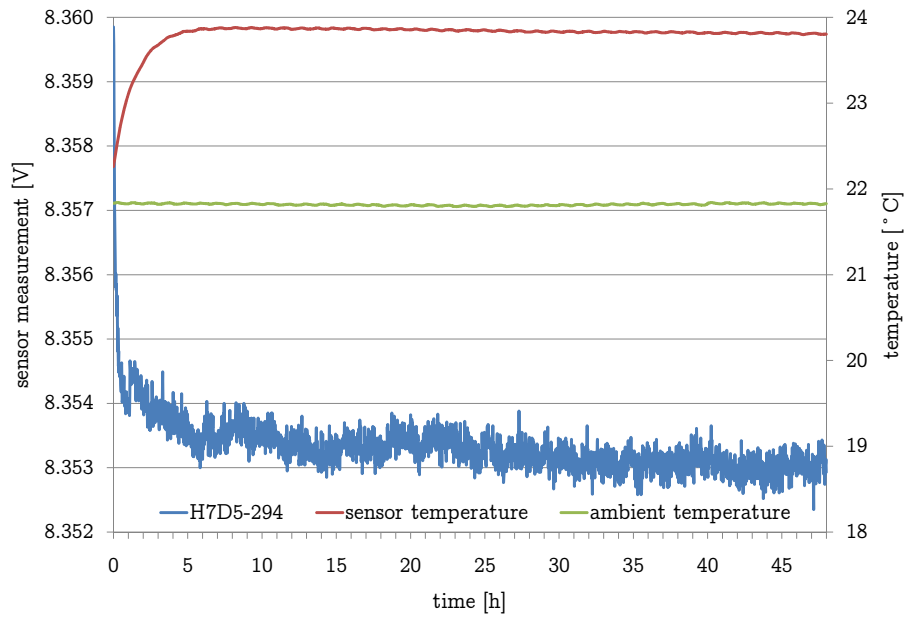


Figure 5.3: HLS warm-up measurement

Measurements The measurements have been registered in intervals of one second and averaged every minute. This gives information about an averaged measurement and its root mean square (RMS) value in the output file. In addition to the integrated temperature probe of the HLS, an external temperature sensor has been used to determine the ambient temperature. The HLS's electrode is heated and therefore transmits heat energy into the measurement pot. The measurements are carried out in a climatically controlled laboratory.

Analysis warm-up The warm-up measurement is taken over a period of 48 hours, which is the time given by the manufacturer for a complete warm-up of the sensor as indicated in table 3.1. Heating effects of the electrode and the electronics warm-up can influence the measurements. As shown in the example of sensor H7D5-294 in figure 5.3, the sensor has a strong warm-up effect in the first 3 hours. The sensor stabilises towards the end of the warm-up period.

For the HLS signal most of the warm-up influence took place within one hour after starting the measurements. The final sensor reading was obtained to 75% within that time. A period of approximately 12 hours is required for the temperature stabilization inside the measurement pot. As the change in the signal is several mV, a distribution of the signal change during warm-up has been calculated. Figure 5.4 shows the distribution, which can be considered as a bell-shaped curve around 0 μm . The peaks at 8 μm , 12 μm and 13 μm can be explained by insufficient temperature

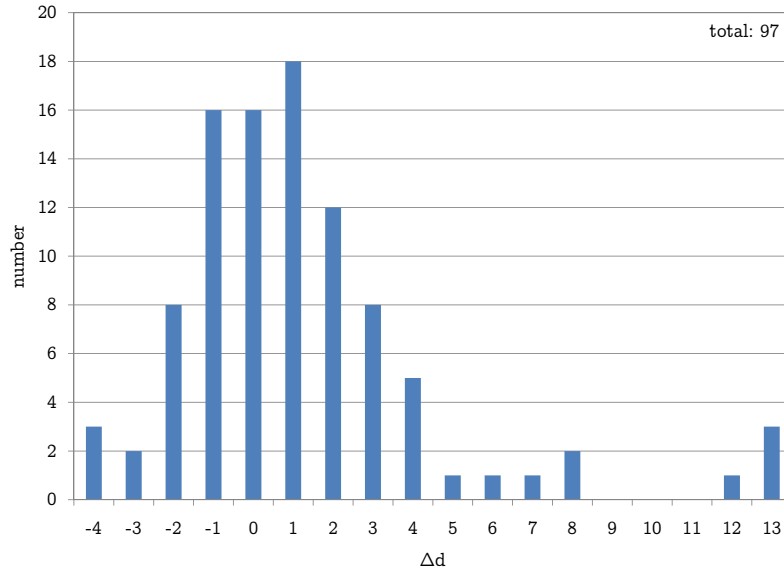


Figure 5.4: HLS warm-up distribution

adaptation in the laboratory before starting the tests. The sensors vary by $\pm 5 \mu\text{m}$ during warm-up. The sensors reproduce their warm-up performance during several warm-up cycles.

Analysis Stability The stability measurement of an HLS takes a period of at least one week. The results conform with the specifications given in table 3.1. An example of a stability graph is given in figure 5.5. The influence of ambient temperature on the measurement has been observed when disruption in the air conditioning system occurred after 70 hours. As FOGALE nanotech cites the influence of temperature change with respect to the electronics, the mechanical change in the distance to the target as calculated in section 5.1 as well as the change in the electronics output signal has to be taken into account. Equation 5.3 shows the different components adding into a worst case calculation for a thermal influence on the measurement:

$$\Delta h = (\Delta O + \Delta G \cdot \frac{\text{sensor reading}}{\text{sensor range}} + \Delta B) \cdot \Delta T \quad (5.3)$$

where the zero change, ΔO , is $0.30 \mu\text{m}\cdot\text{K}^{-1}$, the gain change, ΔG , is $2.50 \mu\text{m}\cdot\text{K}^{-1}$, the thermal expansion of the bench, ΔB , is $0.24 \mu\text{m}\cdot\text{K}^{-1}$ and ΔT is the temperature change.

The difference Δh is a maximum of $2.54 \mu\text{m}$ per Kelvin, which is consistent with the measurements observed.

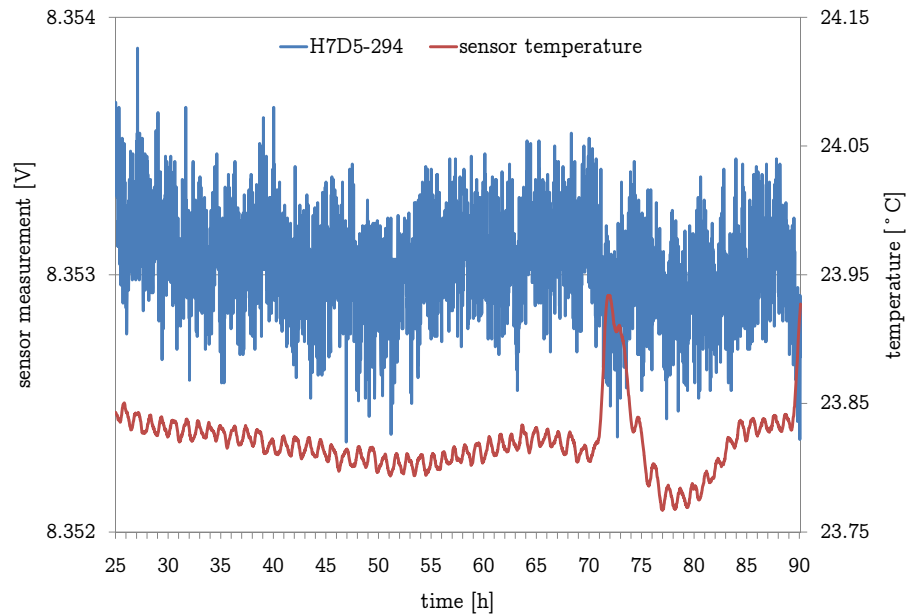


Figure 5.5: HLS stability measurement

Capacitive Reference The capacitive reference measurement is a method using calibrated capacities. Two capacitors are used to ensure one measurement within the lower 10% of the sensor’s range and one at the upper 10%. For this measurement, the sensor and its cable are decoupled from the electronics and instead a cable and the capacitive reference are used.

The measurements allow comparison of the lower signal and the upper signal over time as shown in equations 4.6 and 4.7. The capacitive references have been created by FOGALE nanotech to have a tool for controlling sensors’ drifts at random places outside the laboratory. This tool was available only after the installation of the sensors in the LHC was finished. Therefore the reference measurements were carried out just before the first run of the LHC. Control measurements 6 to 12 months after the initial measurement showed variations of less than $5\ \mu\text{m}$.

Conclusion The concept of a measurement pot serving as fixed target with its bottom used as a stability reference is a suitable solution for performing long-term tests. It avoids the evaporation problems a water surface creates for measurements and it allows testing of single sensors. Mechanical influence on the measurement is limited to a possible temperature variation of the environment which can be avoided by keeping the instrumentation in a climatically controlled environment. Calculations to compensate for the temperature change have not been carried out, as the mix of heating the sensor and the ambient temperature change will not represent

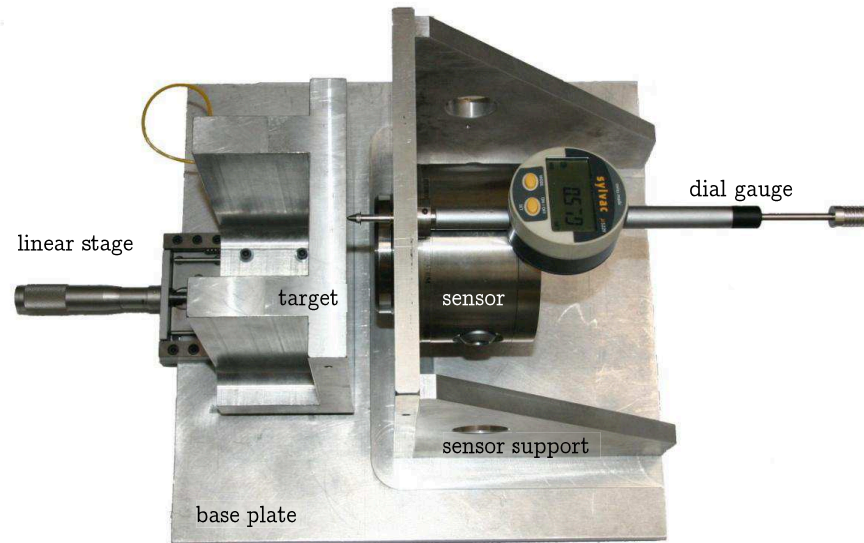


Figure 5.6: HLS linearity check bench

the real temperature of the measurement pot. In addition thermal effects on the electronics, as given in the specification, can be more important than the expansion of the bench.

The in-situ checks with the capacitive reference are an excellent possibility of checking the sensors without removing them from their installation. As a disadvantage of this system can be seen, that the capacitive references have to be controlled against a reference instrument in order to check them before use.

5.2.2 Linearity

To check the linearity of an HLS, a manually operated bench has been designed. The author intends the check of the sensor's calibration parameters with respect to a length reference instrument to be to a few μm . The criteria for a sensor to pass the linearity check is as follows:

- The determination of the polynomial had to be **reproducible** from two independent measurements.
- The polynomials obtained had to be **comparable** to those obtained using the polynomial.

The results of two independent measurements are considered to be reproducible, if the measurement at each position does not differ more than $\pm 0.01\%$ of the sensor's range. Two independent measurements are made to avoid operator errors in

positioning the sensor. The results obtained for the HLS are considered comparable if they do not differ more than $\pm 2\ \mu\text{m}$ for the HLS at the zero point and not more than $\pm 10\ \mu\text{m}$ at the gain point of the sensor.

Design and manufacture The bench, as shown in figure 5.6, has two main components. On a common base plate, a sensor support part is installed, with the sensor in horizontal position and a moving part with the target installed on a linear stage. By moving the stage, different positions with respect to the sensor can be achieved, simulating the different water levels in the measurement pot. For the length reference, the graduation of the stage was not sufficient. This has been shown in prototype tests (Herty et al., 2004). Therefore a digital dial gauge is installed in the fixed part of the system. The principle of Abbe, stating that instrument and standard have to be installed along the same measurement axis, was not respected for this installation. This can result in a second order cosine error if the two measuring axes are not parallel. The measurement can be influenced by non-parallelism of the sensor's measurement axis and the dial gauge axis. A default of $1\ \mu\text{m}$ caused by misalignment throughout a 5 mm sensor range would be caused by an orientation default of 1.15° . This case is excluded as the orientation of the sensor with respect to the target has to be better than 1° as described in section 4.9. The target and sensor are linked electrically to a common ground with the DAQ rack and are isolated from the environment.

Measurements The measurements are carried out using the uncorrected voltage output of the sensor. This allows a recalculation of the polynomial following the method described in section 4.4. The zero reference for the HLS is defined as the 0 V output. The first measurement is locked at this position. Due to the electrical noise of the sensor and limitations in manually positioning, tolerances of $\pm 0.003\ \text{V}$ can be accepted for this position during the check. From this point on, measurements are taken in steps of $1/10$ of the sensor's range throughout the sensor's range. As technical limitations of the DAQ rack do not allow measurements above 10 V, the distance limit for measurements has been set to match the theoretical 9.9 V measurement. This measurement replaces the measurement at the end of the sensor's range. For 5 mm HLS, this means a measurement at 4.950 mm and for 10 mm sensors at 9.900 mm. The measurement series are taken as a go and return measurement, independently, for controlling the validity of the measurements.

A Sylvac digital dial gauge is used in this and all other tests as length reference instrument. The dial gauge has a resolution of $1\ \mu\text{m}$, a maximum error of $7\ \mu\text{m}$ and a repeatability of $2\ \mu\text{m}$, certified in the calibration protocol (Sylvac SA, 2007).

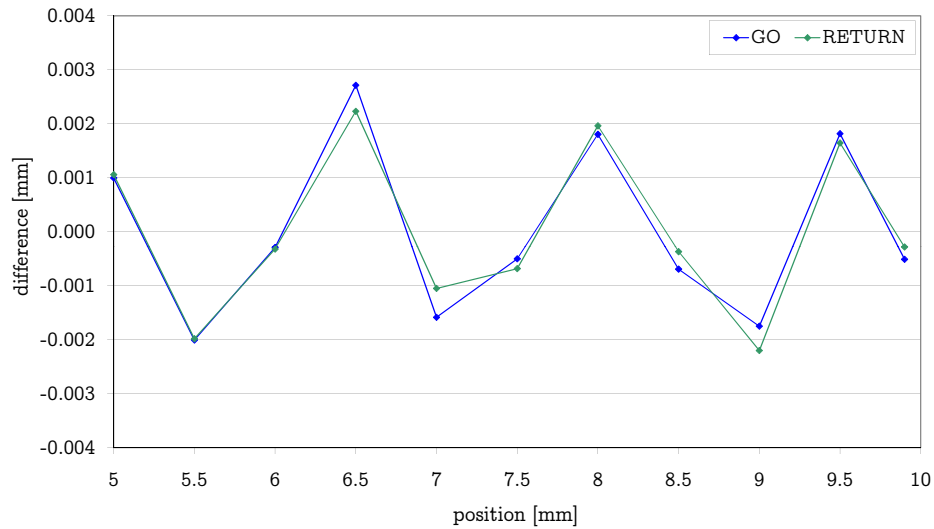


Figure 5.7: recalculated polynomial residuals

Analysis The measurement sets, m , can be written with the voltage measurement, x , the dial gauge reading, d , and the measurements, i , with $i=1$ to 11 as $(x_i/d_i)_m$. They are used for recalculation of the polynomial as proposed in chapter 4.4. An example of the difference between the calculated polynomial and the measurements made with the dial gauge is presented in figure 5.7 for the sensor. The result is better than $\pm 3 \mu\text{m}$.

The calculated polynomials for the two measurement sets, named *GO* and *RETURN*, are subtracted from the polynomial given by the manufacturer as shown in figure 5.8. As the requirement was not to do a calibration of the sensor, the manufacturer's given polynomial is kept after the check. Also a difference between the two polynomials of better than $\pm 3 \mu\text{m}$ has been obtained. The difference between the two measurement sets is shown in the indication *DELTA* and are less than $\pm 1 \mu\text{m}$.

Conclusion All sensors satisfied the condition that the difference between the provided calibration polynomial and the computed polynomial did not exceed more than $\pm 10 \mu\text{m}$. The calibration function provided by FOGALE nanotech was kept.

5.2.3 Zero reference

The HLS measurements are defined with their range of 5 mm or 10 mm starting at the 0 V output of the sensor. This point is defined by the distance, d , of 21.5 mm with respect to the support surface of the HLS on the measurement pot. The variation of d is given by the manufacturer to be less or equal to $50 \mu\text{m}$.

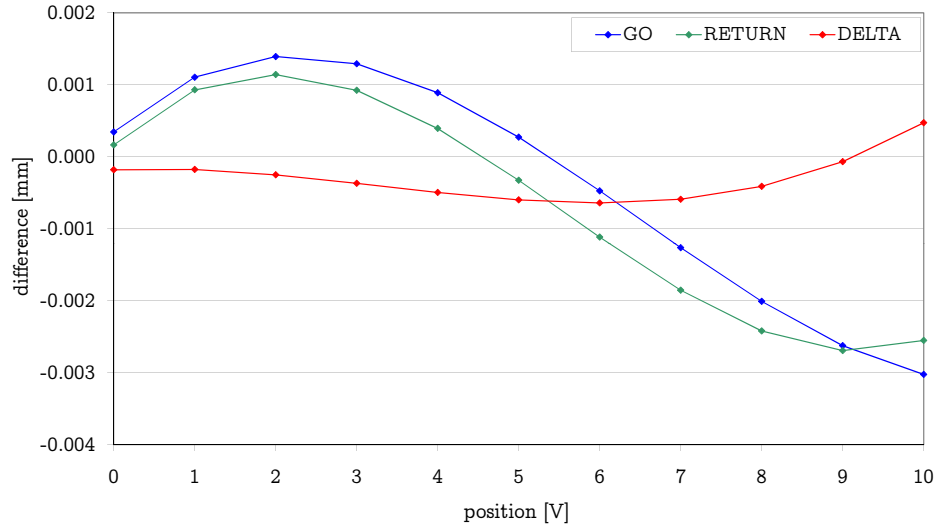


Figure 5.8: check measurements compared to calibration function

The repeatability of the installation of an HLS is better than $2\ \mu\text{m}$. This is shown in table B.1 with a maximum range of 3.8 mV for the repeatability of the tested sensors. The insufficiently determined absolute measurement of the HLS and the good repeatability of the HLS installation led to the concept of modifying the calibration function to an absolute calibration.

Concept The relative measurement within the range of the sensor is linked to the support surface of the HLS, as shown in figure 5.9 and allows absolute measurements of the HLS. A calibrated reference measurement pot with the known distance between the support surface and the fixed target is used for the measurement. The calibrated distance, d_a , corresponds to a measurement of the sensor, m . The corresponding distance in mm to the measurement m is the distance d . The coefficient a_0 of the calibration function shown in equation 3.4 defines the shift of the sensor range with respect to a reference point as it defines the absolute part of the polynomial. This value is calibrated by the manufacturer to a virtual distance given in the coefficient $V\theta$ in their calibration function shown in section A.1. By replacing this coefficient with the absolute distance d_a , the sensor is referenced to the support surface of the HLS.

Measurement pot calibration The HLS measurement pot for zero reference measurements is calibrated on a coordinate-measuring machine (CMM). Support surface points, P , and bottom points, A - E , in the measurement pot are measured in the configuration shown in figure 5.10. One plane with the bottom points of the

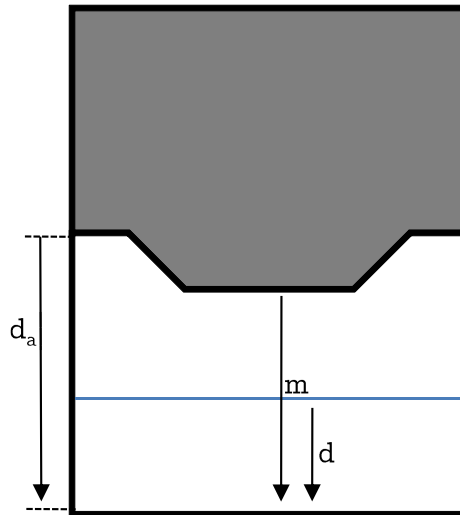


Figure 5.9: HLS absolute zero reference

measurement and a second plane with the points of the support surface is calculated. The distance between the two planes is normalised to 20 °C. The calibration data of a measurement pot is shown in section B.2.

Conclusion The zero reference calibration of an HLS is a step towards a sensor allowing absolute measurements. The concept has been tested for the calibration, but not been implemented for the LHC so far.

5.2.4 External Reference

The standard geodetic interface, as described in section 3.3, allows a link to other geodetic systems. A set of measurements is taken to calculate the distance between the sensor's measurement, h , and the interface, H , as shown in figure 5.11. In the absolute referencing, not only the offset of the sensor has to be taken into account, but also the manufacturing tolerances of the sensor's body. This constant for the distance between internal and external measurement given by the manufacturer is determined to $\pm 50 \mu\text{m}$.

Design and manufacture In order to obtain an individual offset constant for each sensor, measurements on a vertical offset bench have been implemented, as shown in figure 5.12. A first check bench has been improved by replacing the initial incremental gauge with 10 μm resolution by one with 1 μm resolution.

Measurements To calculate the offset between sensor's measurement and the geodetic interface, the following values have to be determined:

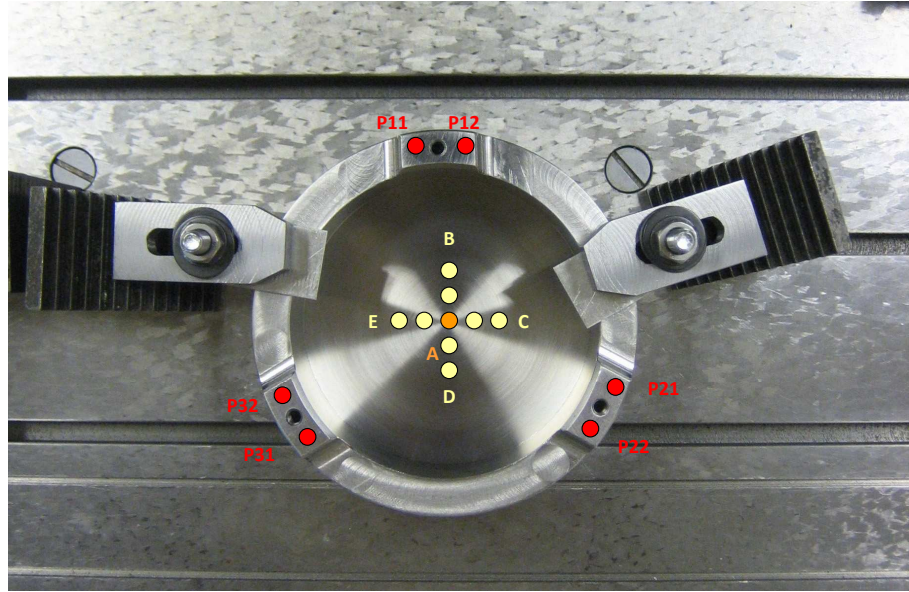


Figure 5.10: measurement pot calibration

- the metric sensor output, h , without temperature compensation
- the readings of the dial gauge at the measurement pot, b and on top of the TH sphere, t
- the ambient temperature, T

In addition the radius, r , of the TH sphere has to be known from calibration. This allows for the calculation of the external reference as shown in equation 5.4

$$H = (|t - b| - h - r) \quad (5.4)$$

Calculating the error propagation in equation 5.4 for this linear case, a standard deviation for the determination of H with of $\sigma_H = 7 \mu\text{m}$ can be calculated as shown in equation 5.5. The assumed standard deviations in the equations input are $\sigma_t = \sigma_b = 3 \mu\text{m}$, $\sigma_h = 2 \mu\text{m}$ and $\sigma_r = 5 \mu\text{m}$.

$$\sigma_H = \sqrt{\sigma_t^2 + \sigma_b^2 + \sigma_h^2 + \sigma_r^2} \quad (5.5)$$

Conclusion The measurements to determine the offset between the HLS measurement and the external, geodetic interface support can be carried out to better than $10 \mu\text{m}$. Compared with the manufacturer's constant, an improvement of factor ten is achieved. The use of this precise determination of the interface is limited to the instruments used on the external reference. Laser tracker instruments can profit from

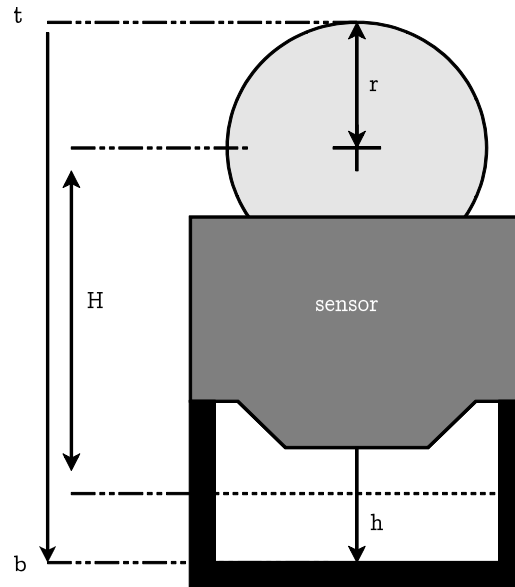


Figure 5.11: HLS external reference

the μm determination of the constant whereas standard instruments, like levels, do not see the improvement to the same extent.

5.3 WPS

The WPS are checked for stability, warm-up and linearity. In addition, the interchangeability of the sensors is determined and confirmed by repeatability tests. The repeatability for the WPS is influenced by the repeatability of the two sensor parts during assembly and the repeatability of the installation of the sensor in its support.

5.3.1 Warm-up and stability

Warm-up and stability checks of a WPS are strongly dependent on the target, which is the wire. As the wire cannot be replaced with a fixed target, the stability of the wire also influences the measurements. Therefore not only the position between the wire and the sensor's electrodes has to be kept stable, but also influences on the anchor points of the wire have to be minimized. The wire has to be stretched in order to keep a horizontal, straight line during the measurements. When a weight is used to establish balance there needs to be a stable environment in the ground where the bench is situated in order to avoid pendulum-like movements of the weight.

The hypothesis that the sensor is stable during the measurement period is true

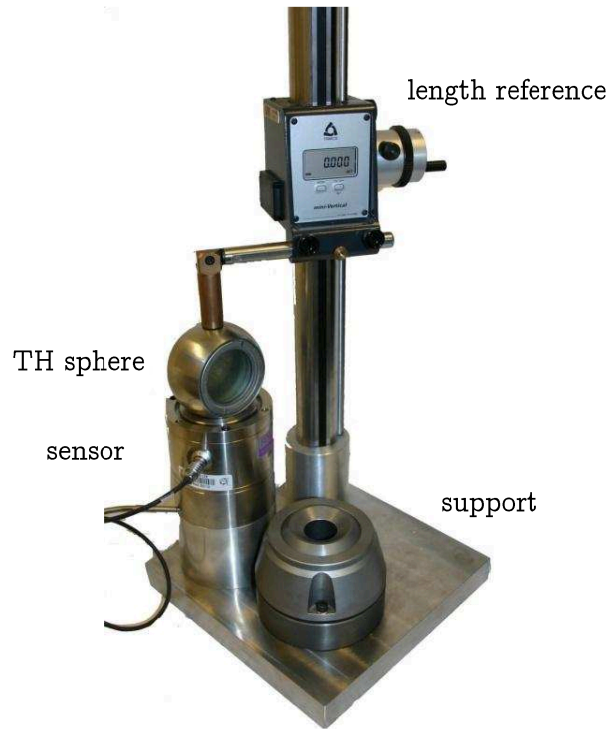


Figure 5.12: external reference calibration bench

in the case that equation 4.2 is satisfied. By using several sensors on the same wire, one can additionally determine the stability of the wire. The stability of the wire during measurements can be determined by calculating the differences, Δz , for each sensor. This is the measurement change of the sensor during the test.

$$\Delta z = z(t) - z(t_0) \quad (5.6)$$

with the measurement, $z(t)$, compared to the reference measurement, z , at the beginning of the stability check, t_0 . This difference, Δz , has to be analysed separately for each sensor and each of the sensor's axes. By knowing the positions of the sensors along the check bench and the displacements seen by each sensor, a verification using the intercept theorem can be calculated. The difference of the sensor's readings, Δz , are considered as parallel lines. They intersect with two lines: the wire at the moment t_0 and the wire at the moment t . A displacement of the wire during the measurement can be calculated as the ratio of two segments on the same line equals the ratio of two segments on the parallels. The wire can be considered

- **stable**, if the displacements Δz do not match the theorem
- **unstable**, if they match it

A movement of the wire can be compensated for by using the outer sensors on the bench for compensation of the displacement and rejecting them from the stability test.

Design and manufacture The WPS stability bench is made of a heavy, aluminium base plate to compensate for the weight used to stretch the wire so that it does not deform under the load. On this plate, five equidistant sensor supports are mounted. Four of the supports can be adjusted radially and vertically in position to bring the sensor to its centre position. The centre support is conceived like a support in the LHC and allows the interchangeability measurements to be carried out on the same bench. The sensors are screwed to the supports. The carbon-peek wire is stretched with a maximum load of 15 kg. The bench is shown in figure 5.13.

Measurements Check measurements are carried out using the calibration function provided by the manufacturer. An acquisition rate of one measurement per second averaged over a period of one minute was chosen.

Analysis The post-processing of the measurements is done by plotting the measurements over time. The measurements presented in figure 5.14 by the blue curves show the sensor at the warm-up check. A warm-up effect of 5 μm can be observed. For the measurement with the electronics already warmed up, no observation of a change can be observed. This shows, that the observed warm-up times of several hours are longer than those suggested by the manufacturer.

Conclusion The sensor's stability is much more difficult to find than that of the one-dimensional sensors. The fact that the wire is not a fixed target needs additional calculations to show that the wire has been stable during measurements. The temperature influence on the bench is not negligible as the distance between the wire stretching units is 80 cm and therefore temperature changes along the bench can change the sensor's position significantly.

The warm-up period of only five minutes as quoted by the manufacturer has not been obtained. Although the sensors have been in the same temperature controlled conditions as the bench, the warm-up time was between three to six hours on average. The noise of the sensor can be a few μm in the case of sensors with long cables.

The tests on the bench have shown that the design is able to allow stability check measurements of WPS over several weeks. The idea to replace the weight of the wire by a stretching unit in order to avoid pendulum movements of the weight has

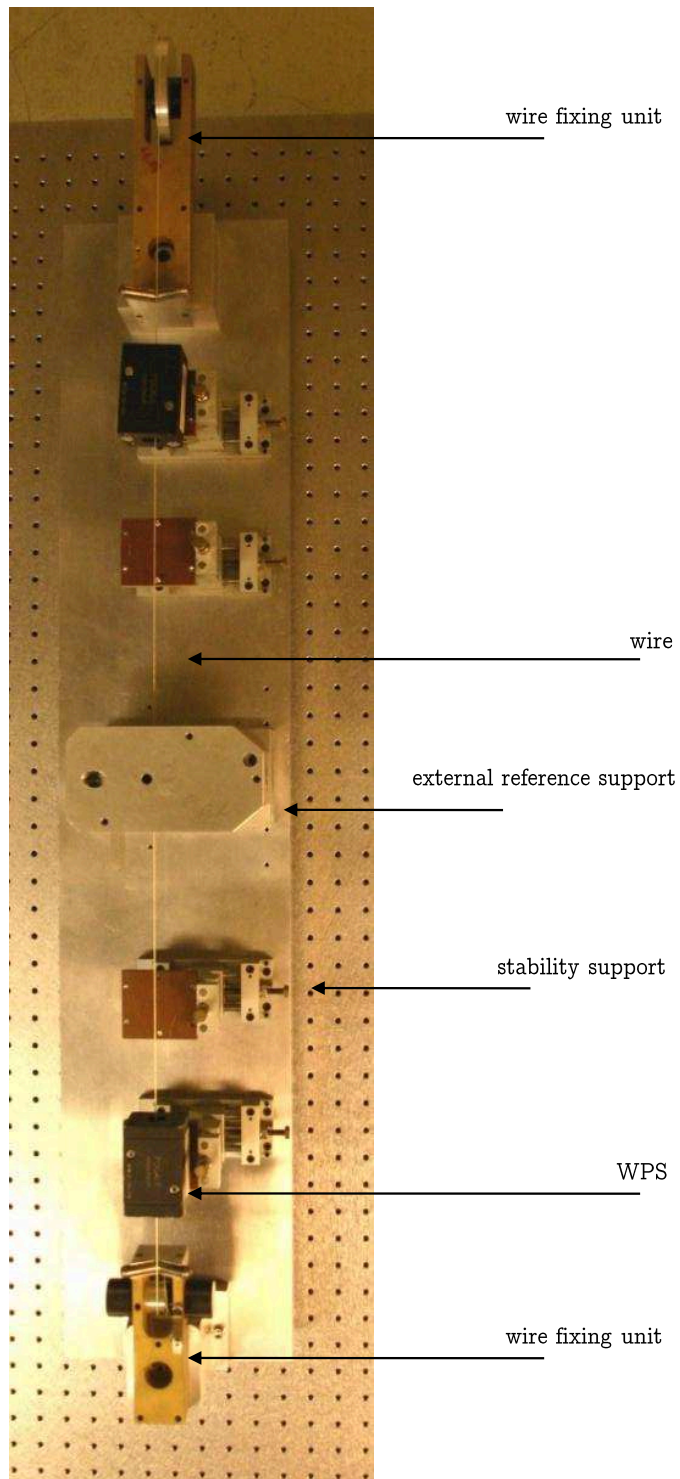


Figure 5.13: WPS stability bench

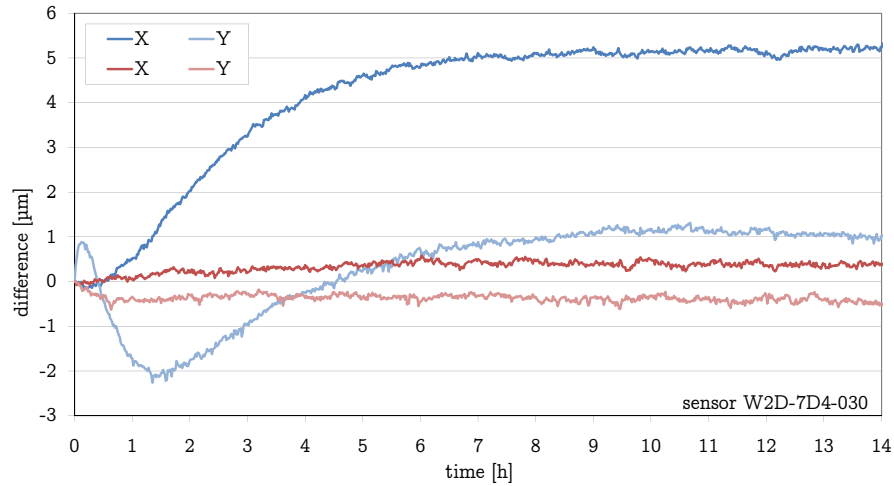


Figure 5.14: warm-up (blue) and stability (red) measurements

not been tested. A granite table with isolation from other short-term test stands has provided sufficient stability.

5.3.2 Linearity

The WPS are checked on a manually operated two-axis bench. The attempt to calculate the two 6 by 6 calibration function matrices for the sensor and compare it to the given calibration matrix, is not feasible for a manually operated bench when checking the sensor with the same number of measurements as the manufacturer during calibration. Measurements along the sensor range in a grid of 11 by 11 would imply 121 measurements. This is not possible given the stability of the bench and the time required for the check. Therefore the concept is based on the check of the sensors' output values which are converted using the matrices given by FOGALE nanotech and comparing them to the dial gauge measurements used for monitoring the displacement. This method was proposed in section 4.4 as direct comparison method.

Design and manufacture The bench is based on the design of the stability bench as shown in section 5.3.1. On the linearity check bench two sensor supports are installed, one at each end. The sensors on both supports are used as reference sensors to monitor the stability of the wire during measurements. The centre support is used for the linearity check of the sensor. This is composed of two linear stages that are fixed perpendicularly and allow displacement of the sensor separately for each axis. The sensor is fixed with bolts and screwed on a support plate. The stages

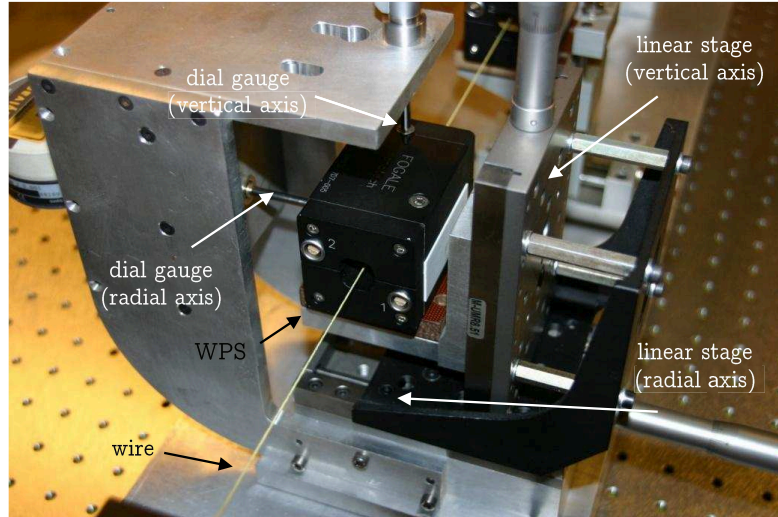


Figure 5.15: WPS linearity bench

are attached to an aluminium structure that hosts two dial gauges, one for each axis. The bench is shown in figure 5.15.

Measurements A set of 10 measurements as shown in figure 5.16 is carried out. The 3 by 3 grid in the corners and on the main axes of the sensor is completed with a measurement to the centre point of the sensor. This centre point is measured at the beginning and at the end in order to close the measurement loop and have an additional control. The measurements of the sensor are converted to metric output using the calibration function provided. The differences are shown in figure 5.16 with scaled arrows and the numerical values, (x/y) , adjacent. The measurements are carried out at 4 mm distance on each axis with respect to the centre of the sensor. The measurement position is indicated in figure 5.16 with crosses. The range of the sensor is given with the thick border line at 5 mm in the same figure.

Analysis The sensor measurements start at the centre point, as for example shown with sensor W2D-7D5-002 in figure 5.16. The return measurement comes back to the initial value within $1\mu\text{m}$. No variation of the wire can be seen during the measurements. The measurement data for this example is provided in section B.3.

Variations of up to $100\mu\text{m}$ can be seen in the corners for some sensors. In all cases, a rotation of the measurement is indicated in the top left corner and in the bottom right corner. The WPS calibration function is less precise compared to that of the HLS and DOMS. Typically residuals range between $\pm 3\mu\text{m}$ in the calibration function given by the manufacturer as shown in the example in section A.2.

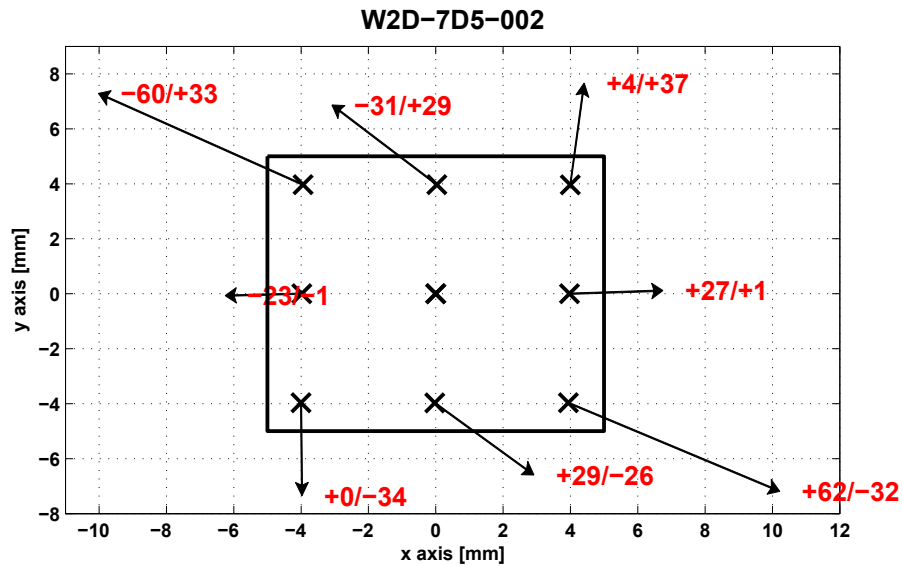


Figure 5.16: WPS linearity measurements

The difference between the sensor measurements and the dial gauge reference readings can be argued with the use of the sensors non-referenced surfaces to probe with the dial gauges.

Conclusion The concept of the linearity check bench was right in principle but was insufficiently investigated to obtain satisfying results. For a modified linearity check bench the following main aspects have to be changed in order to improve the set-up and measurements.

The sensor's fixing to the support has to be designed using both ceramic reference surfaces for fixing points. In the present bench, only the vertical surface is used by screwing the sensor to the support. In addition, the displacement measurement has to be directly taken either on the linear stages or on the ceramic surfaces. With the constraint of already using the sensor's ceramic surface as a fixing, a reading of the linear stage displacement is the preferable solution. The observations during measurements, the analysis of the measurements and the conclusions drawn from the results led to the decision to continue the checks on the future automated calibration bench for WPS.

A second proposal for linearity checks of WPS is based on the use of a CMM. The measurement configuration is based on a stretched wire, which is installed independently from the CMM. The WPS is positioned on the worktop of the CMM

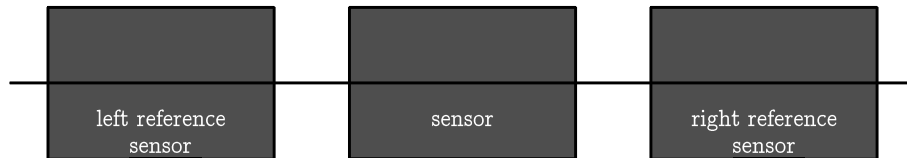


Figure 5.17: WPS assembly and offset bench layout

and can be moved with respect to the wire in both measurement axes.

The linearity check of the WPS was not successful in the configuration chosen. The determination of the calibration function by the manufacturer does not give linearity throughout the range to better than $\pm 3 \mu\text{m}$. In order to improve the residuals of the calibration function, future automated calibration concepts have to provide a suitable calibration bench and review the determination method of the calibration function.

5.3.3 Assembly

The WPS sensor is made of two parts as shown in figure 3.6. For installation the sensor has to be dismantled in two pieces and re-assembled. To quantify possible influence on this operation, a series of tests have been carried out with several sensors.

Design Three of the supports of the calibration bench for the stability measurement are used as illustrated in figure 5.17. The central position of the bench is used to calibrate the sensors, whereas the sensors on the extremities serve as reference sensors to check the stability of the wire during the measurements.

Measurements The inner sensor is dismantled in two parts, keeping the lower part with the fixing screws in place on the support. The assembly procedure was repeated ten times.

Conclusion The range variation of 10 assemblies was 4 mV for the x axis and 3 mV for the y axis. The sensors' assembly therefore can be considered as reproducible. The wider range in the x direction compared to the y direction suggests that the bolts do not allow centring as precisely as fixing the surface that is used for the vertical. The influence on both measuring axes can be disregarded for the check measurements as well as for the monitoring system in the LHC.

Table 5.1: WPS assembly check measurements

#	left reference		sensor		right reference		temperature °C
	X	Y	X	Y	X	Y	
1	5.0692	4.8921	5.0422	4.9184	5.1929	4.9689	22.02
2	5.0691	4.8922	5.0399	4.9183	5.1930	4.9691	22.05
3	5.0692	4.8923	5.0398	4.9191	5.1935	4.9694	22.03
4	5.0691	4.8923	5.0398	8.9198	5.1935	4.9693	22.04
5	5.0691	4.8922	5.0403	4.9194	5.1938	4.9693	22.04
6	5.0691	4.8923	5.0395	4.9192	5.1939	4.9693	22.03
7	5.0690	4.8923	5.0398	4.9194	5.1938	4.9693	22.03
8	5.0691	4.8924	5.0391	4.9200	5.1940	4.9694	22.05
9	5.0690	4.8923	5.0390	4.9195	5.1938	4.9693	22.04
10	5.0690	4.8923	5.0398	4.9198	5.1938	4.9694	22.05
average	5.0691	4.8923	5.0399	5.3193	5.1936	4.9693	22.04
minimum	5.0690	4.8921	5.0390	4.9183	5.1929	4.9689	
maximum	5.0692	4.8924	5.0422	8.9198	5.1940	4.9694	
range	0.0003	0.0003	0.0032	4.0015	0.0011	0.0005	

measurements in mm

5.3.4 External reference

The WPS is referenced to an external coordinate system via two ceramic plates glued to the sensor. These reference surfaces are shown in figure 3.6. The centre of the wire is determined with respect to those surfaces as described in section 3.5. As the interchangeability of the WPS is claimed by FOGALE nanotech to be only within $\pm 50 \mu\text{m}$ as shown in table 3.2 a more precise determination method had to be evaluated. The difference of one sensor, d_i , with respect to a reference sensor, d_r , is defined as the difference of the readings, Δd , in equation 5.7

$$\Delta d_i = d_i - d_r \quad (5.7)$$

In the case of the WPS sensor as a 2D sensor, equation 5.7 has to be applied for both axes of the sensor.

Design and manufacture In contrast to the stability measurement, the positioning of the sensor has to be repeatable for each calibration and each sensor. In order to obtain this constraint, the fixing system for the sensor of the LHC has been used. A positioning system made of three fixing bolts is the interface with reference surfaces as shown in figure 5.18. Two sensors are used as reference sensors to monitor the wire as shown in figure 5.17

Analysis Both reference sensors are used for calculating the stability of the wire. The sensors to which the offset was determined, shown in table 5.2, were used as

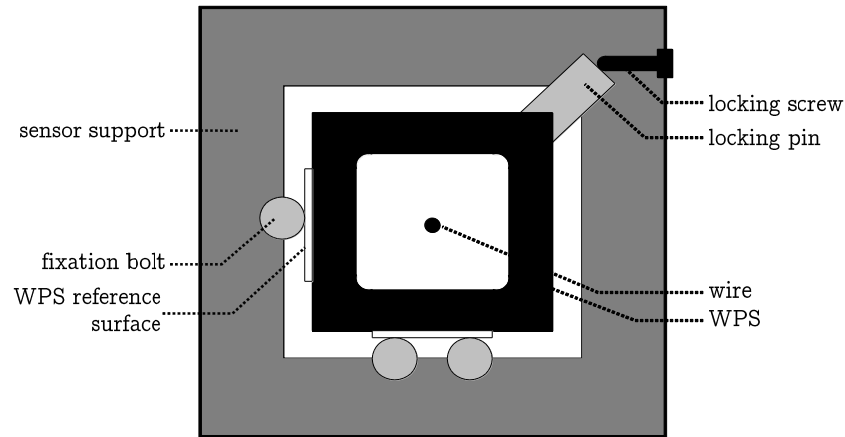


Figure 5.18: WPS offset bench fixation

Table 5.2: External reference determination of WPS reference sensors

attribute	W2D-7D5-018		W2D-7D5-036		difference	
	X	Y	X	Y	X	Y
minimum	-8	-14	-8	-14		
maximum	+11	+16	+1	+11		
range	19	30	9	25		
average	+2.6	+0.6	-3.6	-2.2	6.2	2.8
standard deviation	5.4	9.1	3.4	6.8		

reference sensors. Two sensors were used in case of the failure of one during the measurement period and always to control the measurements with respect to each other. For 9 independent sets of measurements, these values have been obtained.

The analysis of table 5.2 shows that the determination of the external reference can be obtained with $\pm 15 \mu\text{m}$ as required for the installation in the LHC and that the standard deviation of the measurements is less than $10 \mu\text{m}$. The requirements of the bench have therefore be fulfilled. In order to compensate for movement of the wire during measurement a correction is applied to calculate the displacement of the external references with respect to the initial position of the wire.

Conclusion By using a set of measurements for the interchangeability of WPS the position of the external references with respect to each other can be determined. Using several determinations for the calculation of the external reference allows statistical analysis of the calibration.

5.3.5 Reference surfaces

The determination of the interchangeability parameters for the WPS is based on the concept of using the ceramic, external references as presented in paragraph 5.3.4. The support for this calibration uses a support installed for some of the monitoring system reference points in the LHC. Other LHC supports provide a horizontal surface for the vertical axis of the sensor and two vertical bolts for the radial fixing. The height of these bolts can vary and therefore the touch point of the bolts can vary on the ceramic surface. Two cases for a possible influence on the radial position due to this variation can be identified:

- the bolts are not installed vertically;
- the two ceramic reference surfaces are not perpendicular to each other.

The ceramic surfaces are therefore investigated for their perpendicularity and their flatness. CMM measurements scan the two ceramic surfaces of the WPS. The measurement and calculation of the plane and the intersection angle of the two planes is shown in section B.4.

Conclusion Each of the two surfaces has a flatness to better than $\pm 10 \mu\text{m}$. This considers the three measurements with more than $10 \mu\text{m}$ on the Y axis as outliers. This is within the repeatability of measurements for positioning the sensor in its support.

The orthogonality of the two surfaces has been calculated to 1.194 mrad. The height of the ceramic surface is 10 mm, therefore the maximum error for non-orthogonality due to the sensor can be $12 \mu\text{m}$.

5.3.6 Frequency check

The frequency of a WPS is one of its characteristics. Sensors installed on the same wire have to have different frequencies, at least adjusted at steps of 100 Hz as stated in section 3.5. If the frequencies are not sufficiently separated from each other interference between the sensors starts to give an oscillating signal with a period of several minutes. As this problem was seen during stability measurements and in LHC installations, the frequencies of the sensors were checked systematically.

Measurements The frequency of each sensor electronics has been measured with a frequency meter. The measurements are shown in section B.5.

Analysis Changes of the frequencies have been between 1 Hz and 982 Hz the sign of the change disregarded. The range of the changes with respect to the nominal value was 1.476 kHz.

Conclusion The use of sensors with the same frequency on the same wire creates a noisy signal on either one or each of the sensors concerned. The sensors start influencing themselves as soon as they are as close as 10 Hz to each other. The sensor signal is not changed in its value, it gets noisy with a low-frequency oscillation. This oscillation of the signal can be up to $\pm 10 \mu\text{m}$ and this is typically the sign of a frequency problem.

The sensor's frequency can be readjusted and has been observed to be stable after adjustment for short-term observations of a few weeks. Affected sensors can still be used for measurements, when averaging the measurement over a longer period of time. This can be useful in the case that access to readjust the frequency is not immediately possible.

5.3.7 Radiation

The WPS has been tested during a series of radiation tests for LHC equipment in 2005 at the Commissariat à l'Énergie Atomique (CEA) facilities in Saclay, France. The two irradiation tests have been carried out, as described in section 4.7 and were used to investigate the radiation tolerance of the sensor and its electronics as well as the dose rate dependency (DRD) of the sensor.

Total Ionizing Dose The sensors to be tested have been placed in the irradiation facility for a total ionizing dose (TID) test. The electronics of the sensor and the DAQ unit have been placed outside to be protected against radiation. The sensors have been exposed to the gamma radiation of a cobalt 60 (^{60}Co) source. To simulate the limit before break-down of the sensor in this environment, a dose of 2200 Gy per hour has been applied to the sensors. The life-time of the sensors in the LHC before replacement is scheduled to be 10 years, in this time the sensors will be exposed to approximately 160 kGy. The same as the sensors during this test in 72 hours. The sensors are fixed on an aluminium bench with a stretched stainless steel wire and placed around the ^{60}Co source as shown in figure 5.19.

The sensor's signal did not see a degradation during the measurement time of 72 hours. The material used for the sensor housing and the electrodes can resist this applied dose. The measurements during the TID are shown for three WPS in figure 5.20.

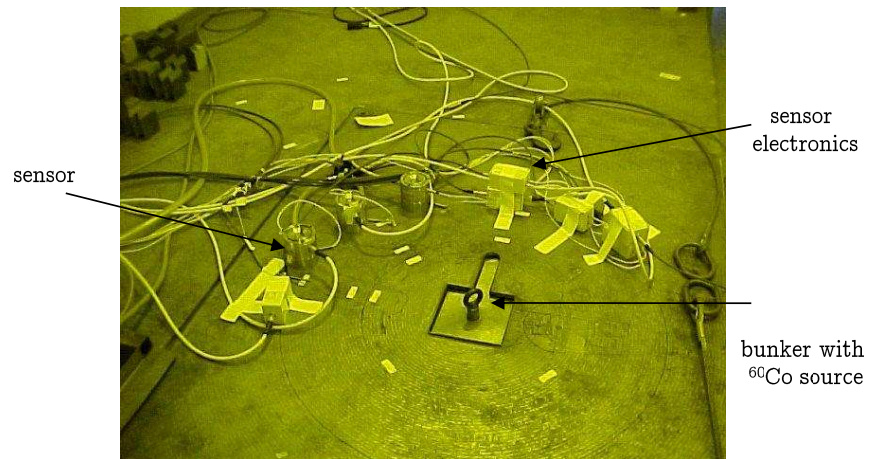


Figure 5.19: TID and DRD set-up

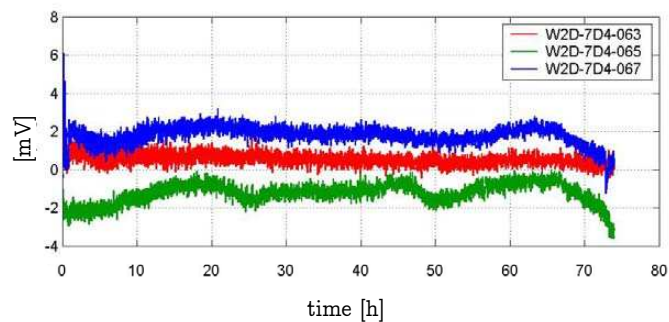


Figure 5.20: TID results sensor

More sensitive is the case of the electronics. They have been tested at lower dose rates in an adjacent irradiation facility. In this configuration, the sensor was installed outside and the electronics were put at a distance from a source with a known dose rate. The degradation of the signal was observed as shown in figure 5.21. The sensor's electronics have to be protected in a radiation-safe environment of the LHC, as they can handle much less radiation than the sensor itself. Therefore cables of up to 30 m in length are used between the sensor and its electronics.

Dose Rate Dependence A DRD test with the WPS did not show any influence of signal to radiation. This can be linked to the fact, that the wire was positioned in the centre of the sensor between the two electrodes. Any ionizing of the air between the electrode and the wire will be seen by both electrodes and therefore compensate in the output. Compared to the HLS, where the influence due to ionised air has been shown, this is not the case for the WPS. By modifying the test installation

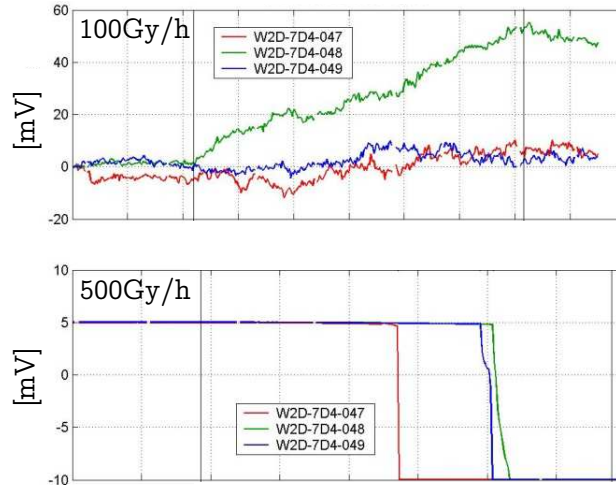


Figure 5.21: TID results electronics

in future tests and moving the wire from the centre to a corner of the sensor's measurement range, different distances between the electrodes are created. If the influence due to ionised air is also an issue for the WPS, it should be detectable with this modification.

5.4 DOMS

The DOMS are checked at reception as stated in chapter 4. The concept of the benches is partially based on the bench designs for HLS. This is possible because of the similar measurement concepts of the sensors.

5.4.1 Warm-up and Stability

The warm-up and stability of the DOMS are checked with the sensor measuring on a fixed target. This is the normal working configuration for the sensor. In consequence, the acceptance criteria are the same as for the HLS as far as the check procedure, installation and analysis methods shown in paragraph 5.2.1 are concerned.

Design The design of the stability test bench was an iterative process of three steps: due to modification of the handling of the bench and due to stability problems with the first sensors delivered. In order to validate the bench and the sensor, the possibility of separation between the instabilities of the sensor and the bench had to be investigated by changing the design.

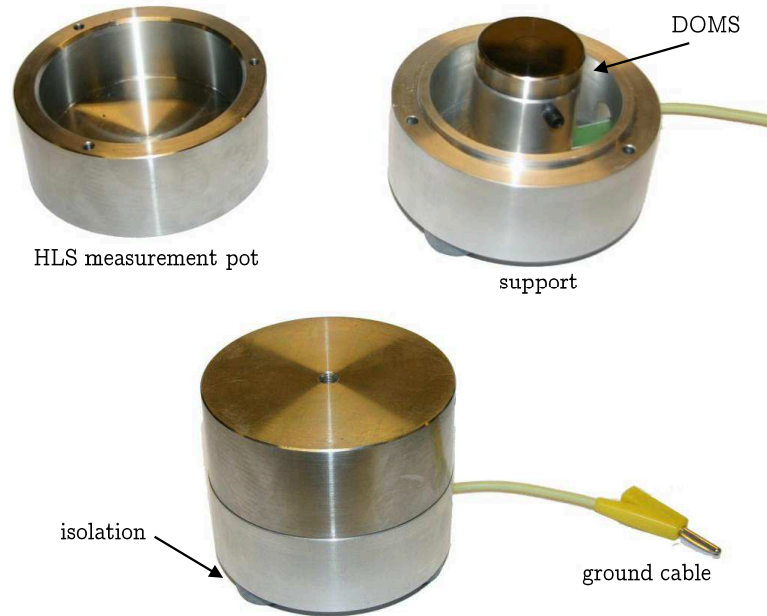


Figure 5.22: DOMS stability check bench (first design)

A first approach for the stability test bench was based on a proposal using the HLS measurement pot and installing the sensor in an adaptor as shown in figure 5.22. The concept was based on the sensor facing the bottom of the measurement pot. This approach was dismissed as the support did not allow control of the sensor's position during tests and because of problems with the sensor installation in the adaptor.

These observations led to a second approach for a stability check bench as shown in figure 5.23. On this bench, the target was fixed to the sensor support and could be adjusted to various distances throughout the range of the sensor. The design followed the installation configuration in the tunnel.

Both designs have the disadvantage that the bench only allows the test of one sensor at a time. This does not allow an investigation of the sensor's behaviour in the case that the sensor is unstable. The second design allows for adjustment of the measurement distance between sensor and target. This advantage allows measurements to be adjusted at the upper range of the sensor between 8 V and 10 V in order to see the influence of zero and gain drift.

To be able to identify drifts, a measurement set-up of several sensors measuring to the same target has been chosen. This concept has been validated with the

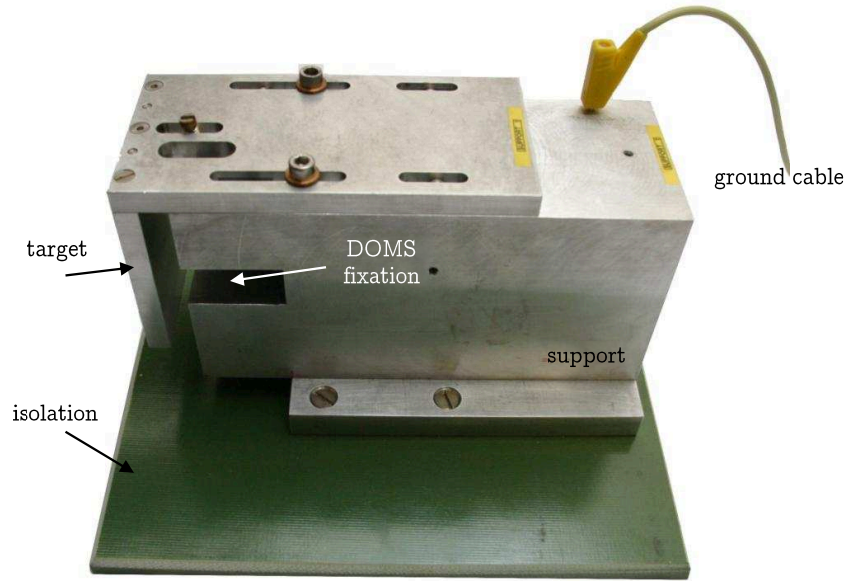


Figure 5.23: DOMS stability check bench (second design)

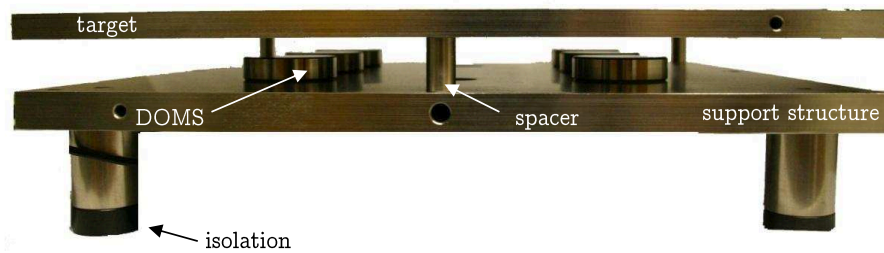


Figure 5.24: DOMS stability check bench (third design)

DOMS linearity measurements as discussed in paragraph 5.4.2. The configuration of the bench is shown in figure 5.24 with the sensors mounted on a support plate, facing a plane machined target. A maximum of 8 sensors can be hosted on the bench. The distance between the target and the sensors can be varied with spacers.

Measurements The measurement configuration for the DOMS is like that of the HLS presented in paragraph 5.2.1.

Analysis warm-up The DOMS warm-up time is determined by the time needed for the electronics to arrive at stable conditions. In contrast to the HLS, the electrode is not heated and the sensor is not installed in a measurement pot, representing a closed volume. The heating time of the sensor support or the target surface can

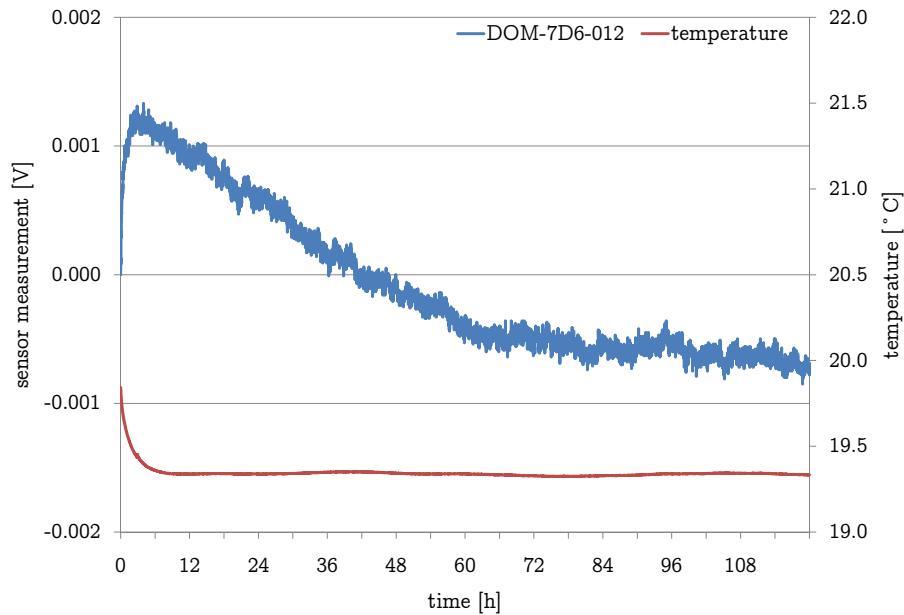


Figure 5.25: DOMS warm-up

therefore be excluded and thermal expansion of the stability bench is captured with a temperature probe. With a constant ambient temperature, the warm-up effects shown, are due to the electronics of the DOMS.

The DOMS shows a warm-up influence of less than $\pm 5 \mu\text{m}$, throughout the warm-up period of 48 hours. Within this time the signal stabilises to a final value.

Analysis stability The stability was a problem in a lot of measurements, as the claimed stability of better than $1 \mu\text{m}$ per month from the manufacturer's specifications cited in table 3.4 was not obtained for some sensors. The stability problem will be also be discussed in paragraph 5.4.2 as linearity measurements also allowed the detection of sensor drifts. The measurements on the single sensor benches of the first and second design did not allow investigation of where this instability came from. The introduction of the third stability bench with several sensors improved measurements in the sense that the stability of the bench could be shown and unstable sensors could be detected. The installation of several sensors on the bench allowed comparison of the results, from the sensors with respect to each other and allowed the elimination of external influences on the bench such as thermal expansion.

Conclusion Compared to the HLS and WPS, DOMS are very delicate to handle with respect to their isolation from the ground and their ground link to the DAQ rack. The first two check benches were of limited use for investigation of the stability

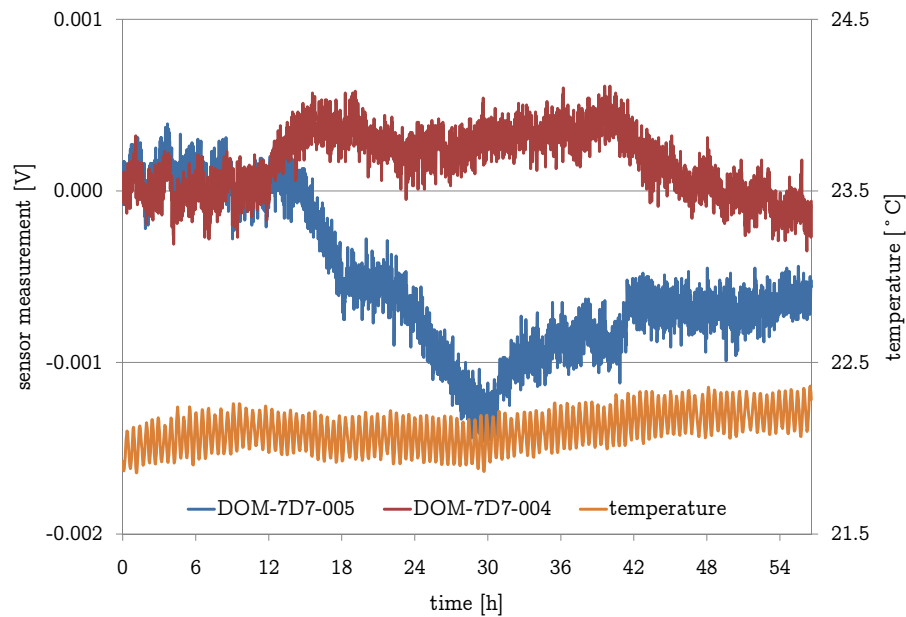


Figure 5.26: DOMS stability

issue as it was not possible to clearly identify if the changes in sensor readings were due to sensor drifts or due to instability of the bench. The solution has been to redesign the warm-up and stability check bench and to have several sensors facing to a common target. The stability measurements led to exchange or repair of one quarter of the sensors, multiple repairs of sensors not being taken into account.

5.4.2 Linearity

The linearity of the DOMS is controlled in a similar way to that of the HLS. Measurements with respect to a length standard and throughout the sensor's range are taken. The polynomial is calculated from the measurements and compared to the manufacturer's calibration function.

Design The configuration of the DOMS linearity check bench, is similar to the HLS bench shown in figure 5.6. The HLS bench is used and the sensor support plate changed in order to host one DOMS. As first sensor checks revealed a discrepancy between the manufacturer's calibration and the check measurements and additional DOMS fixing was integrated in the support plate. This allowed measurements of two sensors at the same time and therefore gave redundant checks on the sensors. Both sensors were situated at the same distance from the centre axis of the bench. The principle of Abbe was no longer respected, so this approach is not a solution for calibration, but comparisons between the sensors themselves and the length reference were possible this way.

Measurements The surface of the sensor's electrode is the electrical zero reference for the sensor. As two sensors were installed at the same time on the linearity bench and the reference installation surface of the sensor is the back side of the sensor, the thickness of the sensor can not be neglected for the zero reference of the DOMS. To avoid mismatch of the zero due to different thicknesses of the sensors, the sensors were no longer plugged on the surface of the mount, but put into contact with the electrode's surface on the target surface and then fixed to the sensor support plate, keeping a short distance of less than 1 mm between the sensor and the mount. As contact of a powered sensor to the target surface causes a short circuit in the electronics, the installation of the sensors in the support was done with the sensors not being powered for the time of installation. The time needed for the installation and orientation of both sensors was less than one minute and therefore the loss of power can be neglected with respect to the warm-up period that was carried out before.

Due to the measurement range configuration of the DOMS, with the electrode as zero reference, the zero measurement of the sensor cannot be carried out and only a gain adjustment of the sensor is possible. The sensor calibration can only start at a distance of 0.5 mm with respect to the electrode to ensure a stable field line distribution. All other measurements are taken at distances equal to 1/10 of the sensor's range. Measurements are carried out twice independently as go and return measurements to calculate the calibration function independently from each other.

Analysis The analysis method used is based on the recalculation of the polynomial and is the same as that of the HLS in section 4.4. In figure 5.27 two linearity measurements are shown. Sensor DOM-7D6-023 shows comparable measurements within tolerance between the linearity check bench measurements (dotted lines) and the calibration of the manufacturer (red line). The difference between the determination of the polynomial at calibration and during check measurements at CERN was less than 2 μm . In this case, the calibration polynomial can be considered as valid and the sensor passed the validation.

Conclusion The DOMS were checked for linearity by modifying the existing HLS bench sensor adaptor plate in order to host two DOMS. A double-check method in combination with a stability check on the second stability bench has been introduced by the author in order to identify drifts. Numerous sensors had been affected by linearity problems and had to be returned to the manufacturer for repair. The method of using two sensors facing to one target made it possible to instantly compare the results of two sensors with respect to each other and with respect

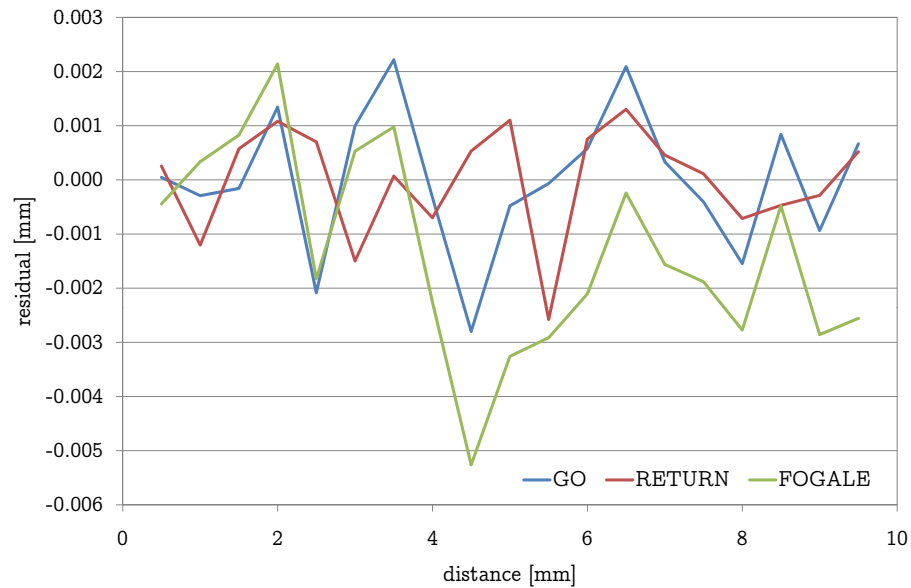


Figure 5.27: DOMS linearity

to the length gauge. The design of a third stability check bench was based on the results showing that two sensors can face the same target without interfering measurements.

5.4.3 External reference and repeatability

The DOMS was designed to perform absolute measurements with respect to the back surface of the sensor. As described in the previous section, the distance measurement is referenced to the electrode of the sensor. This means that to use the sensors external referencing of the back surface of the sensor with respect to the measurement depends on the thickness of the sensor, t , and the variation in the calibration of the zero reference of the sensor. The external reference can be deduced as long as all the sensors can be referenced relative to each other. In order to validate these measurements, the repeatability of the sensor installation in the support had to be tested before calculating the external reference.

Repeatability The repeatability of the installation of the DOMS has been shown to be better than $3\ \mu\text{m}$ for each sensor.

External reference The concept for this determination uses the DOMS stability bench shown in figure 5.23. This bench has the advantages that the distance to the sensor is adjustable and the target can be kept in place while changing sensors. The absolute distance between the target and the sensor surface was unknown. Therefore

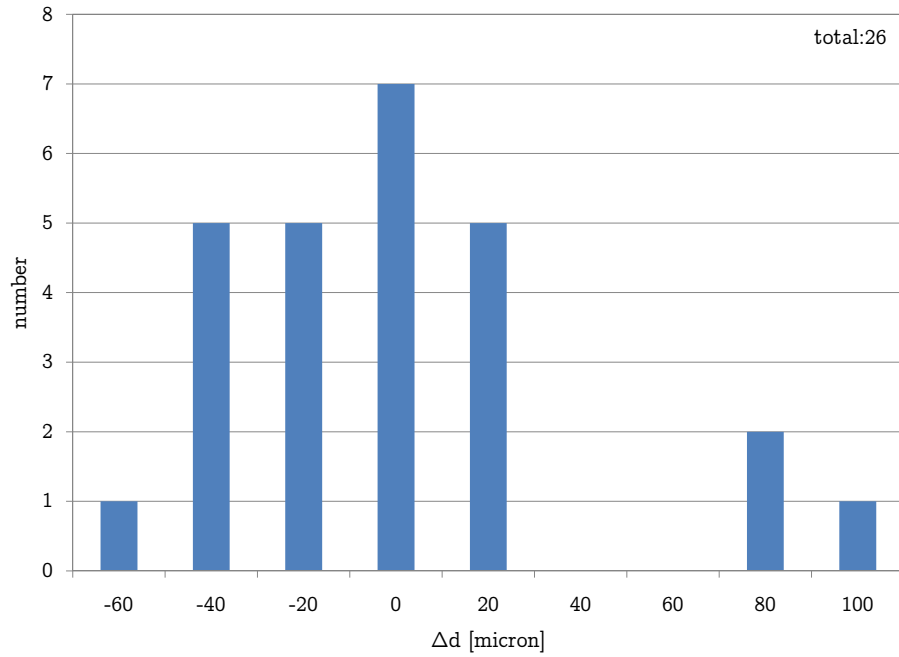


Figure 5.28: DOMS external reference

relative interchangeability parameters were found with respect to a reference sensor. By comparing the different measurements to each other one can get the offset difference between two sensors. The offset and differences in the thickness of the sensor are presented in one interchangeability constant. The constant Δd_i is defined as the difference of the measurements between the tested sensor, i , and the reference sensor, r , to the same target at the same distance.

$$\Delta d_i = d_i - d_r \quad (5.8)$$

The interchangeability of DOMS is given by FOGALE nanotech to be better than $\pm 50 \mu\text{m}$ as shown in figure 3.4. The maximum difference between the sensors was $150 \mu\text{m}$. The histogram in figure 5.28 shows three sensors which are outliers to the normal distribution; all other sensors fit in the defined slot.

Change of reference surface The method of interchangeability between the sensors does not separate the thickness of the sensor from the determination of the zero point of the sensor.

For a future calibration bench, the definition of the sensor's measurement should be referenced to the back surface of the sensor. In this case the thickness of the sensor is included in the absolute part of the calibration polynomial. This can be done by determining the distance, d , between the back of the mounting surface of the

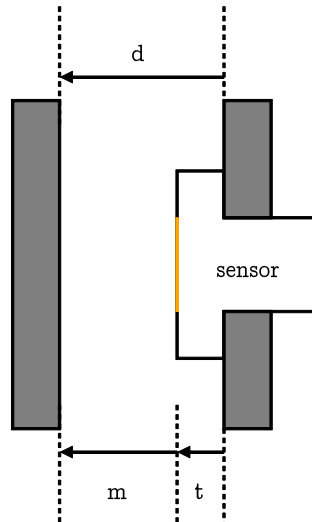


Figure 5.29: DOMS external reference

sensor and the target on a CMM. The measurement of the sensor, m , on this bench is combined with measurements for the determination of the calibration function of the sensor. This approach eliminates the thickness, t , of the DOMS in the external referencing.

5.4.4 Magnetic field

The DOMS was the only sensor tested in a magnetic field. This was due to instabilities of the IRS during low-beta magnets powering tests. The test on the DOMS was carried out in order to exclude the influence of magnetic stray fields on the measurements.

Design and manufacture The sensor uses both supports of the second stability bench. The sensors are installed on a common base plate facing their fixed target as shown in figure 5.30. The situation in the tunnel with the sensor facing the invar rod is not used for this test as the invar rod is magnetic and therefore interacting with the magnetic field of the magnets. During this test set-up only the sensor is exposed to the magnetic field. Most of the cable and the electronics are outside the field of the magnet.

Measurements The DOMS was installed for warm-up during an overnight period and stability was recorded for this period. The measurements were carried out at steps of 0.1 T throughout the range of the magnet up to its limit of 0.54 T. A gaussmeter which measures magnetic flux is used for recording the magnetic field at

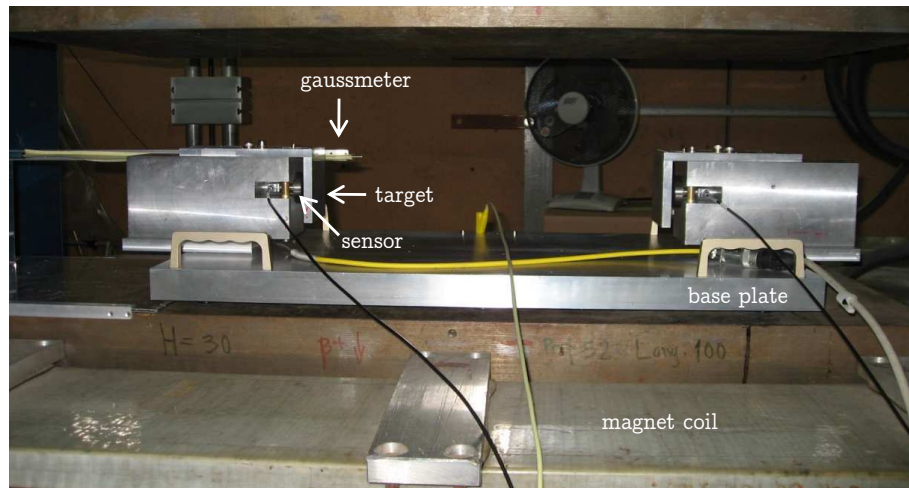


Figure 5.30: magnetic field test installation

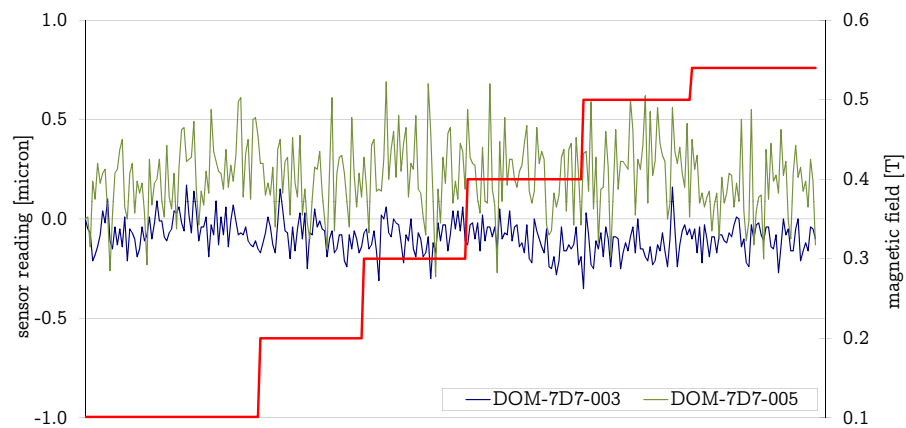


Figure 5.31: magnetic field measurements

the position of the sensors. The measurements of the sensor and the corresponding magnetic fields are shown in figure 5.31.

Conclusion The sensors are not subject to variation due to the applied magnetic field. The signal is not perturbed and the noise level of the sensor does not vary. As exposure of sensors to a magnetic field can destroy the electronics due to a malfunction of components, the electronics have not been tested so far.

5.5 Summary

The measurements, checks and benches presented in this chapter showed the approaches chosen for validation of the HLS, WPS and DOMS for the LHC. Results of the measurements led to exchange and repair of sensors. The check benches allowed for the check of the sensors and furthermore the identification and quantification of errors of the sensors. Calibration methods for additional parameters of the sensors have been introduced by the author.

The following chapter draws conclusions from the results, taking into account the sensors, methods and benches.

Chapter 6

Conclusions and recommendations

In this chapter, the author draws conclusions from the investigation and summarises the results obtained about the sensors, test methods and benches. The studies on monitoring sensors used in the LHC had several objectives. First, the sensor check and calibration methods have been defined. Measurements for the validation of the sensors according to the concepts proposed and test infrastructure have been created. Based on these results, recommendations will be given for future, additional checks and calibrations as well as for the manufacture and operation of automated calibration benches.

6.1 Sensors

In the check and calibration series, three types of sensors were investigated: HLS, WPS and DOMS. All sensors were chosen to be used in the LHC low-beta magnet monitoring and repositioning system.

The HLS are designed with cable lengths of up to 30m and have, together with the WPS, the longest cable configuration. The results for stability, linearity and noise tests obtained were within the claims of the manufacturer. Problems during measurements were mostly related to mechanical failure, for example, the connector of the cable. This resulted in some non-conformities that were eliminated after repair.

HLS For the HLS, additional calibrations were introduced. The stability bench concept was modified in order to be used for zero reference and interchangeability calibration. This reduced the variety of benches. An approach to redefine the zero reference of the HLS was proposed and validated in a series of tests. The new

zero reference has not been applied to the LHC alignment so far, but can easily be implemented during the next recalibration.

WPS The WPS showed several severe problems during the tests. The most incomprehensible one was the phenomenon of burning the electronics during tests. The problem is linked to excess voltage in the electronics. As a precaution for future tests, sensors may no longer be connected or disconnected while the electronics are live. The problem has not been reproduced so far.

As the WPS is a biaxial sensor, the linearity check bench design had to follow two displacement axes. The approach of using the body of the sensor as an external reference was not suitable. The normal, non-ceramic surfaces of the sensor are not manufactured sufficiently precisely to be used for the linearity measurements; only the ceramic surfaces can be used.

Concerning the sensor design one result is, that the possibility of fixing the sensor only in the vertical axis is not sufficient for a sensor that is used for radial and vertical measurements in the case that both axes have to be known with respect to an external reference.

Using a stretched wire as a reference is the only possibility for checking and calibrating the sensor. A problem in this configuration arises from the fact that the wire is a light target that has to be stretched to be stabilised. Using a weight for stretching the wire and the configuration of the suspension which is part of the wire stretching unit, are source of instabilities during long-term measurements. For measurements like external referencing the risk of touching the wire is high, although one is working with precaution. The wire will come back to its initial position to within $\pm 20 \mu\text{m}$ with respect to the v-shaped radial fixing. The stability problem of the wire has been solved by monitoring with additional reference sensors situated on the extremities of the bench.

The WPS were successfully validated for the LHC. The linearity bench did not achieve its objective because an orientation problem with the fixing caused rotated measurements between the measurement axes and the reference axes. There was also a scaling problem of the measurements on this bench. The problem of destroyed electronics will remain under investigation until the phenomenon can be recreated in a reproducible way and will then be discussed with the manufacturer.

DOMS The DOMS showed better results after a change of the primary signal transmission technology by the manufacturer. Drift effects as observed for the prototype production have been eliminated. The sensor's cable is the most fragile part of the measurement chain and led to the high number of returns to the manufacturer.

Drift problems significantly influenced the sensor's stability and were the second major problem identified during tests. The long-term stability of the sensors has now to be evaluated with measurements in the LHC.

Measurements on the linearity check bench are carried out in a similar way to those of the HLS. Using two sensors in the check bench design was possible and did not influence the measurements. It was useful at the beginning of the series of tests to have two sensors on the bench in order to cross-check the observations for unstable measurements on the linearity bench by using a validated sensor and the sensor in doubt.

The initial stability check benches were only of limited success as the stability problem of the DOMS did not allow a comparison with other sensors. After successful validation of the concept with several sensors measuring on the same target, this led to a stability bench with a maximum of 8 sensors checked at the same time. The second designed stability bench was used for magnetic field tests and external reference determination as it allowed the sensor to be mounted and dismounted from the support without changing the target.

6.2 Checks and calibrations

In chapter 4 the different tests planned for the sensors of the low-beta magnets monitoring system were presented. Some of these checks are carried out for the type of sensor, e.g. the radiation or magnetic field tests and other checks for each sensor. All calibrations have to be carried out for each sensor in order to determine each sensor's parameters.

The chosen checks and calibrations are appropriate to evaluate the necessary parameters to be able to use the sensors in the LHC. The checks of functioning, warm-up, stability and linearity were the core tests of the sensors. The stability and linearity measurements are also part of the quality control at manufacturer. The main reason to carry out these tests again at CERN was because of stability and linearity problems encountered with some sensors. Those sensors have been

identified and returned for repair. These checks avoided the installation of faulty equipment in a complex alignment system, where the identification of the defective equipment could be more difficult.

The introduction of external reference calibrations and the check on repeatability of the installation of the sensor allow a realistic estimation of the error model for the sensor in the monitoring system. The tolerances for the determination of the external reference were guaranteed by the manufacturer within the machining and assembly tolerances for the sensors and were in the order of $\pm 50 \mu\text{m}$. By determining the true parameters, the range of the variation was not reduced, but the true values are now known to better than $\pm 10 \mu\text{m}$. This reduced the individual error for each sensor in the error propagation model of the alignment system. The tolerances announced by the manufacturer were exceeded in some cases.

The TID radiation test has been carried out for HLS and WPS. Both types of sensors passed the test for a 10 year equivalent dose of LHC operation. The DOMS sensors have not been tested as they were not available for the tests in 2005. They have to be validated in future radiation tests. The DRD test was successfully completed for the HLS and resulted in a correction model for the sensor's measurements with respect to the dose rate applied. The WPS have been tested, but did not show any influence depending on the dose rate. This can be possible due to the symmetric installation of the wire with respect to the electrodes in the central position of the sensor. A modified configuration with an off-centre installation of the wire has to be tested in future radiation tests.

The magnetic field compatibility of the sensors has not been tested. The DOMS has only been tested for magnetic field influence in combination with a model of the IRS monitoring system. The magnetic field tests will have to comprise sensor, cable and electronics for each of the types of sensors.

6.3 Benches

The three types of sensors needed special benches for the checks and calibrations which were proposed. In consideration of the variety of tests the author intended to design benches that can be used for different checks with only a few modifications.

To conform with this objective, the linearity check bench for HLS and DOMS was designed. It is possible to modify the bench by changing the support plate of the sensor. The WPS stability check bench has been modified to allow external reference

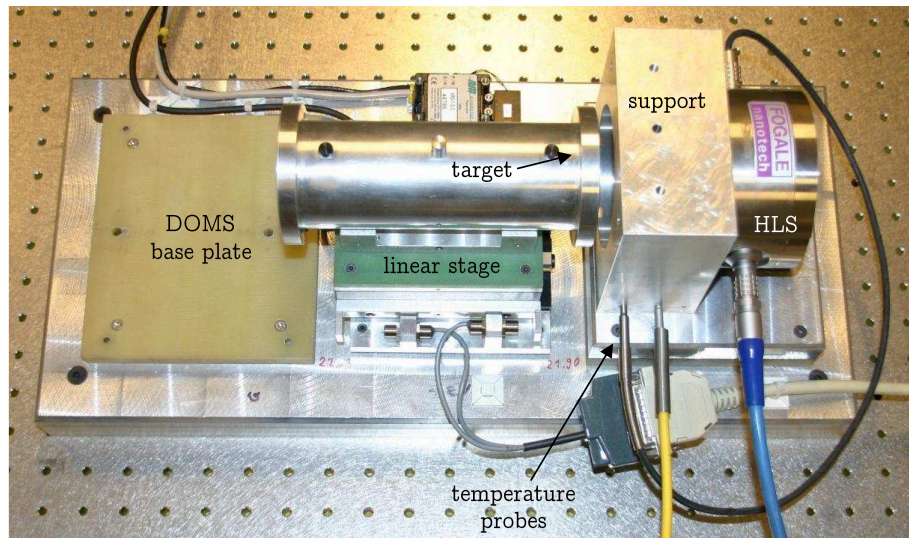


Figure 6.1: automated linearity calibration bench

measurements by replacing the central, standard sensor support by a special one. In the case of the first stability bench for DOMS, that used the HLS measurement pot as fixed target, this approach failed due to practical problems relating to operating the bench.

All check benches for HLS and DOMS achieved the defined tolerances. The WPS only achieved this objective for the warm-up, stability and external reference bench. The linearity check bench was not sufficiently well designed to obtain measurement results within the required tolerances.

The linearity benches will be automated in order to allow recalibration of the sensors at CERN. Based on experience with manually operated benches, an HLS calibration bench has been designed and put into preproduction operation. First calibration results show an improvement of the determination with respect to the manual check bench. The recalculated calibration function reproduces to within $2\ \mu\text{m}$ with respect to the polynomial given by the manufacturer. Figure 6.1 shows the automated HLS linearity calibration bench. Keeping the concept of one bench for different sensors, the automated calibration bench is also designed to host the DOMS.

6.4 Recommendations

The investigation of check and calibration methods, sensors and benches covered the range of tests necessary for the installation of the sensors in the LHC. In this

section, some recommendations for future tests are presented in order to improve upon knowledge of the performance of the sensors.

Radiation and magnetic field The three types of sensors have to complete a series of tests under the accelerator-related influences of radiation and magnetic field. The radiation tests for the HLS showed a radiation related influence with respect to the dose rate applied. The WPS measurement set-up for the DRD test, was not appropriate as outlined in section 6.2. For the DOMS, a validation of the sensor, the cable and the electronics has to be carried out in the radiation environment.

Radiation tests with the HLS sensor showed a drift in the electronics of the temperature probe at the very beginning of the tests. The drift was strongly correlated with the radiation dose applied to the electronics. SEE tests have to be carried out for all sensors.

The influence of magnetic fields has to be tested for all types of sensors and all components of the sensor. HLS and WPS have not been tested at all; the DOMS has been tested for the sensor in a magnetic field of up to 0.54 T.

HLS range extension The HLS is designed to carry out measurements at a range that is neither starting at the electrode, as for the DOMS, nor limited by mechanical housing constraints, as for the WPS. The range of fourth generation HLS starts at a distance of 5 mm from the target. As the DAQ system is able to carry out measurements between -10 V and +10 V, the range of the HLS could be extended by -5 mm without losing resolution. Extending the range increases the risk of getting the electrode into contact with water and creating a short-circuit as the water level can rise closer to the sensor's electrode.

Sensor cables The calibration of the sensors, their cables and their electronics as one unit is an integral part of the working principle of the sensors. Studies on the properties of the cable have shown, that using a different cable, either of the same or a different length, devalues the calibration. In case of failure of a sensor in the LHC, all three components of the sensor have to be changed. Following these first tests on the cables' properties, additional tests have to be carried out to learn more about the possibility of separating the cable from the calibration.

The aspect of making the sensor's reading independent from the cable used is also important for the capacitive references as they depend on the set of cables that are used for the measurements. The cables are the most fragile part of the system and

they are most likely to fail. A backup solution without dependence on the cables is desirable.

DOMS absolute reference The measurement range of the DOMS is referenced with respect to its electrode surface. The point of reference for the sensor is its back. This includes the thickness of the sensor. In paragraph 5.4.2, the concept, similar to the HLS absolute referencing, was presented. This theoretical specification has to be validated with measurements.

WPS wire The use of the carbon-peek wire, with specifications as shown in table 3.3, could not be changed for the LHC. The measurement supports were optimised to follow the wire sag along the installation. For future installations, other wires can be used in case they are suitable. This necessitates investigation of properties of the wire and a possible change in the calibration parameters of the sensor. If an easy-to-handle wire can be found with similar properties with respect to the calibration of the sensor, one could think about using this wire for calibrations and in future installations.

Linearity calibration The linearity calibration will be carried out on automated benches. A calibration in two steps can be proposed for the automated calibration bench. The sensors presented in this thesis are used for monitoring and repositioning of magnets. In the case that the reference points on the magnets are well enough designed to have the sensors at the centre of their range, a high-resolution calibration for this central part and a lower resolution calibration for the outer part can be considered. This allows the measurements to be tracked more precisely in the centre of the measurement range where no repositioning needs to be carried out.

6.5 Summary

Already with the conclusions on the monitoring sensors obtained from the test conceived, presented and carried out by the author, the HLS, WPS and DOMS are no longer black boxes for the user. The presented tests identified the strong and weak points of these sensors.

With these recommendations additional tests can be planned. This can lead to a further improvement for the LHC alignment system. In addition to the tests, careful investigation of any abnormal behaviour of the sensors in the LHC is important. Observations from the LHC can result in new check methods and new aspects of the long-term characteristics of the sensor.

Especially with regard to future accelerator projects understanding of the sensors has to be improved. This includes the low-beta magnet upgrade planned after some years of LHC use and the linear collider project CLIC that is currently under investigation at CERN.

Reference List

- Anon. (2002). *Linac Coherent Light Source (LCLS) - Conceptual Design Report [online]*, SLAC, USA, available at: http://www-ssrl.slac.stanford.edu/lcls/cdr/lcls_cdr.pdf. Accessed: 11.04.2006.
- Bader, F. and Dorn, F. (1993). *Physik Oberstufe - Gesamtband 12/13*, Schroedel Schulbuch Verlag, Hannover, Germany.
- Becker, F., Coosemans, W., Pittin, R. and Wilson, I. (2003). *An active pre-alignment system and metrology network for CLIC [online]*, CLIC note 553, CERN, Switzerland, available at: <http://doc.cern.ch/archive/electronic/cern/preprints/open/open-2003-011.pdf>. Accessed: 15.07.2007.
- Bestmann, K. and Missiaen, D. (2006). *Naming conventions for Fiducials on LHC LSS special magnets [online]*, CERN, Switzerland, available at: <http://edms.cern.ch/document/776046>. Accessed: 13.02.2008.
- Blobel, V. and Lohrmann, E. (1998). *Statistische und numerische Methoden der Datenanalyse*, Teubner Studienbücher, Stuttgart.
- British Standards Institution (1996). *BS EN 60751: 1996. Industrial platinum resistance thermometer sensors*, British Standards Institution.
- Busch, W. (1981). *Eigenschaften stationärer hydrostatischer Präzisions-Höhenmeßsysteme für kontinuierliche Langzeitbeobachtungen untersucht an einem neuentwickelten Schlauchwaagensystem*, Geodätisches Institut der Rheinisch-Westfälischen Technischen Hochschule Aachen.
- CERN (2008). *CERN FAQ - LHC the guide [online]*, CERN, Switzerland, available at: <http://cdsmedia.cern.ch/img/CERN-Brochure-2008-001-Eng.pdf>. Accessed: 20.02.2009.
- Coosemans, W. and Mainaud, H. (1997). *Prealignment of CLIC using the double-wire method [online]*, 5th International Workshop on Accelerator Alignment, Argonne National Laboratory, USA, available at: http://www-group.slac.stanford.edu/met/IWAA/TOC_S/Papers/WCoos97.pdf. Accessed: 01.11.2006.
- Coosemans, W., Mainaud Durand, H., Marin, A. and Quesnel, J.-P. (2002). *The Alignment of the LHC Low Beta Triplets: Review of Instrumentation and*

- Methods [online]*, 7th International Workshop on Accelerator Alignment, SPring-8, Japan, available at: <http://www.spring8.or.jp/pdf/en/iwaa02/proceedings/2002/WCoos02.pdf>. Accessed: 11.04.2006.
- Dimovasili, E., Herty, A., Mainaud Durand, H., Marin, A., Ossart, F. and Wijnands, T. (2005a). *Radiation induced effects on the sensors of the Hydrostatic Leveling System for the LHC low beta quadrupoles [online]*, Technical Note CERN-TS-2005-052, CERN, Switzerland, available at: <https://edms.cern.ch/file/629483>. Accessed: 11.04.2006.
- Dimovasili, E., Herty, A., Mainaud Durand, H., Marin, A., Ossart, F. and Wijnands, T. (2005b). *Radiation induced effects on the sensors of the Hydrostatic Leveling System for the LHC low beta quadrupoles [online]*, 8th European conference on radiation and its effects on components and systems (RADECS), Cap d'Agde, France, available at: <http://ieeexplore.ieee.org/stamp/stamp.jsp?arnumber=4365621&isnumber=4365538>. Accessed: 03.10.2008.
- Fogale Nanotech (2006). *Accelerator alignment [online]*, company flyer, FOGALE nanotech, 125 rue de l'hostellerie, Bâtiment A, 30900 Nîmes, France, available at: <http://www.fogale.fr/media/GC/acceleratoralignment.pdf>. Accessed: 14.01.2007.
- Fogale Nanotech (2007a). *Certificat de contrôle N° 07-02 [online]*, FOGALE nanotech, 125 rue de l'hostellerie, Bâtiment A, 30900 Nîmes, France, available at: <https://edms.cern.ch/file/883782/1>. Accessed: 04.01.2009.
- Fogale Nanotech (2007b). *Etalonnage des capteurs HLS et WPS [online]*, presentation, FOGALE nanotech, 125 rue de l'hostellerie, Bâtiment A, 30900 Nîmes, France, available at: https://edms.cern.ch/file/856493/1/etalonnage_wps_hls.pdf. Accessed: 14.07.2007.
- Gieck, K. (1995). *Technische Formelsammlung*, Gieck Verlag, Germering, Germany.
- Herty, A., Dimovasili, E., Mainaud Durand, H., Marin, A., Ossart, F. and Wijnands, T. (2006). *Radiation induced effects on Hydrostatic Levelling Systems [online]*, 9th International Workshop on Accelerator Alignment, SLAC, USA, available at: <http://www.slac.stanford.edu/econf/C06092511/papers/WEP016.PDF>. Accessed: 31.12.2006.
- Herty, A., Mainaud Durand, H. and Marin, A. (2004). *Test and Calibration Facility for HLS and WPS sensors [online]*, 8th International Workshop on Accelerator alignment, CERN, Switzerland, available at: http://iwaa2004.web.cern.ch/IWAA2004/subsite/PDF/20041006_TS08-2_Andreas-Herty.pdf. Accessed: 11.04.2006.
- Herty, A. and Mergelkuhl, D. (2008). *Alignment of the low-beta magnets and the experiments in the LHC [online]*, TS Workshop 2008, CERN, Switzerland, available at: <http://edms.cern.ch/document/936560/1>. Accessed: 22.02.2009.

- Hofmann-Wellenhof, B., Kienast, G. and Lichtenegger, H. (1994). *GPS in der Praxis*, Springer Verlag, Germany.
- Ingensand, H., Meier, E. and Ruland, R. (2002). *Developments and Experiences with Hydrostatic Height Monitoring Systems*, 2nd Symposium on Geodesy for Geotechnical and Structural Engineering, Berlin, Germany.
- International Organization for Standardization (2000). *Optics and optical instruments - Geodetic and surveying instruments - Vocabulary*, International Organization for Standardization.
- International Organization for Standardization (2004). *International vocabulary of basic and general terms in metrology (VIM) [online]*, ISO VIM, available at: <http://www.ntmdt.ru/download/vim.pdf>. Accessed: 26.06.2007.
- Jones, M. (2001). *Geodetic Definition (Datum Parameters) of the CERN coordinate system*, CERN, Geneva, Switzerland, available at: <http://edms.cern.ch/document/107981>. Accessed: 27.02.2008.
- Kivioja, L., Friedsam, H. and Penicka, M. (1997). *A new hydrostatic leveling system developed for the Advanced Photon Source [online]*, 5th International Workshop on Accelerator Alignment, Argonne National Laboratory, USA, available at: http://www-group.slac.stanford.edu/met/IWAA/TOC_S/Papers/LKivi97.pdf. Accessed: 03.01.2007.
- Löffler, F., Dobers, T. and Neubauer, G. (1992). *High precision levelling system for the HERA detectors and interaction quadrupoles [online]*, 15th International Conference on High Energy Accelerators, available at: http://geo.desy.de/sites/site_mea2/content/e4/e11/e15/e94/infoboxContent95/HLS_ger.pdf. Accessed: 21.01.2007.
- Lippitsch, A. (2007). *A Deformation Analysis Method for the Metrological ATLAS Cavern Network at CERN*, Shaker Verlag, Achen, Germany.
- Mainaud, H. (1996). *Une nouvelle approche métrologique: L'écartométrie biaxiale. Application à l'alignement des accélérateurs linéaires*, Thèse de doctorat, Ecole Nationale Supérieure des Arts et Industries de Strasbourg, France.
- Mainaud Durand, H. (2006). *Alignment Requirements for the LHC low-beta triplets [online]*, CERN, Switzerland, available at: <https://edms.cern.ch/document/344496/1.2>. Accessed: 13.01.2007.
- Mainaud Durand, H., Herty, A., Marin, A., Mathieu, A. and Rénaglia, T. (2004). *Status of the Alignment of the LHC Low Beta Quadrupoles [online]*, 8th International Workshop on Accelerator Alignment, CERN, Switzerland, available at: http://iwaa2004.web.cern.ch/IWAA2004/subsite/PDF/20041005_TS03-1_Andreas-Herty.pdf. Accessed: 18.01.2007.

- Mainaud Durand, H., Quesnel, J.-P. and Touzé, T. (2008). *Stretched wire offset measurements: 40 years of practice of this technique at CERN [online]*, 10th International Workshop on Accelerator Alignment, KEK, Tsukuba, Japan, available at: <http://www.slac.stanford.edu/econf/C0802113/papers/P053.pdf>. Accessed: 20.01.2009.
- Martin, D. (2002). *The European Synchrotron Radiation Facility hydrostatic leveling system - twelve years experience with a large scale hydrostatic leveling system [online]*, 7th International Workshop on Accelerator Alignment, SPring-8, Japan, available at: <http://www.slac.stanford.edu/econf/C0211115/papers/032.PDF>. Accessed: 14.05.2007.
- Martin, D. (2004). *Some reflections on the validation and analysis of HLS data [online]*, 8th International Workshop on Accelerator Alignment, CERN, Switzerland, available at: <http://www.slac.stanford.edu/econf/C04100411/papers/030.PDF>. Accessed: 14.05.2007.
- Meier, E., Wei, F., Rivkin, L., Wrulich, A., Zelenika, S., Ingensand, H., Haberecht, M. and Akeret, F. (2004). *Long term results of the hydrostatic levelling system at the Swiss Light Source [online]*, 8th International Workshop on Accelerator Alignment, CERN, Switzerland, available at: <http://www.slac.stanford.edu/econf/C04100411/papers/034.PDF>. Accessed: 13.05.2007.
- Meyer-Dietrich, U. and Felshart, M. (1999). *Untersuchung eines kapazitiven hydrostatischen Messsystems für die ingenieurgeodätische Anwendung in einem geplanten, über 30 km langen Linearbeschleuniger*, Universität Hannover, Universität Hannover.
- Peters, F. (2005). *The Undulator - Wire Position System [online]*, LCLS Undulator Alignment and Motion Review, available at: http://www-ssrl.slac.stanford.edu/lcls/undulator/meetings/2005-10-20_intl_align_review/talks/wps-oct21-05-review-peters.ppt. Accessed: 08.07.2007.
- Prochnow, J., Coosemans, W., Dehning, B., Hildreth, M., Marin, A., Matheson, J., Mugnai, G., Roncarolo, F. and Torrence, E. (1999). *Performance of wire position sensors in a radiation environment [online]*, 6th International Workshop on Accelerator Alignment, ESRF, France, available at: http://www-group.slac.stanford.edu/met/IWAA/TOC_S/PAPERS/JProc99.pdf. Accessed: 13.01.2007.
- Quesnel, J.-P. (1997). *Review of the Metrology Aspects of the LHC Alignment [online]*, 5th International Workshop on Accelerator Alignment, Argonne National Laboratory, USA, available at: <http://www.aps.anl.gov/conferences/iwaa97/papers/quesnel.pdf>. Accessed: 18.01.2007.

- Quesnel, J.-P. (2004). *LHC Design Report - Volume II - Chapter 11*, CERN, Geneva, Switzerland, available at: http://edms.cern.ch/file/445932/5/Vol_2_Chapter_11_v6.pdf. Accessed: 27.02.2008.
- Rausch, R., Pignard, C. and Wijnands, T. (2002). *Qualification of electronic components and systems in a LHC tunnel radiation environment [online]*, 8th European Particle Accelerator Conference, Paris, France, available at: <http://accelconf.web.cern.ch/Accelconf/e02/PAPERS/WEALA003.pdf>. Accessed: 14.01.2007.
- Roux, D. (1993). *A historical first on accelerator alignment [online]*, 3rd International Workshop on Accelerator alignment, Geneva, Switzerland, available at: http://www-group.slac.stanford.edu/met/IWAA/TOC_S/Papers/DRoux93.pdf. Accessed: 21.01.2007.
- Ruland, R. (1995). *Some alignment considerations for the next linear collider [online]*, 4th International Workshop on Accelerator Alignment, Tsukuba, Japan, available at: <http://www.slac.stanford.edu/econf/C951114/papers/045.PDF>. Accessed: 20.11.2007.
- Schlösser, M. (2004). *The rapid tunnel reference surveyor for a future linear collider [online]*, 8th International Workshop on Accelerator Alignment, CERN, Switzerland, available at: <http://www.slac.stanford.edu/econf/C04100411/papers/048.PDF>. Accessed: 13.05.2007.
- Schlösser, M. and Herty, A. (2002). *High Precision Survey and Alignment of Large Linear Colliders - Vertical Alignment [online]*, 7th International Workshop on Accelerator Alignment, SPring-8, Japan, available at: <http://www.spring8.or.jp/pdf/en/iwaa02/proceedings/2002/MSchl102.pdf>. Accessed: 18.01.2007.
- Schwarz, W. (1990). *Wire measurements for the control of the FFTB-magnets [online]*, 2nd International Workshop on Accelerator Alignment, CERN, Switzerland, available at: http://www-group.slac.stanford.edu/met/IWAA/TOC_S/Papers/WSchw90b.pdf. Accessed: 15.07.2007.
- Schwarz, W. (1997). *Concept for the Alignment of the planned Linear Collider at DESY [online]*, 5th International Workshop on Accelerator Alignment, Argonne National Laboratory, USA, available at: <http://www.slac.stanford.edu/econf/C971013/papers/029.PDF>. Accessed: 16.05.2007.
- Schwarz, W., Baumann, E., Dold, J., Grabowski, J., Gröne, A., Hagemann, M., Meyer, R., Pelzer, H., Ritter, R., Wendt, K. and Wittmann, G. (1995). *Vermessungsverfahren im Maschinen- und Anlagenbau*, Konrad Wittwer Verlag, Germany, Band 28.
- Sylvac SA (2007). *General specifications for all dial gauges [online]*, Sylvac SA, Chemin du Closalet 16, 1023 Crissier, Switzerland, available at: http://www.sylvac.ch/index.php?option=com_docman&task=doc_download&gid=11&Itemid=41&lang=en. Accessed: 13.09.2007.

- Wei, F. Q., Dreyer, K. and Umbricht, H. (2002). *Status of the SLS alignment system [online]*, 7th International Workshop on Accelerator Alignment, SPring-8, Japan, available at: <http://www.spring8.or.jp/pdf/en/iwaa02/proceedings/2002/FQWei02.pdf>. Accessed: 21.01.2007.
- Zhang, C., Fukami, K. and Matsui, S. (2002). *Primary hydrokinetics study and experiment on the hydrostatic leveling system [online]*, 7th International Workshop on Accelerator Alignment, SPring-8, Japan, available at: <http://www.slac.stanford.edu/econf/C0211115/papers/031.PDF>. Accessed: 13.01.2009.

Appendix A

Calibration files

A.1 HLS calibration file

The calibration file of the HLS is designed for the FOGALE nanotech software MSM. The fourth order polynomial for the sensor are the parameters V0 to V4 in section [LIN_CAPT_A]. The correction of the temperature probe is a linear regression function with the parameters V0 and V1 in section [SONDE_T].

```
[DEF]
numero_serie = H7D7-011
type = 1
09/12/2008
nom = ?

[TREF]
tref = 20

[CAPT]
correction_eau = 1
pt_equilibre_eau = 11
type_eau = eau_simple

hauteur_differentiel = 54

coef_dil_pot = 17

[LIN_CAPT_A]
Degre_lin = 3
Resolution = 1000
V0 = 5.00001
V1 = 1.060988
V2 = -0.0179514
V3 = 0.00094883
V4 = 0.000023763
V5 =
V6 =
V7 =
V8 =
V9 =

[SONDE T]
Degre_lin = 1
Resolution = 100
V0 = -0.4045
V1 = +5.00352
V2 =
V3 =
V4 =
V5 =
V6 =
V7 =
V8 =
V9 =
```

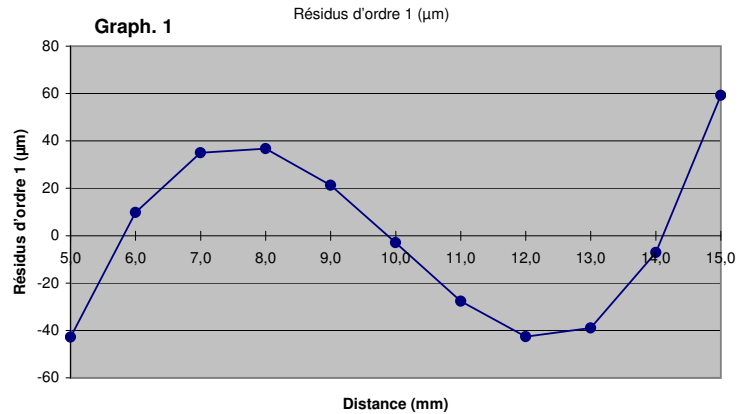
H7D7-011

H7D7-011

Date : 09/12/2008

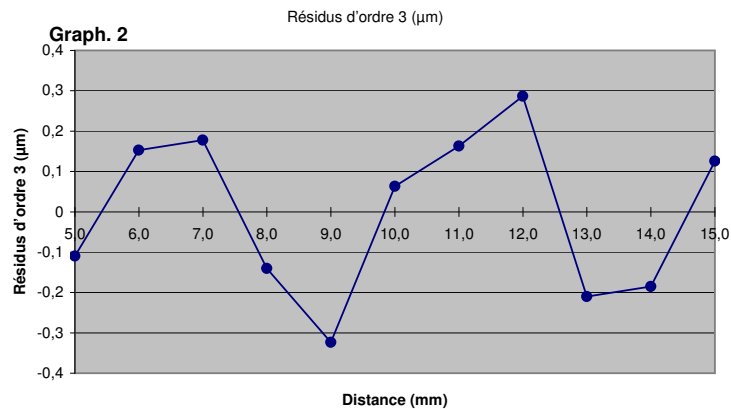
Linéarisation du 1^{er} ordre

Coefficients de régression du 1^{er} ordre
 $d = 5,0427 + 0,98993 V$



Linéarisation du 3^{er} ordre

Coefficients de régression du 3^{er} ordre (équa. 1)
 $d = 5,0000 + 1,06099 V - 0,017951 V^2 + 0,0009488 V^3 + 0,00002376 V^4$



Légende : Les polynômes de linéarisation expriment la distance d en fonction de la tension V .
 - la distance est exprimée en mm
 - la tension est exprimée en V

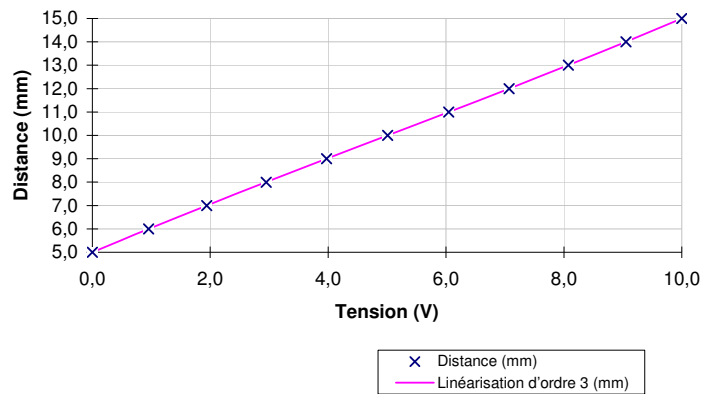
H7D7-011

H7D7-011

Type : HLS.REM5 5/ 0-50

Date : 09/12/2008

Linéarisation du capteur



Résultats

Distance (mm)	Tension (V)
4,9995	-0,0004
5,9989	0,9560
6,9985	1,9403
7,9986	2,9489
8,9988	3,9748
9,9985	5,0091
10,9990	6,0448
11,9991	7,0702
12,9992	8,0768
13,9994	9,0550
15,0004	9,9991

A.2 WPS calibration file

The calibration file of the WPS is designed for the FOGALE nanotech software MSM. The calibration parameters are given in a 6 by 6 matrix for each of the two measurement axes with the parameters A0 to A35 for the x axis in section [LIN_CAPT_WPS2D_X] and B0 to B35 for the y axis in section [LIN_CAPT_WPS2D_Y].

```
[DEF]
numero_serie = WPS2D-7D7-011
type = 30
date = 12/07/2007
nom = ?

[LIN_CAPT_WPS2D_X]
Degre lin = 5
Resolution = 1000
A0 = -5.770343889646
A1 = 0.330173099854
A2 = -0.034076054766
A3 = 0.000232808237
A4 = -0.000086334255
A5 = 0.000005570398
A6 = 0.901966824356
A7 = -0.052396395669
A8 = 0.005261699776
A9 = 0.000512388169
A10 = -0.000112081808
A11 = 0.000006315621
A12 = 0.030330414452
A13 = 0.008970511011
A14 = -0.001592079595
A15 = -0.000276316835
A16 = 0.000087309671
A17 = -0.000005375045
A18 = 0.014071673976
A19 = -0.005154728227
A20 = 0.000842639319
A21 = 0.000034940335
A22 = -0.000019514659
A23 = 0.000001301826
A24 = -0.002409885516
A25 = 0.000692249281
A26 = -0.000118632970
A27 = 0.000000196531
A28 = 0.000001702112
A29 = -0.000000125674
A30 = 0.000096678819
A31 = -0.000028238840
A32 = 0.000005159377
A33 = -0.000000138851
A34 = -0.000000051105
A35 = 0.000000004272

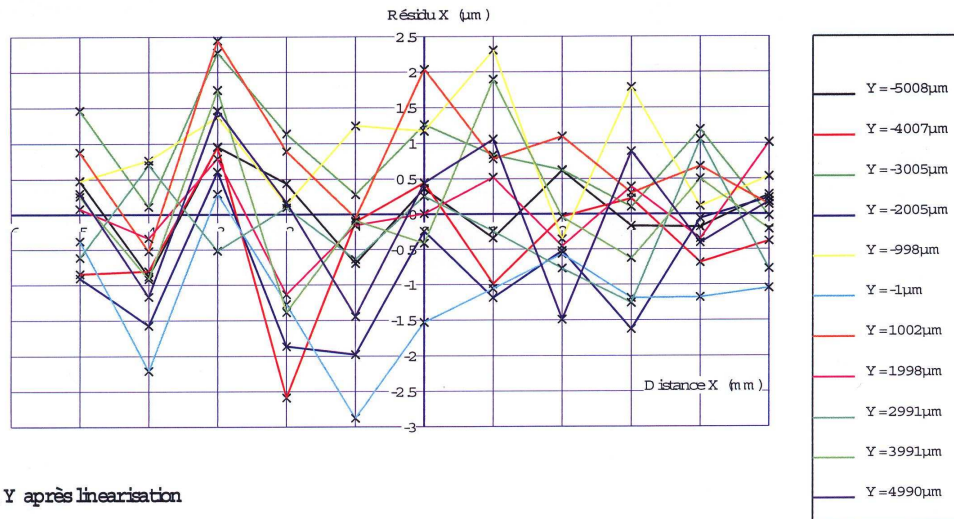
[LIN_CAPT_WPS2D_Y]
Degre lin = 5
Resolution = 1000
B0 = -5.933518304216
B1 = 0.917837998767
B2 = 0.030651175414
B3 = 0.014582483244
B4 = -0.002519217878
B5 = 0.000101922935
B6 = 0.333889475458
B7 = -0.031044943109
B8 = -0.002136530882
B9 = -0.002773442887
B10 = 0.000451327316
B11 = -0.000019012869
B12 = -0.019761439778
B13 = -0.009797269648
B14 = 0.005947240575
B15 = -0.000955233304
B16 = 0.000076823995
B17 = -0.000002575406
B18 = -0.003472738221
B19 = 0.004136329482
B20 = -0.002102265024
B21 = 0.000484958625
B22 = -0.000049937483
B23 = 0.000001873221
B24 = 0.000332672721
B25 = -0.000490249469
B26 = 0.000276109836
B27 = -0.000066642901
B28 = 0.000007021810
B29 = -0.000000266416
B30 = -0.000011762871
B31 = 0.000020802492
B32 = -0.000012491668
B33 = 0.000003087291
B34 = -0.000000328834
B35 = 0.000000012538
```

W PS2D

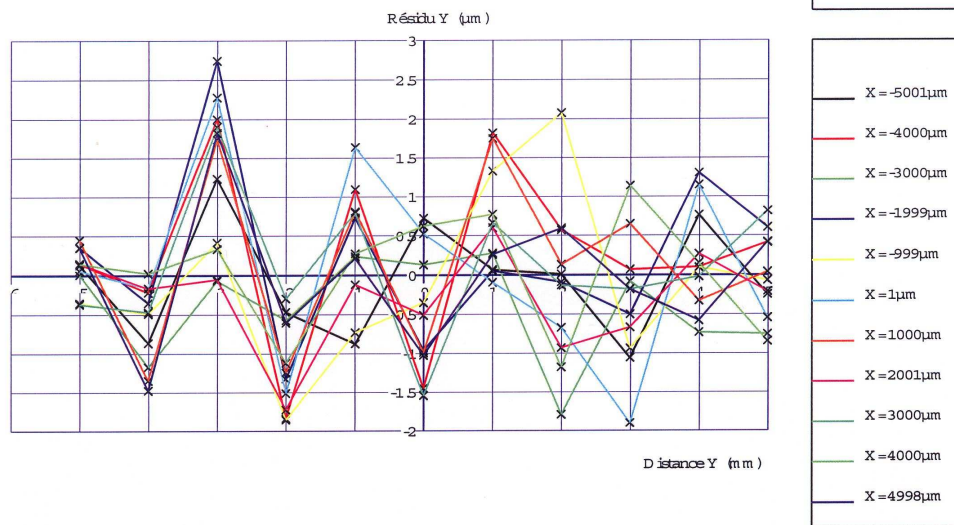
W PS2D -7D 7-011 -29M

Date:12/07/2007

Résidus en X après linearisation



Résidus en Y après linearisation



W PS2D

W PS2D -7D 7-011 -29M

Date:12/07/2007

Résidus en X (µm)

$\begin{matrix} X \\ \backslash \\ Y \end{matrix}$	-5.002	-4.000	-3.000	-1.999	-0.999	0.002	1.000	2.002	3.000	4.000	4.998
-5.008	0.5	-0.9	1.0	0.4	-0.7	0.4	-0.3	0.6	-0.2	-0.2	0.3
-4.008	-0.8	-0.8	1.0	-2.6	-0.1	0.5	-1.0	-0.0	0.2	-0.7	-0.4
-3.005	1.5	0.1	2.3	1.1	0.3	1.3	0.8	0.6	0.1	1.2	-0.0
-2.006	-0.9	-1.6	0.6	-1.9	-2.0	-0.2	-1.2	-0.5	-1.6	-0.1	0.2
-0.998	0.5	0.8	1.4	0.1	1.2	1.2	2.3	-0.4	1.8	0.1	0.5
-0.001	-0.4	-2.2	0.3	-1.3	-2.9	-1.5	-1.1	-0.6	-1.2	-1.2	-1.0
1.003	0.9	-0.5	2.5	0.9	-0.1	2.0	0.8	1.1	0.3	0.7	0.1
1.998	0.1	-0.3	0.8	-1.1	-0.2	0.0	0.5	-0.5	0.4	-0.3	1.0
2.991	-0.6	0.7	-0.5	0.1	-0.6	0.3	-0.2	-0.8	-1.3	1.1	-0.8
3.991	0.3	-0.9	1.8	-1.4	-0.1	-0.4	1.9	-0.0	-0.6	0.5	-0.2
4.990	0.3	-1.2	1.5	0.2	-1.4	0.4	1.1	-1.5	0.9	-0.4	0.2

Résidus en Y (µm)

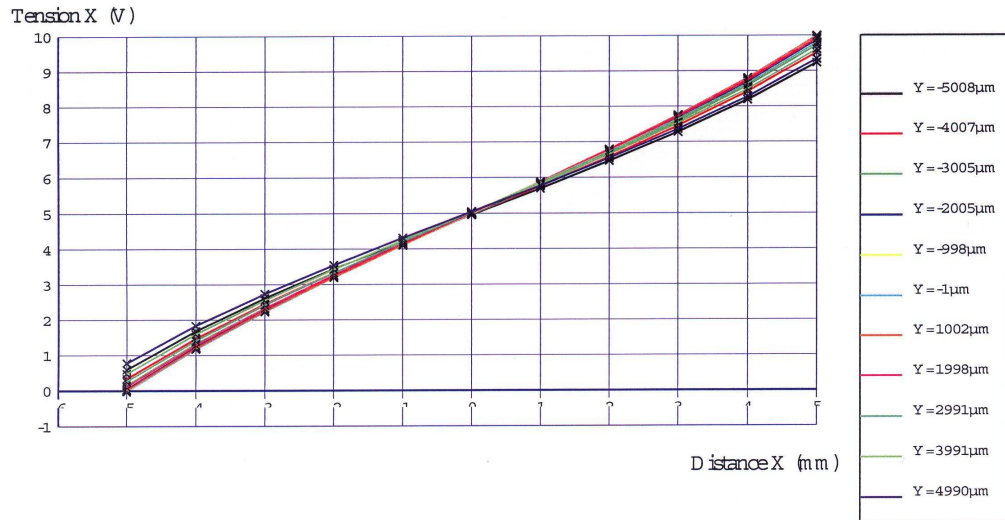
$\begin{matrix} X \\ \backslash \\ Y \end{matrix}$	-5.002	-4.000	-3.000	-1.999	-0.999	0.002	1.000	2.002	3.000	4.000	4.998
-5.008	0.1	0.1	0.00	0.4	-0.4	0.1	0.4	0.2	-0.4	0.1	0.3
-4.008	-0.9	-0.2	-1.2	-0.4	-0.5	-0.2	-1.3	-0.2	-0.5	0.0	-1.5
-3.005	1.2	2.0	-0.1	2.7	0.4	2.3	1.7	-0.0	1.9	0.3	1.8
-2.006	-0.5	-1.8	-0.6	-1.3	-1.9	-1.5	-1.2	-1.7	-0.3	-1.1	-0.6
-0.998	-0.9	1.1	0.2	0.7	-0.7	1.6	0.8	-0.1	0.8	0.3	0.2
-0.001	0.7	-1.4	0.1	-1.0	-0.4	0.5	-1.0	-0.5	-1.5	0.6	-1.0
1.003	0.1	1.8	0.3	0.1	1.3	-0.1	1.8	0.6	0.7	0.8	0.3
1.998	0.0	0.6	-1.8	-0.1	2.1	-0.7	0.1	-0.9	-0.1	-1.2	0.6
2.991	-1.1	0.1	-0.1	-0.5	-0.9	-1.9	0.7	-0.7	-0.2	1.1	-0.2
3.991	0.8	0.1	-0.7	1.3	0.1	1.2	-0.3	0.3	-0.0	0.2	-0.6
4.990	-0.2	0.4	-0.8	0.6	-0.1	-0.5	0.0	-0.2	0.8	-0.8	0.4

W PS2D

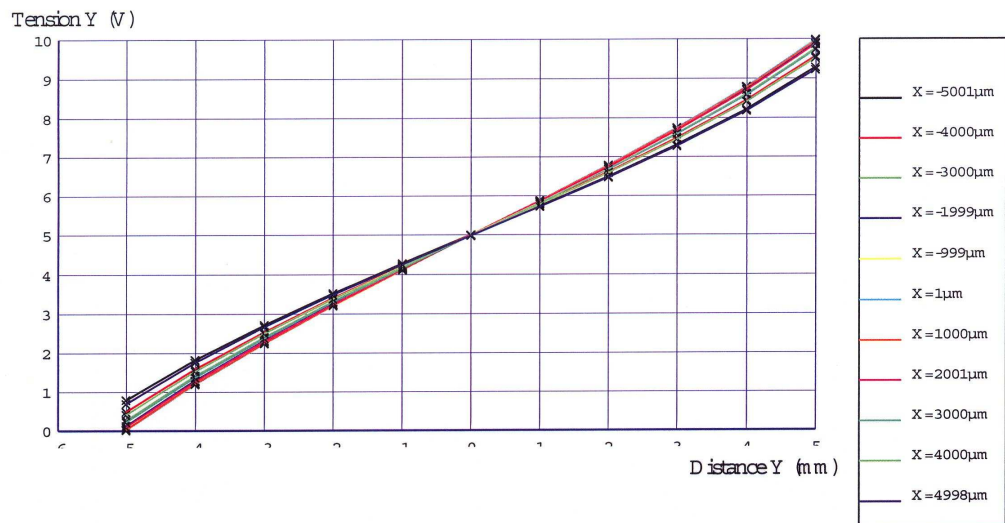
W PS2D -7D 7-011 -29M

Date:12/07/2007

R elevé capteur X



R elevé capteur Y



W PS2D

W PS2D -7D 7-011 -29M

Date:12/07/2007

Tension en X

$y = X =$	-5.002	-4.000	-3.000	-1.999	-0.999	0.002	1.000	2.002	3.000	4.000	4.998
-5.008	0.594	1.684	2.615	3.448	4.220	4.962	5.702	6.466	7.283	8.192	9.241
-4.008	0.332	1.472	2.455	3.345	4.168	4.967	5.763	6.583	7.456	8.423	9.529
-3.005	0.148	1.321	2.341	3.267	4.133	4.972	5.808	6.671	7.585	8.590	9.736
-2.006	0.036	1.227	2.270	3.223	4.115	4.981	5.845	6.735	7.677	8.709	9.876
-0.998	-0.023	1.175	2.233	3.198	4.105	4.988	5.867	6.775	7.730	8.780	9.960
-0.001	-0.029	1.173	2.231	3.201	4.114	5.000	5.884	6.795	7.757	8.811	9.996
1.003	0.013	1.207	2.259	3.222	4.128	5.007	5.887	6.792	7.749	8.798	9.981
1.998	0.108	1.288	2.324	3.270	4.157	5.020	5.881	6.771	7.712	8.747	9.917
2.991	0.262	1.415	2.425	3.339	4.198	5.031	5.864	6.726	7.641	8.650	9.802
3.991	0.482	1.598	2.561	3.436	4.250	5.042	5.831	6.652	7.528	8.499	9.616
4.990	0.779	1.835	2.741	3.557	4.316	5.049	5.783	6.547	7.364	8.283	9.346

Tension en Y

$y = X =$	-5.002	-4.000	-3.000	-1.999	-0.999	0.002	1.000	2.002	3.000	4.000	4.998
-5.008	0.791	0.495	0.281	0.135	0.050	0.016	0.033	0.102	0.228	0.421	0.695
-4.008	1.829	1.590	1.418	1.297	1.226	1.198	1.214	1.271	1.377	1.536	1.759
-3.005	2.723	2.545	2.415	2.321	2.269	2.246	2.258	2.305	2.384	2.506	2.672
-2.006	3.527	3.410	3.321	3.259	3.222	3.208	3.215	3.245	3.298	3.380	3.491
-0.998	4.283	4.223	4.179	4.146	4.128	4.117	4.121	4.135	4.160	4.200	4.256
-0.001	5.007	5.008	5.005	5.003	5.001	4.997	4.996	4.993	4.991	4.987	4.987
1.003	5.741	5.796	5.838	5.866	5.880	5.884	5.874	5.856	5.824	5.779	5.720
1.998	6.496	6.609	6.695	6.749	6.778	6.789	6.774	6.739	6.678	6.592	6.473
2.991	7.309	7.479	7.603	7.686	7.733	7.747	7.724	7.673	7.583	7.453	7.279
3.991	8.224	8.452	8.614	8.720	8.782	8.798	8.774	8.705	8.588	8.417	8.184
4.990	9.290	9.569	9.767	9.895	9.967	9.987	9.956	9.873	9.731	9.522	9.230

W PS2D

W PS2D -7D 7-011 -29M

Date: 12/07/2007

Coefficients de régression

LN_CAPT_W PS2D_X	LN_CAPT_W PS2D_Y
A 0 = -5.7703438896	B 0 = -5.9335183042
A 1 = 0.3301730999	B 1 = 0.9178379988
A 2 = -0.0340760548	B 2 = 0.0306511754
A 3 = 0.0002328082	B 3 = 0.0145824832
A 4 = -0.0000863343	B 4 = -0.0025192179
A 5 = 0.0000055704	B 5 = 0.0001019229
A 6 = 0.9019668244	B 6 = 0.3338894755
A 7 = -0.0523963957	B 7 = -0.0310449431
A 8 = 0.0052616998	B 8 = -0.0021365309
A 9 = 0.0005123882	B 9 = -0.0027734429
A 10 = -0.0001120818	B 10 = 0.0004513273
A 11 = 0.0000063156	B 11 = -0.0000190129
A 12 = 0.0303304145	B 12 = -0.0197614398
A 13 = 0.0089705110	B 13 = -0.0097972696
A 14 = -0.0015920796	B 14 = 0.0059472406
A 15 = -0.0002763168	B 15 = -0.0009552333
A 16 = 0.0000873097	B 16 = 0.0000768240
A 17 = -0.0000053750	B 17 = -0.0000025754
A 18 = 0.0140716740	B 18 = -0.0034727382
A 19 = -0.0051547282	B 19 = 0.0041363295
A 20 = 0.0008426393	B 20 = -0.0021022650
A 21 = 0.0000349403	B 21 = 0.0004849586
A 22 = -0.0000195147	B 22 = -0.0000499375
A 23 = 0.0000013018	B 23 = 0.0000018732
A 24 = -0.0024098855	B 24 = 0.0003326727
A 25 = 0.0006922493	B 25 = -0.0004902495
A 26 = -0.0001186330	B 26 = 0.0002761098
A 27 = 0.0000001965	B 27 = -0.0000666429
A 28 = 0.0000017021	B 28 = 0.0000070218
A 29 = -0.0000001257	B 29 = -0.000002664
A 30 = 0.0000966788	B 30 = -0.0000117629
A 31 = -0.0000282388	B 31 = 0.0000208025
A 32 = 0.0000051594	B 32 = -0.0000124917
A 33 = -0.0000001389	B 33 = 0.0000030873
A 34 = -0.0000000511	B 34 = -0.0000003288
A 35 = 0.0000000043	B 35 = 0.0000000125

A.3 DOMS calibration file

The calibration file of the DOMS is designed for the FOGALE nanotech software MSM. The parameters V0 to V4 in section [LIN_CAPT_A] represent the coefficients for the fourth order polynomial. The parameters in [SONDE_T] are set to 0 as this channel is not used.

```
[DEF]
nom = DOMS
numero_serie = DOM-7D6-012
type = 10

[SURF APPUI]
zero_capt_surf_appui_A = 0

[LIN_CAPT_A]

Degre_lin = 4
Resolution = 1000
V0 = -0.0184
V1 = +1.03003
V2 = -0.001971
V3 = -0.0013203
V4 = +0.00012193
V5 =
V6 =
V7 =
V8 =
V9 =

[SONDE T]
Degre lin = 0
Resolution = 100
V0 = 0.0
V1 = 0.0
V2 = 0.0
V3 = 0.0
V4 =
V5 =
V6 =
V7 =
V8 =
V9 =
```

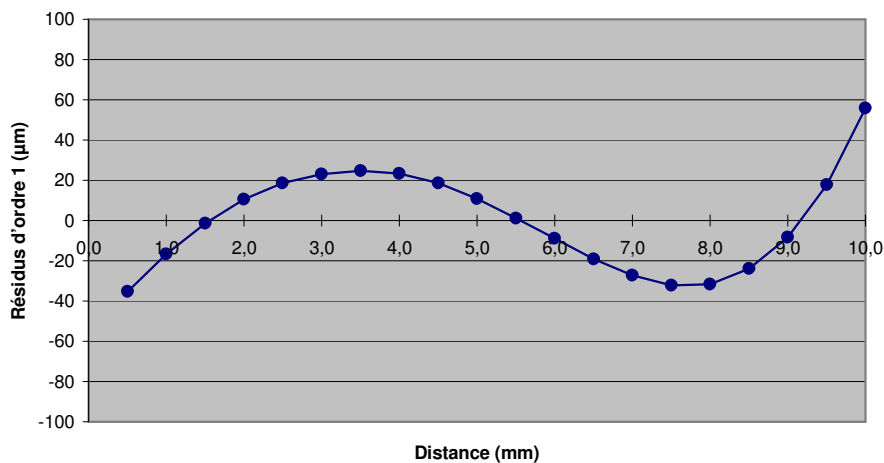
DOM-7D6-012

MCC50 n°: 50-832 Câble 16m

Date : 27/05/2008

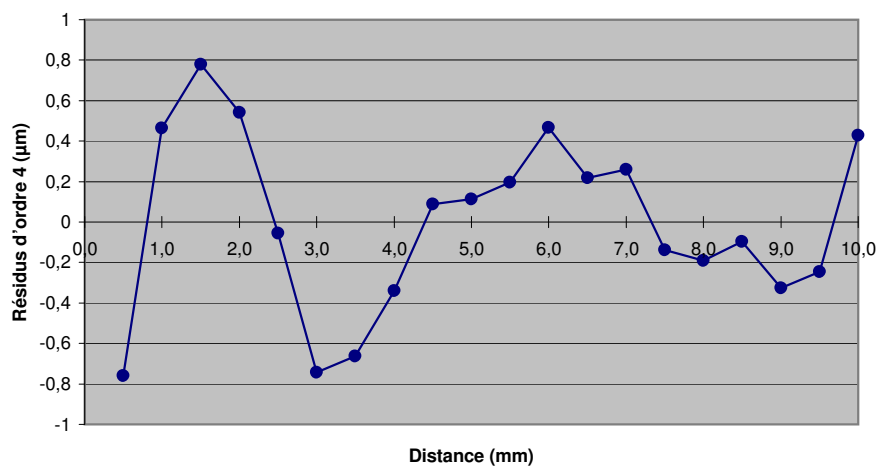
$$d = 0,0359 + 0,98938 V$$

Résidus d'ordre 1 (μm)



$$d = -0,0184 + 1,03003 V - 0,001971 V^2 - 0,0013203 V^3 + 0,00012193 V^4$$

Résidus d'ordre 4 (μm)



Légende : Les polynômes de linéarisation expriment la distance d en fonction de la tension V .
 - la distance est exprimée en μm
 - la tension est exprimée en V

Appendix B

Measurements

B.1 HLS repeatability

Table B.1 shows a series of measurements for the determination of the HLS repeatability. Three measurements are carried out for each sensor by fixing the sensor on the measurement pot. The measurements in this table are given in V. The average (AVG), the minimum (MIN) and the maximum (MAX) are shown. The range between the measurements for each sensor is shown in the column *RANGE*. The largest value is 3.8 mV for sensor H7D5-280.

SENSOR	MEASUREMENT				MIN	MAX	RANGE
	1	2	3	AVG			
H7D5-280	8.3052	8.3060	8.3090	8.3067	8.3052	8.3090	0.0038
H7D5-282	8.3162	8.3164	8.3156	8.3161	8.3156	8.3164	0.0008
H7D5-286	8.3330	8.3330	8.3329	8.3330	8.3329	8.3330	0.0001
H7D5-291	8.3313	8.3302	8.3307	8.3307	8.3302	8.3313	0.0011
H7D5-293	8.2724	8.2718	8.2714	8.2719	8.2714	8.2724	0.0010
H7D5-296	8.3355	8.3380	8.3390	8.3375	8.3355	8.3390	0.0035
H7D5-297	8.3216	8.3219	8.3214	8.3216	8.3214	8.3219	0.0005
H7D5-329	8.3100	8.3101	8.3098	8.3100	8.3098	8.3101	0.0003
H7D5-330	8.3220	8.3190	8.3200	8.3203	8.3190	8.3220	0.0030
H7D5-332	8.3061	8.3063	8.3061	8.3062	8.3061	8.3063	0.0002
H7D5-333	8.2961	8.2965	8.2962	8.2963	8.2961	8.2965	0.0004
H7D5-335	8.3061	8.3053	8.3052	8.3055	8.3052	8.3061	0.0009
H7D5-337	8.3064	8.3072	8.3073	8.3070	8.3064	8.3073	0.0009
H7D5-338	8.3276	8.3297	8.3263	8.3279	8.3263	8.3297	0.0034
H7D5-339	8.3141	8.3115	8.3117	8.3124	8.3115	8.3141	0.0026
H7D5-340	8.2916	8.2897	8.2903	8.2905	8.2897	8.2916	0.0019
H7D5-342	8.3342	8.3337	8.3339	8.3339	8.3337	8.3342	0.0005
H7D5-343	8.3307	8.3295	8.3297	8.3300	8.3295	8.3307	0.0012
H7D5-344	8.3140	8.3137	8.3132	8.3136	8.3132	8.3140	0.0008
H7D5-346	8.3278	8.3272	8.3271	8.3274	8.3271	8.3278	0.0007
H7D5-351	8.3139	8.3119	8.3125	8.3128	8.3119	8.3139	0.0020
H7D5-376	8.3255	8.3252	8.3251	8.3253	8.3251	8.3255	0.0004

B.2 HLS measurement pot

The HLS measurement pot is determined on a CMM. The distances, Z , are the vertical measurements to calibrate the depth of the measurement pot. The average of the bottom and the average of the surface are calculated and corrected for temperature variation with respect to 20°C.

PET-CER-001

HLS reference measurement pot

name	date	time	X	Y	Z raw	Z offset	Z
A	19.12.2008	8:12:52 AM	0.000017	0.000023	1.871511	0.0423	1.8292
B05	19.12.2008	8:13:25 AM	0.000021	4.992468	1.871523	0.0448	1.8267
B10	19.12.2008	8:13:55 AM	0.000010	9.995286	1.871491	0.0473	1.8242
C10	19.12.2008	8:14:31 AM	-9.995727	-0.006357	1.871490	0.0440	1.8275
C05	19.12.2008	8:14:58 AM	-4.995326	-0.006341	1.871406	0.0429	1.8285
D05	19.12.2008	8:15:37 AM	-0.002718	-4.991584	1.871473	0.0432	1.8283
D10	19.12.2008	8:16:00 AM	-0.002672	-10.005513	1.871499	0.0458	1.8257
E10	19.12.2008	8:16:32 AM	9.994736	0.003800	1.871391	0.0483	1.8231
E05	19.12.2008	8:16:55 AM	4.995573	0.003766	1.871431	0.0449	1.8265
P11	19.12.2008	8:17:34 AM	0.149749	44.418955	-24.630958	0.0444	-24.6754
P12	19.12.2008	8:17:57 AM	-11.510240	43.722305	-24.630888	0.0413	-24.6722
P21	19.12.2008	8:18:38 AM	-39.967554	-22.021264	-24.612184	0.0434	-24.6556
P22	19.12.2008	8:19:05 AM	-33.900455	-31.495064	-24.612233	0.0425	-24.6547
P31	19.12.2008	8:19:45 AM	39.264673	-22.898010	-24.632388	0.0452	-24.6776
P32	19.12.2008	8:20:12 AM	43.169342	-13.617097	-24.632387	0.0470	-24.6794

average	minimum	maximum	difference	
1.8266	1.8231	1.8292	0.0061	bottom
-24.6691	-24.6794	-24.6547	0.0247	surface

temperature	22.4	°C
thermal expansion	13.0	ppm

distance	uncorrected	thermal expansion	corrected
	26.49577		

measurements in mm

B.3 WPS linearity measurement

This figure shows the measurements taken for the linearity check of a WPS. The tested sensor, W2D-7D5-002, gives the pair of measured distances with respect to the length gauge measurements. The references left and right are used to monitor the stability of the wire during measurements.

length gauge		reference left		W2D-7D5-002		reference right		X	Y
X	Y	X	Y	X	Y	X	Y	X	Y
0.0000	0.0000	-0.0031	-0.0021	0.0004	0.0000	0.0035	0.0013	0	0
-4.0000	0.0000	-0.0023	-0.0025	-3.9770	0.0007	0.0040	0.0014	-23	-1
-4.0000	4.0000	-0.0025	-0.0024	-3.9394	3.9671	0.0040	0.0013	-60	33
0.0000	4.0000	-0.0027	-0.0020	0.0313	3.9713	0.0038	0.0017	-31	29
4.0000	4.0000	-0.0027	-0.0021	3.9963	3.9632	0.0038	0.0016	4	37
4.0000	0.0000	-0.0027	-0.0023	3.9730	-0.0012	0.0041	0.0015	27	1
4.0000	-4.0000	-0.0033	-0.0019	3.9383	-3.9682	0.0039	0.0012	62	-32
0.0000	-4.0000	-0.0031	-0.0021	-0.0288	-3.9741	0.0037	0.0018	29	-26
-4.0000	-4.0000	-0.0031	-0.0020	-3.9999	-3.9665	0.0036	0.0017	0	-34
0.0000	0.0000	-0.0025	-0.0023	0.0001	0.0003	0.0034	0.0017	0	0
								μm	μm

range	0.0010	0.0006
return		

0.0003	-0.0004
--------	---------

0.0007	0.0007
--------	--------

measurements in mm unless indicated different

B.4 WPS surface measurement

The ceramic reference surfaces of the WPS are checked for flatness and orthogonality. The range of variation to the surface is shown below the tables. The three measurements for dY with more than 10 μm are considered as outliers.

The angle between X and Y plane is 1.194 mrad. This is a maximum error of 12 μm for the position of the radial reference surface.

	X	Y	Z	dX
	(mm)	(mm)	(mm)	(micron)
X.01	1.21386	-0.00002	0.00006	-3.2
X.02	1.19607	-7.49857	0.00005	-4.5
X.03	1.17635	-14.99025	0.00003	-3.9
X.04	1.18565	-14.99027	-5.00497	-4.6
X.05	1.19799	-7.49800	-5.00493	2.2
X.06	1.21988	0.00027	-5.00500	-0.6
X.07	1.22811	0.00024	-9.99622	-0.2
X.08	1.20842	-7.49781	-9.99624	0.3
X.09	1.19428	-15.00219	-9.99616	-4.7
X.10	1.19288	-15.00211	-14.99217	5.3
X.11	1.21368	-7.49892	-14.99215	3.7
X.12	1.23654	-0.00725	-14.99215	-0.1
X.13	1.23642	-0.00718	-19.99565	8.6
X.14	1.21711	-7.50519	-19.99564	8.8
X.15	1.20106	-15.00400	-19.99562	5.8
X.16	1.21350	-15.00379	-24.99302	1.9
X.17	1.22934	-7.49588	-24.99304	5.2
X.18	1.25109	0.00196	-24.99303	2.6
X.19	1.26517	0.00188	-29.99075	-2.9
X.20	1.24554	-7.50162	-29.99073	-2.4
X.21	1.22224	-14.99617	-29.99073	1.8
X.22	1.23760	-14.99635	-34.99402	-5.0
X.23	1.25861	-7.49957	-34.99407	-6.8
X.24	1.27847	-0.00289	-34.99403	-7.6

	X	Y	Z	dY
	(mm)	(mm)	(mm)	(micron)
Y.01	40.99628	-29.46347	-34.99400	9.2
Y.02	32.98764	-29.45637	-34.99399	13.0
Y.03	22.99357	-29.42255	-34.99399	-7.2
Y.04	14.99446	-29.41543	-34.99403	-3.5
Y.05	14.99451	-29.40904	-29.99914	-6.9
Y.06	23.00333	-29.42609	-29.99920	-0.7
Y.07	32.99447	-29.43982	-29.99916	-0.6
Y.08	40.99615	-29.44915	-29.99915	-2.2
Y.09	40.99616	-29.44599	-25.00105	-2.4
Y.10	33.00058	-29.41609	-25.00108	-21.4
Y.11	22.99233	-29.43070	-25.00104	6.8
Y.12	15.00388	-29.41063	-25.00106	-2.3
Y.13	15.00385	-29.41190	-19.99936	1.9
Y.14	22.99775	-29.42939	-19.99933	8.5
Y.15	32.99792	-29.44146	-19.99940	6.9
Y.16	40.99420	-29.44492	-19.99934	-0.5
Y.17	40.99413	-29.43838	-14.99757	-4.1
Y.18	32.99132	-29.42975	-14.99755	-1.8
Y.19	23.00233	-29.43564	-14.99758	17.7
Y.20	14.99984	-29.40425	-14.99755	-2.8
Y.21	14.99975	-29.39615	-10.00002	-7.9
Y.22	23.00281	-29.42211	-10.00001	7.1
Y.23	32.99492	-29.42994	-10.00003	1.4
Y.24	40.99377	-29.43133	-10.00004	-8.1

minimum	-7.6
maximum	8.8
range	16.4

minimum	-21.4
maximum	17.7
range	39.1

angle between X and Y plane 1.194 mrad

W2D-7D7-005

B.5 WPS frequency measurement

The WPS frequency measurement compares the nominal frequency, as adjusted by the manufacturer, to the measured frequency. Differences with respect to the nominal value of maximum 1 kHz are found. The variation is in a range of 1.5 kHz.

name	nominal	frequency	difference
W2D-7D4-003	4.0	4.075	0.075
W2D-7D4-004	4.1	4.147	0.047
W2D-7D4-006	4.3	4.195	-0.105
W2D-7D4-007	4.4	4.440	0.040
W2D-7D4-008	4.5	4.545	0.045
W2D-7D4-009	4.6	4.720	0.120
W2D-7D4-010	4.7	4.834	0.134
W2D-7D4-011	4.8	4.917	0.117
W2D-7D4-012	4.9	5.004	0.104
W2D-7D4-013	5.0	5.141	0.141
W2D-7D4-014	5.1	5.196	0.096
W2D-7D4-016	5.3	5.174	-0.126
W2D-7D4-017	5.4	5.309	-0.091
W2D-7D4-019	5.6	5.526	-0.074
W2D-7D4-020	5.7	5.551	-0.149
W2D-7D4-021	5.8	5.763	-0.037
W2D-7D4-022	5.9	5.738	-0.162
W2D-7D4-023	6.0	5.919	-0.081
W2D-7D4-024	6.1	6.115	0.015
W2D-7D4-025	6.2	6.208	0.008
W2D-7D4-026	6.3	6.367	0.067
W2D-7D4-027	6.4	6.432	0.032
W2D-7D4-028	6.5	6.612	0.112
W2D-7D4-029	6.6	6.606	0.006
W2D-7D4-030	6.7	6.692	-0.008
W2D-7D4-031	6.8	6.864	0.064
W2D-7D4-032	6.9	6.963	0.063
W2D-7D4-033	7.0	7.076	0.076
W2D-7D4-034	7.1	7.220	0.120
W2D-7D4-035	7.2	7.392	0.192
W2D-7D4-036	7.3	7.794	0.494
W2D-7D4-037	7.4	7.370	-0.030
W2D-7D4-038	7.5	7.753	0.253
W2D-7D4-039	7.6	7.668	0.068
W2D-7D4-040	7.7	7.719	0.019
W2D-7D4-041	7.8	8.007	0.207
W2D-7D4-042	7.9	8.061	0.161
W2D-7D4-043	8.0	8.183	0.183
W2D-7D4-044	8.1	8.263	0.163
W2D-7D4-045	8.2	7.744	-0.456
W2D-7D4-046	8.3	7.318	-0.982
W2D-7D4-080	5.5	5.589	0.089

name	nominal	frequency	difference
W2D-7D5-001	3.0	3.030	0.030
W2D-7D5-002	3.1	3.167	0.067
W2D-7D5-003	3.2	3.247	0.047
W2D-7D5-004	3.3	3.352	0.052
W2D-7D5-005	3.4	3.339	-0.061
W2D-7D5-007	3.5	3.531	0.031
W2D-7D5-008	3.6	3.540	-0.060
W2D-7D5-009	3.7	3.717	0.017
W2D-7D5-010	3.8	3.871	0.071
W2D-7D5-012	4.0	3.893	-0.107
W2D-7D5-014	4.2	4.137	-0.063
W2D-7D5-016	4.4	4.316	-0.084
W2D-7D5-017	4.5	4.546	0.046
W2D-7D5-021	4.9	4.929	0.029
W2D-7D5-022	5.0	4.850	-0.150
W2D-7D5-024	5.2	5.188	-0.012
W2D-7D5-025	5.3	5.478	0.178
W2D-7D5-028	3.9	3.973	0.073
W2D-7D5-036	5.4	5.410	0.010
W2D-7D5-038	4.7	4.549	-0.151
W2D-7D5-039	4.3	4.221	-0.079

name	nominal	frequency	difference
W2D-7D7-001	3.5	3.495	-0.005
W2D-7D7-002	3.6	3.599	-0.001
W2D-7D7-003	3.7	3.691	-0.009
W2D-7D7-004	3.8	3.781	-0.019
W2D-7D7-005	3.9	3.887	-0.013
W2D-7D7-006	4.0	3.969	-0.031
W2D-7D7-007	4.1	4.067	-0.033
W2D-7D7-008	4.2	4.178	-0.022
W2D-7D7-009	4.3	4.238	-0.062
W2D-7D7-010	4.4	4.373	-0.027
W2D-7D7-011	4.5	4.459	-0.041
W2D-7D7-012	4.6	4.570	-0.030
W2D-7D7-013	4.7	4.658	-0.042
W2D-7D7-014	4.8	4.769	-0.031
W2D-7D7-015	4.9	4.863	-0.037

minimum 0.001
maximum 0.982
range 1.476

frequencies given in kHz

Appendix C

Publications

C.1 Radiation induced effects on the sensors of the Hydrostatic Levelling System for the LHC low beta quadrupoles

E. Dimovasili, A. Herty, H. Mainaud Durand, A. Marin, F. Ossart and T. Wijnands

The dose rate dependence of the Hydrostatic Leveling System (HLS) for the final focusing quadrupole magnets in the Large Hadron collider is discussed. At high dose rates, ionization of the air inside the sensors causes charge deposition and this perturbs the position measurement. A model is presented that corrects the HLS signal offset as a function of the dose rate. The model compares the HLS with condenser ionization chambers and in this note the results of the comparison are presented.

CERN Technical Note TS-2005-052, CERN, 2005



EUROPEAN ORGANIZATION FOR NUCLEAR RESEARCH
ORGANISATION EUROPÉENNE POUR LA RECHERCHE NUCLÉAIRE

CERN - TS Department

EDMS Nr: 629483
Group reference: TS-LEA

TS-Note-2005- 052
1 August 2005

Radiation induced effects on the sensors of the Hydrostatic Leveling System for the LHC low beta quadrupoles

E. Dimovasili¹, A. Herty¹, H. Mainaud Durand¹, A. Marin¹, F. Ossart², T. Wijnands¹

¹ CERN 1211 Geneva 23, Switzerland

² FOGALE Nanotech, Parc Kennedy-Bât A3, 285 Rue Gilles Roberval, F-30915, Nimes Cedex

Abstract

The dose rate dependence of the Hydrostatic Leveling System (HLS) for the final focusing quadrupole magnets in the Large Hadron collider is discussed. At high dose rates, ionization of the air inside the sensors causes charge deposition and this perturbs the position measurement. A model is presented that corrects the HLS signal offset as a function of the dose rate. The model compares the HLS with condenser ionization chambers and in this note the results of the comparison are presented.

Keywords: *Low beta quadrupoles, alignment, HLS, radiation, ionization*

CONTENTS

1. Introduction.....	1
2. Hydrostatic Leveling System.....	1
2.1. <i>Operating principles of the HLS</i>	1
2.2 <i>Radiation induced effects</i>	3
3. Experimental set –up.....	4
4. Experimental results.....	5
4.1 <i>Recombination in the sensors</i>	5
4.2 <i>The HLS sensors as condenser ionization chambers</i>	5
4.3. <i>The validity of the calibration polynomials</i>	8
4.4. <i>General recombination in the HLS</i>	9
4.5. <i>The HLS and the LHC radiation environment</i>	10
5. Summary and conclusions.....	10
References.....	11
APPENDIX.....	12

1. Introduction

The Large Hadron Collider (LHC) [1] is a high energy, high intensity proton collider presently under construction at CERN which will become operational in 2007. The ultimate aim of this machine is to inject, accelerate and collide two proton beams of 10^{11} particles head-on each at energy of 7 TeV. At the location where the beams collide, large detectors are used to detect the collision products. A key performance parameter for a detector is the luminosity which is a quantity proportional to the number of collisions per second. In past and present colliders, luminosity is culminated at rate of around $L = 10^{32} \text{cm}^{-2} \text{s}^{-1}$ while in the LHC it will reach $L = 10^{34} \text{cm}^{-2} \text{s}^{-1}$. In order to achieve this goal, it is required to focus the counter rotating beams -before they collide- using 3 quadrupole magnets, the so called inner triplet. The size of the beam is very small and therefore the alignment of the magnets in the inner triplet is very important, concerning both the position of the inner triplet with respect to the detector and the position of the quadrupoles with respect to each other inside the inner triplet.

The Hydrostatic Leveling System (HLS) has been designed to provide relative measurement of the magnet position, in particular the vertical position and transverse tilt. The sensors of the HLS system have to operate reliable in a complex radiation field created by particles that did not collide head-on in the detector but that were deflected by the strong electromagnetic field of the opposing bunch. These so called collision products have a high forward momentum and are usually lost in first few meters after the experimental cavern, i.e. where the inner triplet is located. Under the cryostat of the low beta quadrupoles where the position sensors are located, there is a strong radiation field with dose rates up to 16,000 Gy/year.

During previously conducted aging tests with ^{60}Co , it was found that the HLS sensors show a strong dependence on the dose rate. In this paper, it will be shown that the charge produced by radiation in the air cavity of the HLS, is deposited on the surface of a capacitance and interpreted by the read-out electronics as a movement of a magnet. It will be shown that this can be corrected with the data provided in this note.

2. Hydrostatic Leveling System

2.1. Operating principles of the HLS

The basic principle of the HLS system consists in measuring the water levels in a closed circuit at various locations. The HLS systems that are used for the particle detectors of the LHC are composed of one hundred hydrostatic sensor units¹ (produced by Fogale Nanotech [2]) interconnected with fluid and air pipes and located in referenced points onto the final focusing quadrupoles. The HLS that are used in this study are shown in Figure 1. A cross section of a sensor is shown in Figure 2.

¹ The term *sensor unit* has to be regarded as the ensemble of measuring sensor surface, electronics and connecting cables.



Figure 1. Two different types of HLS sensors (left: 1st generation, right: 4th generation)

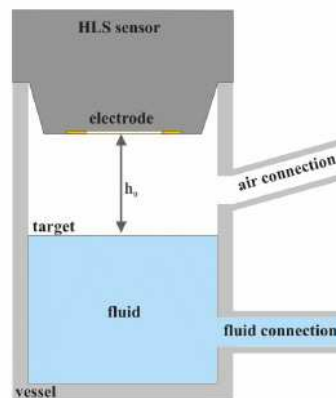


Figure 2. Cross section of a HLS sensor.

The HLS sensors perform hydrostatic leveling measurements with respect to a plane which is the free surface of a water network following the principle of communicating vessels. The continuous monitoring of the relative position is performed by the sensor's surface (electrode) and the water surface (the target). The electrode and the target are separated by air. The electrode is integrated in the top of the vessel. The principle of operation is based on capacitive measurements that determine the distance to the target. When a voltage is applied to one of the plates, the difference between the charge stored on the surfaces of the plates will cause an electric field to exist between them. The amount of existing charge determines the amount of current required to change the voltage on the electrode.

The driver electronics continuously change the voltage on the electrode with an excitation frequency of 4 kHz. The amount of current required to change the voltage on the electrode is detected by the electronics and indicates the amount of capacitance between sensor and target. The change ΔC in capacitance is directly related to the change in the distance between the electrode and the target level [3] as:

$$\Delta C = \frac{\epsilon_o \cdot \epsilon_r \cdot S}{\Delta h} \quad (1)$$

where ε_0 the absolute permittivity of free space (8.85×10^{-12}), ε_r the relative permittivity (dielectric constant) of air, S the surface of the electrode and Δh the variation of the distance between the electrode and the target.

The resulting output voltage is given by equation (2) [3]

$$V_{out} = (V_{offset} + \frac{1}{C_e} \cdot V_e \cdot C_{ref}) \cdot G \quad (2)$$

In this formula C_e is the capacitance value during the measurement, C_{ref} is the reference value of the capacitance (i.e the capacitance for a reference distance between electrode and target that was measured during calibration), V_e is the voltage applied between the plates of the capacitor and G is the gain² of the electronics.

The manufacturing company [2] provides calibration polynomials to compute the offset. For each sensor there is a different polynomial. The one for sensor H7D5-361 is given in equation (3) and the others in Table A1 in the Appendix.

$$h [\text{mm}] = 4.999 + 5.010 \cdot 10^{-1} \cdot V_{out} - 2.647 \cdot 10^{-4} \cdot V_{out}^2 + 1.688 \cdot 10^{-5} \cdot V_{out}^3 \quad (3)$$

The three sensors studied here have undergone a calibration procedure by the manufacturing company during which specific voltage changes are recorded for predefined variations of the gap size. The amount of voltage change for a given amount of gap change is called the sensitivity and for the HLS it is 0.2V/ 100 μm , i.e. for every 100 μm of change in the gap, the output voltage will change 0.2V.

The ambient temperature is measured continuously as the signal ΔV_{out} needs correction for the vessel and water dilatation.

2.2 Radiation induced effects

The physical process inside the sensor is assumed to be similar to those inside an ionization chamber. The technique is based upon the Bragg Gray principle [4], which states that the absorbed dose in a given material can be estimated from the ionization produced in a small gas-filled cavity within the material. The Bragg-Gray principle is presented in detail in the Appendix. This principle applies here because the secondary electron ranges are long compared to the internal dimensions of the HLS chamber.

Ionizing radiation creates ions and electrons in the air between the electrode and the target. In the presence of the applied potential difference, the ions and electrons move in opposite directions. The charge deposited by the particles on the target plate changes the electric field and varies the excitation voltage. The more the ionization, the more the charge produced and collected on the electrode. The amount of existing charge determines how much the voltage has to vary so as to keep the electric field between the electrode and the target stable. Since some charge is already produced by radiation, the system needs to make less 'effort' to charge the electrode.

² Gain is the ratio of signal output from a system to signal input to the system.

At low dose rates, the amount of electron-ion pairs produced in the air between the target and the water level is proportional to the dose. At higher dose rates, more positive and negative ions recombine so that the signal of the HLS eventually saturates.

There are two types of recombination considered in such a chamber: initial (or columnar) recombination and general (or volume) recombination. During initial recombination ions recombine with electrons from the same track while during general recombination ions recombine with electrons from another track.

As the dose rates to the sensors are high, ions are uniformly distributed in the air cavity [5] and therefore general recombination is the dominant effect.

3. Experimental set –up

Three HLS sensors were irradiated with gamma rays from a ^{60}Co source. The source consisted of ten pencil-like sticks with a height of 16 cm and a diameter of 1 cm, with a total activity 13850 Ci. Gamma rays from cobalt-60 are of relatively high energy and have relatively high penetration³ which makes them suitable for these tests. Two different types of HLS were used: the H7D5-361 with a ceramic electrode (1st generation) and the H7D5-372 and H7D5-001, both with a glass electrode (4th generation).

The irradiation was done at different distances from the source so as to vary the dose rate. Measurements were performed at the dose rates 50 Gy/hr, 100 Gy/hr, 500 Gy/hr, 100 Gy/hr and 1500 Gy/hr. The measurements were repeated at the same dose rates but with descending order, i.e from 1500 Gy/hr to 50 Gy/hr, to obtain better statistics of the recorded data. After the end of each irradiation, access was granted so as to change the distance from the source. The data acquisition was performed with two different racks and the data were recorded on two computers, outside the irradiation hall. The HLS electronics were switched on 4 hours before the first irradiation session, for the signal to stabilize. The vacuum pump system was also installed outside the hall in order to be able to perform tests in parallel.

During the experiments the dose rates inside the irradiation hall were monitored by the Radiation Protection Group of the host facility. An independent parallel assessment of the dose received by the sensors (for each dose rate), was also done with the radiophotoluminescent (RPL) glass dosimeters and Alanine dosimeters [6]. The readings of the dosimeters agree within 15% with the reference values. The temperature in the hall remained constant within 10 degrees of Celsius.

³Each disintegration of a ^{60}Co nucleus, which entails the emission of a beta particle, is accompanied by the emission of two gamma photons of energies 1.17 and 1.33 MeV. The gamma photon from ^{60}Co on travels a longer distance than a lower-energy gamma photon (e.g. In the case of a ^{137}Cs source).

4. Experimental results

4.1 Recombination in the sensors

Figure 3 shows the variation of the output voltage as a function of the dose rate (see also Figures a-1 and a-2 in the Appendix for the other sensors). This curve indicates the existence of recombination in the sensor; otherwise it should be a straight line. The analysis is described in the next sections only for sensor H7D5-361. The graphs and Tables for sensors H7D5-372 and H7D5-001 are given in the Appendix.

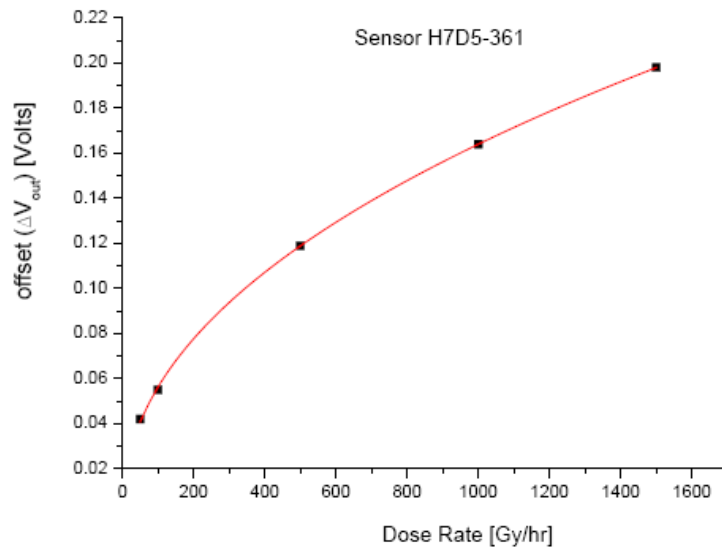


Figure 3. The offset variation of a HLS sensor as a function of the dose rate [Gy/hr] (irradiation with a ^{60}Co source).

4.2 The HLS sensors as condenser ionization chambers

It was initially assumed that the HLS sensors show a similar response with condenser ionization chambers. A condenser chamber is built as a capacitor. A central anode, insulated from the rest of the chamber, is given an initial charge from a charge-reader device. When exposed to photons, the secondary electrons liberated in the walls and enclosed air tend to neutralize the charge on the anode and lower the potential difference between it and the wall. The change in potential difference is directly proportional to the total ionization produced and hence to the exposure. Thus, after exposure to photons, measurement of the change in potential difference from its original value (when the chamber was fully charged) can be used to find the exposure.

The initial assumption that the HLS sensor behaves similarly to condenser chamber and satisfies the Bragg-Gray conditions allows the calculation of the ionization current by the following equation⁴ [7]:

⁴ The reader can find the explanation about the Bragg- Gray principle and the derivation of equation (4) in the Appendix.

$$I_{ion} = \frac{D \cdot m \cdot S_g}{W \cdot S_w} \quad (4)$$

where D is the dose rate in the air inside the sensor, I_{ion} the induced ionization current, m the mass of air inside the sensor, S_g/S_w the ratio of the mass stopping power of the gas and the wall and W a constant that depends on the gas and it has the value 34.1 J/C for air.

This current was calculated assuming that it is a dc current, that the electric field remains constant and that this current can be added to the one flowing in the circuit. In this case, the ionization current induced in the sensor at all different dose rates was calculated and it is given in the second column of Table 1. The third column is the output voltage reduction ΔV_{out} , that is the difference between the sensor's signal during irradiation, V_{out}^{rad} , and the sensor's signal before the irradiation, V_{out} , i.e.

$$\Delta V_{out} = V_{out}^{rad} - V_{out} \quad (5)$$

In order to verify that the ionization current I_{ion} is related to the output voltage of the HLS sensor, the voltage reduction was also calculated by equation (2). The results are presented in the last column of Table 1 (see Table A2 in the Appendix for the other sensors).

Table 1. The ionization current and the voltage decrease in the H7D5-361 sensor at various dose rates.

D [Gy/hr]	I_{ion} [nA] (calculated)	ΔV_{out} [Volts] (measured)	ΔV_{out} [Volts] (calculated)
50	0.50	0.042	0.047
100	1.00	0.055	0.061
500	4.98	0.119	0.132
1000	10.31	0.164	0.183
1500	15.65	0.198	0.221

This table shows that the I_{ion} is not linearly proportional to the offset ΔV_{out} and this verifies the existence of recombination in the HLS sensors.

The ionization current versus the measured output for all different dose rates is shown in Figure 4 along with an exponential growth fit of first order. The errors are less than 0.1% in all cases and it is not possible to show them on the graphs.

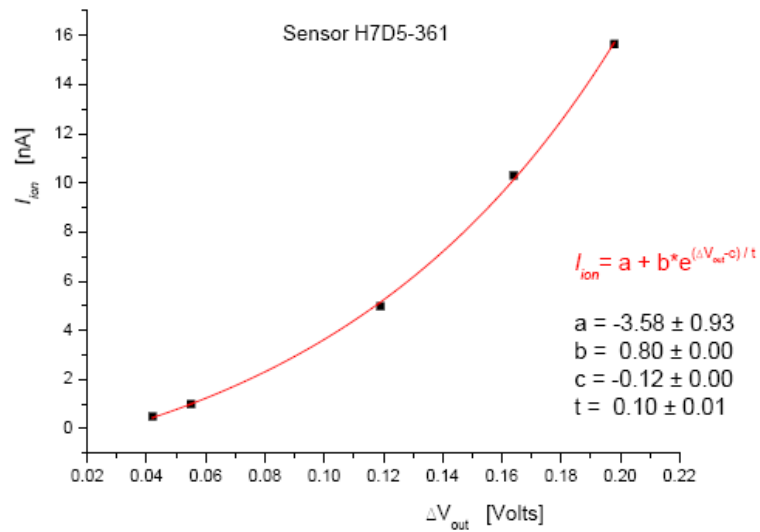


Figure 4. Ionization current versus output potential difference for sensor H7D5-361. The red line is an exponential growth fit of first order.

The corresponding curves for sensors H7D5-372 and H7D5-001 are given in Figures a-3 and a-4 in the Appendix. Figure 5 shows the experimental points for all the sensors and it provides an average polynomial.

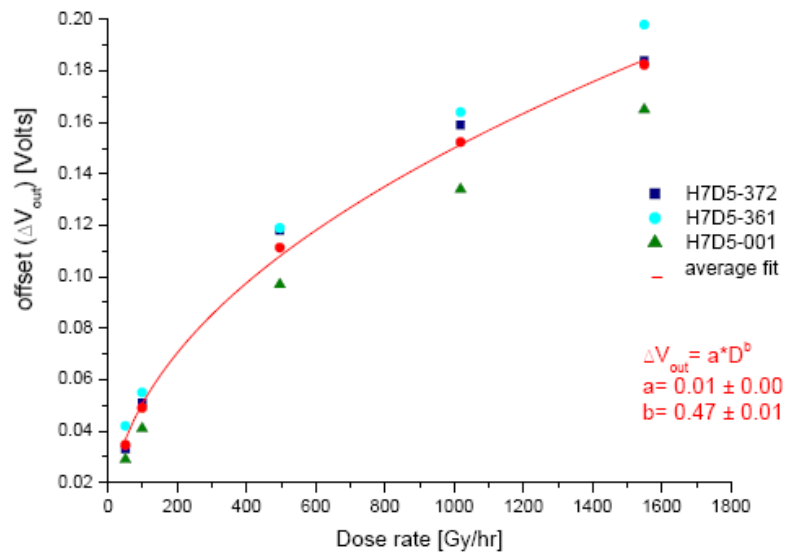


Figure 5. The measured voltage offset for all sensors and the average variation (in red).

4.3. The validity of the calibration polynomials

As discussed in section 2.2, the charge on the electrode is increasing due to ionization in the air inside the sensor and therefore the voltage that is needed to maintain the electric field is reduced. This is interpreted by the electronics as a capacitance change and the output voltage decreases. In other words this effect is due to the electronics design rather than a real ‘internal movement’ of the HLS sensor and it explains the fact that the offset is observed only during the exposure of the HLS to radiation.

To correct the signal, the calibration polynomials can be used. Using equation (2) with the values of the parameters given in Table 2, one can calculate the theoretical variation of capacitance, for different dose rates. Then, by equation (4), the distance between electrode and target can be derived. Since the nominal distance between electrode and target is known (from the value of the capacitance before irradiation), the *hypothetical* offset (in microns) due to radiation can be obtained.

Table 2: Parameters used for the calculation of the capacitance variation.

Parameter	offset [mm] (theoretical)
V_{off}	-4.55
C_{ref}	0.11
V_e	9.00
G	2.23

The offsets that were calculated as described above are denoted as ‘experimental’ while the calculations with the use of polynomials are denoted as ‘theoretical’. The comparison between experimental and theoretical values is given in Table 3 for sensor H7D5-361 (see also Table A3 in the Appendix for the other sensors).

Table 3: Comparison of the two methods (experimental –theoretical) for the offset calculation.

Dose rate [Gy/hr]	Δh [mm] (theoretical)	Δh [mm] (experimental)	Difference (%)
50	21.10	21.06	0.21
100	27.34	27.29	0.21
500	59.18	59.06	0.20
1000	81.79	81.64	0.19
1500	98.96	98.79	0.18

This comparison confirms that the calibration polynomials are valid under irradiation.

4.4. General recombination in the HLS

A proof of the existence of recombination in the chamber is the non linear variation of the collection efficiency of the electrode with radiation [5]. The collection efficiency of a condenser chamber at a voltage V is given by the following equation:

$$f_{av} = \frac{1}{[1 + (1/6\lambda) \cdot \xi_0^2]} \quad (6)$$

where the parameter ξ_0 is given by the formula $\xi_0 = m \cdot (h^2 \sqrt{q/V_0})$, λ is the ratio of the original voltage over the final voltage (i.e. V/V_0), m a constant depending on the gas in the chamber, h is the distance between electrode and target and q the ionization intensity in units $[\text{esu}/\text{cm}^3/\text{s}]$.

It was possible to find in the bibliography [5], curves that predict the collection efficiency at certain dose rates (Figure 6). These curves were calculated in the 80's for condenser ionization chambers and due to lack of high energy experiments at that time, there are no reference data for very high dose rates.

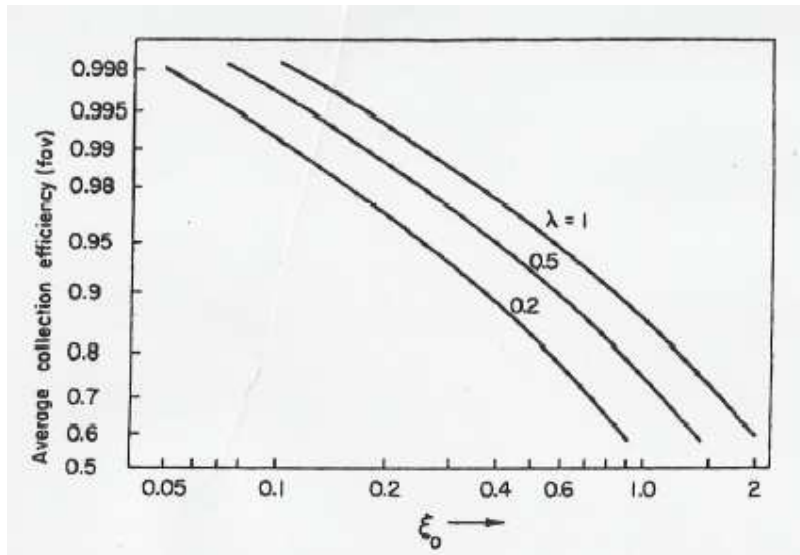


Figure 6. Average collection efficiency of a condenser chamber exposed to continuous radiation. For accuracy in reading, logarithmic scale is used. ξ_0 is based on the initial voltage and λ is the ratio of the voltage on the chamber after irradiation to the initial voltage.

The results for the collection efficiency are presented in Table 4 for all sensors. The agreement between the reference data and the calculations is very good and there is no evidence that the reference data provide correct results for low dose rates but not for high ones.

From the collection efficiency one can easily calculate the saturation current I_{sat} . This is given in the third column of Table 4. The I_{sat} is the current that should be measured if all the ions formed in chamber by the radiation were able to reach the electrode. The difference between I_{ion} and I_{sat} indicates the recombination in the

chamber. This is given in the last column of Table 4. The values for the other sensors are given in Table A4 in the Appendix.

Table 4: The collection efficiency of the electrode of HLS (all types). The data are compared with theoretical values derived from graphs in the bibliography [5].

SENSOR 361					
Dose Rate [Gy/hr]	Average calculated collection efficiency f_{av}	Theoretical collection efficiency (bibliography)	$I_{sat} = I_{ion} / f_{av}$	ionization current I_{ion} (calculated)	General recombination (%)
50	0.85	0.87	0.56	0.47	16.07
100	0.74	0.77	1.26	0.93	26.19
500	0.37	no exp. data available	12.72	4.66	63.36
1000	0.22		43.73	9.67	77.88
1500	0.16		92.20	14.67	84.09

4.5. The HLS and the LHC radiation environment

The HLS will be installed on the external metrological reference points of the low beta quadrupoles of the LHC, in a very high radiation environment. The ATLAS and CMS experiments involve the highest dose rates and only these cases are considered and discussed. Rough estimates of various radiological parameters associated with the inner triplet of the high luminosity insertions of the LHC can be found in [8, 9]. Monte Carlo calculations have shown that very close to the quadrupoles, any equipment installed will have to resist an irradiation of 16 kGy per year of operation. A year of operation corresponds to around 140 days for production physics. Assuming an optimum run time of 12 hours, it follows that the HLS will have to resist dose rates up to 10 Gy/hr for the first year of the LHC operation. Such dose rates will have no effect on the lifetime of the HLS but as it can be seen by the previous graphs they will provoke an offset of about 10 microns to the HLS reading. The dose rates however will be monitored on line by the RADMON system and a fill-to-fill correction will be possible.

5. Summary and conclusions

The signal from the sensors for the Hydrostatic Leveling System of the LHC will be modified when exposed to ionizing radiation. The radiation induced charge is accumulated on the capacitor plates and provokes a voltage variation in the sensor which is operated at a constant electric field. By assuming a constant ionization current, the HLS can be compared to a condenser type ionization chamber. This model is in good agreement with the experimental data and can be used to predict the HLS offset at arbitrary dose rates.

In addition, the experiments at Saclay have shown that the HLS sensors do not show any signs of aging. The radiation resistance of the HLS electronic readout is approximately 200 Gy Total Ionising Dose and comparable to standard Commercial Off the Shelf Components.

Within the purposes of this technical note it was also possible to verify that the collection efficiency of the electrode varies with the dose and in particular that the approach to saturation depends on the dose rate, a well known effect in condenser ionization chambers.

During the LHC operation, the HLS may show radiation induced offsets of the order of a few microns. The signal of the HLS can be corrected with a model based on the study provided in this note.

References

1. LHC Design Report, Volumes I- III, CERN.
2. <http://www.fogale.fr>
3. F. Ossart, Fogale Nanotech [private communication]
4. Attix F.H., Roesch W.C. and Tochilin E., 'Radiation Dosimetry, II; 9. Academic Press, New York (1966).
5. J. W. Boag, *The Dosimetry of Ionizing Radiation*, edited by K. R. Kase B. E. Bjarngard, and F. H. Attix, Vol. 2 Chap. 3, Academic Press, Orlando, (1987).
6. H. Vincke, SC-RP, CERN (private communication).
7. J. Turner 'Atoms, Radiation and Radiation Protection' Eds J. Wiley & Sons Inc, 2nd Edition, (1995).
8. M. Huhtinen and G.R Stevenson, *Energy deposition, star densities and shielding requirements around the inner triplet of the high luminosity insertions of the LHC*, CERN Divisional Report TIS-RP/IR/95-16 (1995), LHC Note 338.
9. M. Huhtinen and G.R Stevenson, *Estimates of dose to Components in the LHC Tunnel close to the Quadrupoles of the High- luminosity Low- beta regions*, LHC Project Note 22.

APPENDIX

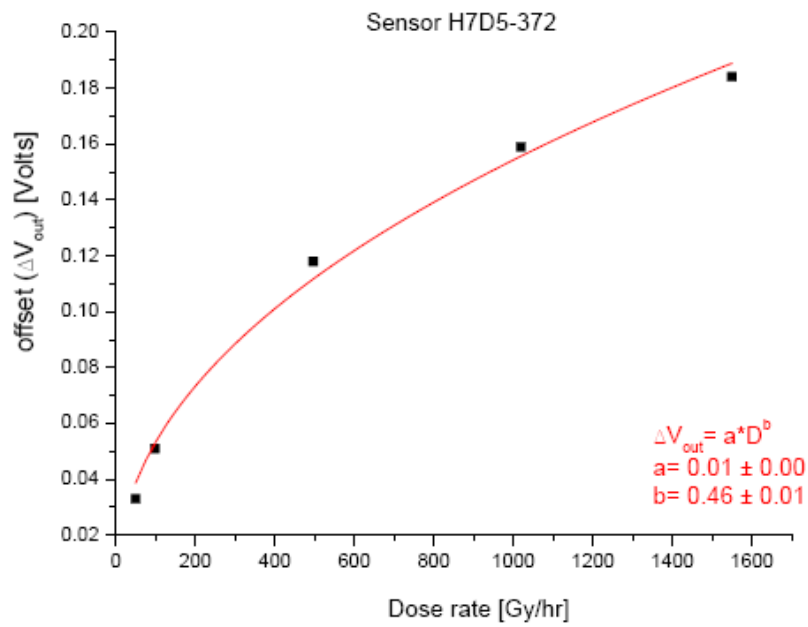


Figure a-1. The offset variation as a function of the dose rate [Gy/hr] (irradiation with a ^{60}Co source).

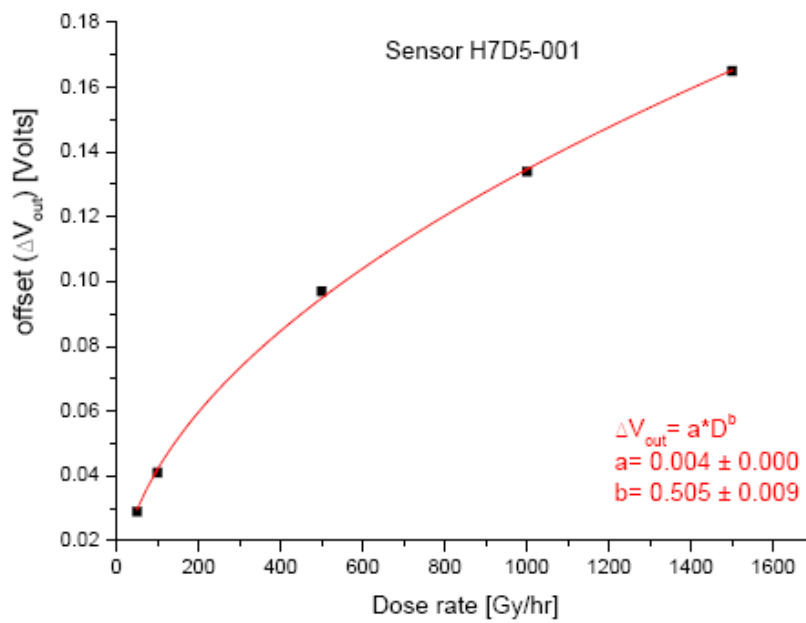


Figure a-2. The offset variation as a function of the dose rate [Gy/hr] (irradiation with a ^{60}Co source).

The Bragg- Gray principle

The Bragg- Gray principle states that if a gas is enclosed by a wall of the same atomic composition and if the wall thickness is not so great to attenuate appreciably the incident radiation, then the energy absorbed per unit mass in the gas is equal to the number of ion pairs produced there times the W value divided by the mass m of the gas. Furthermore, the absorbed dose D_g in the gas is equal to the absorbed dose D_w in the wall. Denoting the number of ions in the gas by N_g , one can write:

$$D_w = D_g = \frac{N_g \cdot W}{m} \quad (i)$$

When the wall and gas are of different atomic composition, the absorbed dose in the wall can still be obtained from the ionization in the gas. In this case, the cavity size and gas pressure must be small, so that secondary charged particles lose only a small fraction of their energy in the gas. The absorbed dose scales as the ratio S_w/S_g of the mass stopping powers of the wall and gas:

$$D_w = \frac{D_g \cdot S_w}{S_g} = \frac{N_g \cdot W \cdot S_w}{m \cdot S_g} \quad (ii)$$

If the dose rate \dot{D} is measured, then equation (ii) becomes

$$\dot{D}_w = \frac{I_{ion} \cdot W \cdot S_w}{m \cdot S_g}$$

where I_{ion} is the ionization current induced by radiation.

Table A1. The calibration polynomials of Fogale Nanotech for the HLS sensors

Sensor	Polynomial ($y \rightarrow$ [mm], $V \rightarrow$ [Volts])
372	$y = 4.99927 + 0.509377 \cdot V - 0.0023040 \cdot V^2 + 0.00013632 \cdot V^3$
001	$y = 4.99913 + 0.508767 \cdot V - 0.0022748 \cdot V^2 + 0.00013938 \cdot V^3$

Table A2.

Type of sensor	Dose rate [Gy/hr]	Ionisation current [nA] (calculated)	dV(Volts) (measured)
H7D5-372 (generation 4)	50	0.50	0.033
	100	1.00	0.051
	500	4.98	0.118
	1000	10.31	0.159
	1500	15.65	0.184
H7D5-001 (generation 2)	50	0.77	0.029
	100	1.53	0.041
	500	7.64	0.097
	1000	15.83	0.134
	1500	24.03	0.165

Table A3: Comparison of the two methods (experimental –theoretical) for the offset calculation.

Sensor	offset [mm] (theoretical)	Offset [mm] (experimental)	Difference (%)
372	16.55	16.53	0.13
	22.12	25.61	15.78
	52.93	58.82	11.12
	73.30	79.03	7.82
	88.87	91.74	3.23
001	14.70	14.71	0.05
	18.02	18.04	0.07
	44.27	44.30	0.07
	61.88	61.92	0.07
	77.18	77.22	0.06

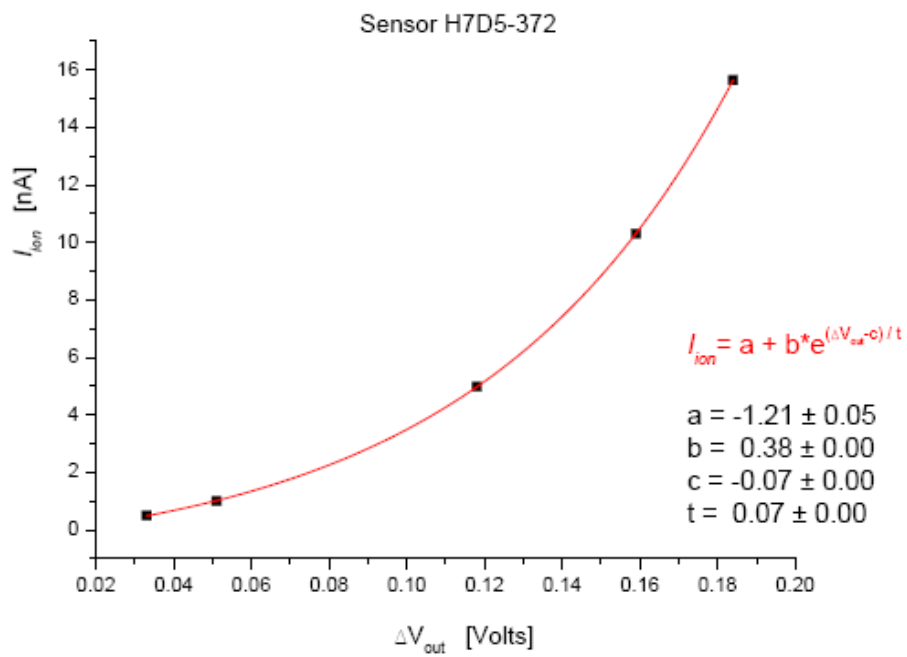


Figure a-3. Ionization current versus output potential difference for sensor H7D5372.

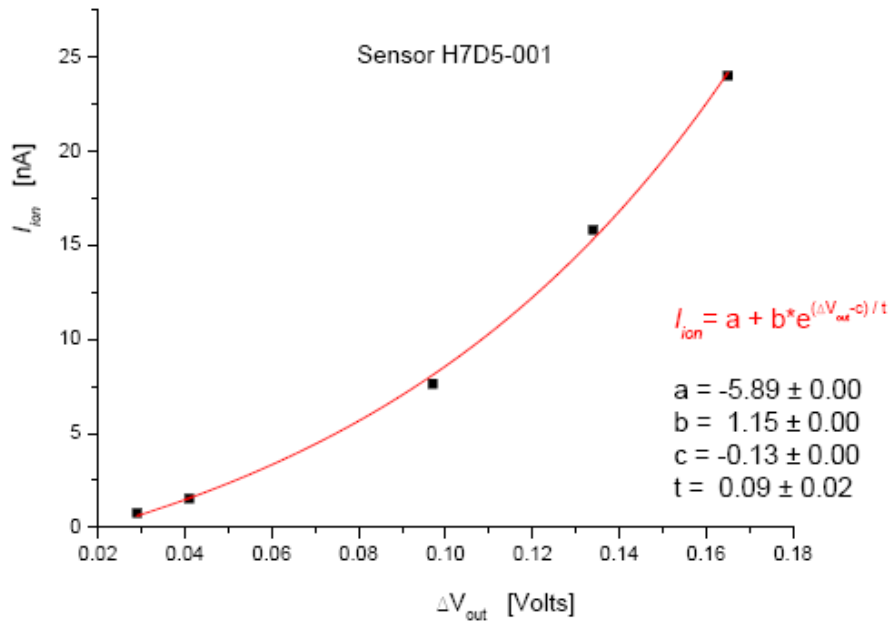


Figure a-4. Ionization current versus output potential difference for sensor H7D5001.

Table A4. The collection efficiency of sensors H7D5-372 and H7D5-001

	f_{av}	Theoretical (bibliography)	$I_s = I / f_{av}$	measured I_{ion}	Recombination (%)
Sensor H7D5372	0.85	0.87	0.59	0.50	15.25
	0.74	0.77	1.35	1.00	26.12
	0.37	no value available	13.57	4.98	63.33
	0.22		46.72	10.31	77.93
	0.16		98.76	15.65	84.15
Sensor H7D5001	0.85	0.87	0.91	0.77	15.07
	0.74	0.77	2.06	1.53	25.88
	0.37	no value available	20.72	7.64	63.12
	0.22		71.22	15.83	77.77
	0.16		149.94	24.03	83.97

C.2 Radiation induced effects on the sensors of the Hydrostatic Levelling System for the LHC low beta quadrupoles

E. Dimovasili, A. Herty, H. Mainaud Durand, A. Marin, F. Ossart and T. Wijnands

The response of the Hydrostatic Leveling System (HLS) for the final focusing quadrupole magnets in the Large Hadron collider is dose rate dependent. At high dose rates, ionization of the air inside the sensors causes charge deposition and this perturbs the position measurement. A model is presented that corrects the HLS signal offset as a function of the dose rate.

Radiation and its Effects on Components and Systems (RADECS) conference, Cap d'Agde, France, 2005



Radiation induced effects on the sensors of the Hydrostatic Leveling System for the LHC low beta quadrupoles

E. Dimovasili, A. Herty, H. Mainaud Durand, A. Marin, F. Ossart, T. Wijnands

Abstract— The response of the Hydrostatic Leveling System (HLS) for the final focusing quadrupole magnets in the Large Hadron collider is dose rate dependent. At high dose rates, ionization of the air inside the sensors causes charge deposition and this perturbs the position measurement. A model is presented that corrects the HLS signal offset as a function of the dose rate.

Index Terms—LHC, Low beta quadrupoles, alignment, HLS, radiation, ionization

I. INTRODUCTION

The Large Hadron Collider (LHC) [1] is a 7 TeV energy proton collider under construction at CERN. The aim of this machine that will become operational in 2007 is to inject, accelerate and collide two proton beams of 10^{11} particles. At the interaction points large detectors will detect the collision products. A very important performance parameter is the luminosity which is proportional to the number of collisions per second and for the LHC it will reach the value $10^{34} \text{cm}^{-2} \text{s}^{-1}$. In order to achieve this goal, it is required to focus the two beams -before collision- using 3 quadrupole magnets, the so called inner triplet. The size of the beam is very small and therefore the alignment of the magnets in the inner triplet is very important, concerning both their relative position with respect to the detector and with respect to each other.

The Hydrostatic Leveling System (HLS) will provide relative measurements of the vertical magnet position and its transverse tilt. The sensors of the HLS system have to operate reliable in a complex radiation field, as at their location (under the cryostat of the low beta quadrupoles) there is a strong radiation field with dose rates up to 16,000 Gy/year.

Manuscript received September 16, 2005.

E. Dimovasili, A. Herty H. Mainaud Durand, A. Marin and T. Wijnands are with CERN (The European Organisation for Nuclear Research, 1211 Geneva 23 Switzerland), phone: +41-22 767 3212, Fax: +41-22 767 9080, e-mail: Evangelia.Dimovasili@cern.ch.
F. Ossart is with FOGALE Nanotech, Parc Kennedy-Bât A3, 285 Rue Gilles Berberal, F-30915, Nîmes Cedex

During previously conducted aging tests with ^{60}Co , it was found that the HLS sensors show a strong dependence on the dose rate. In this paper, it will be shown that the charge produced by radiation in the air cavity of the HLS, is deposited on the surface of a capacitance and interpreted by the read-out electronics as a movement of a magnet. This offset can be corrected with the data provided in this paper.

II. HYDROSTATIC LEVELING SYSTEM

A. Operating principles of the HLS

The basic principle of the HLS system consists in measuring the water levels in a closed circuit. The systems that are used for the particle detectors of the LHC are composed of one hundred hydrostatic sensor units [2] interconnected with fluid and air pipes and located in referenced points onto the final focusing quadrupoles. The HLS along with a cross section are shown in Fig. 1.

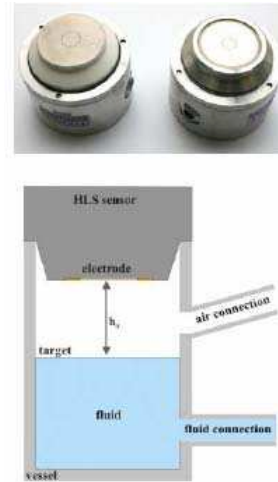


Fig. 1. (upper) Two different HLS sensors, (lower) a cross section of a HLS sensor.

The HLS sensors perform hydrostatic leveling measurements with respect to a plane which is the free surface of a water network following the principle of communicating vessels. The continuous monitoring of the relative position is performed by the sensor's surface (electrode) and the water surface (the target). The electrode and the target are separated by air. The electrode is integrated in the top of the vessel. The principle of operation is based on capacitive measurements that determine the distance to the target. When a voltage is applied to one of the plates, the difference between the charge stored on the surfaces of the plates will cause an electric field to exist between them. The amount of existing charge determines the amount of current required to change the voltage on the electrode.

The driver electronics continuously change the voltage on the electrode with an excitation frequency of 4 kHz. The amount of current required to change the voltage on the electrode is detected by the electronics and indicates the amount of capacitance between sensor and target. The change ΔC in capacitance is directly related to the change in the distance between the electrode and the target level [3] as:

$$\Delta C = \frac{\epsilon_0 \cdot \epsilon_r \cdot S}{\Delta h} \quad (1)$$

where ϵ_0 the absolute permittivity of free space (8.85×10^{-12} F/m), ϵ_r the relative permittivity (dielectric constant) of air, S the surface of the electrode and Δh the variation of the distance between the electrode and the target.

The resulting output voltage is given by equation (2) [3]

$$V_{out} = (V_{offset} + \frac{1}{C_e} \cdot V_e \cdot C_{ref}) \cdot G \quad (2)$$

B. Radiation induced effects

The physical process inside the sensor is assumed to be similar to those inside an ionization chamber. The Bragg Gray principle is applied here [4], which states that the absorbed dose in a given material can be estimated from the ionization produced in a small gas-filled cavity within the material. This principle is valid because the secondary electron ranges are long compared to the internal dimensions of the HLS chamber.

Ionizing radiation creates ions and electrons in the air between the electrode and the target. In the presence of the applied potential difference, the ions and electrons move in opposite directions. The charge deposited by the particles on the target plate changes the electric field and varies the excitation voltage. The more the ionization, the more the charge produced and collected on the electrode. The amount of existing charge determines how much the voltage has to

vary so as to keep the electric field between the electrode and the target stable. Since some charge is already produced by radiation, the system needs to make less 'effort' to charge the electrode. At low dose rates, the amount of electron-ion pairs produced in the air between the target and the water level is proportional to the dose. At higher dose rates, more positive and negative ions recombine so that the signal of the HLS eventually saturates. The dose rates to the sensors are high and ions are uniformly distributed in the air cavity [5], therefore it is assumed that general recombination is the dominant effect.

C. Experimental set-up

Three HLS sensors were irradiated with gamma rays from a ^{60}Co source. Two different types of HLS were used: the H7D5-361 with a ceramic electrode (1st generation) and the H7D5-372 and H7D5-001, both with a glass electrode (4th generation).

The irradiation was done at different distances from the source so as to vary the dose rate. Measurements were performed at the dose rates 50 Gy/hr, 100 Gy/hr, 500 Gy/hr, 100 Gy/hr and 1500 Gy/hr. The measurements were repeated once at the same dose rates but with descending order, i.e from 1500 Gy/hr to 50 Gy/hr. The HLS electronics were switched on 4 hours before the first irradiation session, for the signal to stabilize. The vacuum pump system was also installed outside the hall in order to be able to perform tests in parallel. The temperature in the hall remained constant within 10 degrees of Celsius.

D. Experimental results

The variation of the output voltage as a function of the dose rate is shown in Fig. 2. The experimental data for all the sensors are plotted along with an average exponential growth polynomial. The shape of the curve indicates the existence of recombination in the sensor.

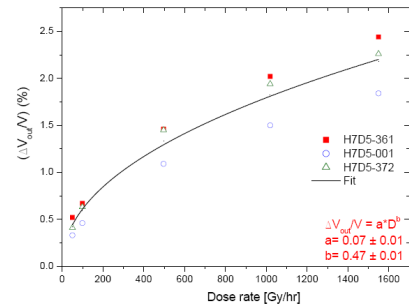


Fig. 2. The measured voltage offset for all sensors and the average variation (in black).

It was initially assumed that the HLS sensors show a similar response with condenser ionization chambers [5]. This allows the calculation of the ionization current by the following equation [7]:

$$I_{ion} = \frac{D \cdot m \cdot S_g}{W \cdot S_w} \quad (3)$$

where D is the dose rate in the air inside the sensor, I_{ion} the induced ionization current, m the mass of air inside the sensor, S_g/S_w the ratio of the mass stopping power of the gas and the wall and W a constant that depends on the gas and it has the value 34.1 J/C for air.

This current was calculated assuming that it is a dc current, that the electric field remains constant and that it can be added to the one flowing in the circuit. In this case, the ionization current induced in the sensor at all different dose rates was calculated and it is given in Table 1. The fourth column is the relative output voltage reduction $\Delta V_{out}/V$, (ΔV_{out} is the difference between the sensor's signal during irradiation, V_{out}^{rad} , and the sensor's signal before the irradiation, V_{out} , i.e.

$$\Delta V_{out} = V_{out}^{rad} - V_{out} \quad (4)$$

In order to verify that the ionization current I_{ion} is linked to the variation of the output voltage of the HLS sensor, the relative voltage reduction was calculated by equation (2). The results are given in Table 1.

TABLE I
THE IONIZATION CURRENT AND THE VOLTAGE DECREASE
IN THE HLS SENSORS AT VARIOUS DOSE RATES

Sensor	Dose rate [Gy/hr]	I_{ion}	$\Delta V_{out}/V$ (%) (meas)	$\Delta V_{out}/V$ (%) (calc)
H7D5-361	50	0.50	0.52	0.46
	100	1.00	0.67	0.60
	500	4.98	1.46	1.29
	1000	10.31	2.02	1.79
	1500	15.65	2.44	2.16
H7D5-001	50	0.77	0.33	0.29
	100	1.53	0.46	0.41
	500	7.64	1.09	0.98
	1000	15.83	1.50	1.34
	1500	24.03	1.84	1.65
H7D5-372	50	0.50	0.41	0.36
	100	1.00	0.63	0.56
	500	4.98	1.45	1.28
	1000	10.31	1.94	1.72
	1500	15.65	2.26	2.00

Table 1 shows that the ionization current (I_{ion}) is not

linearly proportional to the offset ΔV_{out} . This verifies the existence of recombination in the HLS sensors. The ionization current versus the measured output for all different dose rates is shown in Fig. 3 along with exponential growth fits of first order. The errors are less than 0.1% in all cases and they do not appear on the plot.

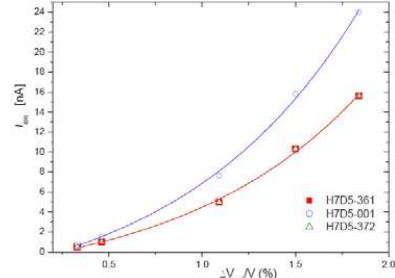


Fig. 3. Ionization current versus output potential difference for all sensors. The lines are exponential growth fits of first order.

III. DISCUSSION AND CONCLUSIONS

The signal from the sensors for the Hydrostatic Leveling System of the LHC will be modified when exposed to ionizing radiation. The radiation induced charge is accumulated on the capacitor plates and provokes a voltage variation in the sensor which is operated at a constant electric field. By assuming a constant ionization current, the HLS can be compared to a condenser type ionization chamber. This model is in good agreement with the experimental data and can be used to predict the HLS offset at arbitrary dose rates. It was found that the charge on the electrode is increasing due to ionization in the air inside the sensor and therefore the voltage that is needed to maintain the electric field is reduced. This is interpreted by the electronics as a capacitance change and the output voltage decreases. In other words this effect is due to the electronics design rather than a real 'internal movement' of the HLS sensor and it explains the fact that the offset is observed only during the exposure of the HLS to radiation.

In addition, the experiments at Saclay have shown that the HLS sensors do not show any signs of aging. The radiation resistance of the HLS electronic readout is approximately 200 Gy Total Ionising Dose and comparable to standard Commercial Off the Shelf Components. During the LHC operation, the HLS may show radiation induced offsets of the order of a few microns. The signal of the HLS can be corrected with a model based on the study provided here.

The HLS will be installed on the external metrological reference points of the low beta quadrupoles of the LHC, in a very high radiation environment. Rough estimates of various

radiological parameters associated with the inner triplet of the high luminosity insertions of the LHC can be found in [8, 9].

The HLS will have to resist dose rates up to 10 Gy/hr for the first year of the LHC operation. Such dose rates will have no effect on the lifetime of the HLS but they will provoke an offset of about 10 microns to the HLS reading.

REFERENCES

- [1] LHC Design Report, Volumes I- III, CERN.
- [2] <http://www.fogale.fr>
- [3] F. Ossart, Fogale Nanotech [private communication]
- [4] Attix F.H., Roesch W.C. and Tochilin E., 'Radiation Dosimetry, II; 9. Academic Press, New York (1966).
- [5] J. W. Boag, The Dosimetry of Ionizing Radiation, edited by K. R. Kase B. E. Bjarngard, and F. H. Attix, Vol. 2 Chap. 3, Academic Press, Orlando, (1987).
- [6] H. Vincke, SC-RP, CERN (private communication).
- [7] J. Turner 'Atoms, Radiation and Radiation Protection' Eds J. Wiley & Sons Inc, 2nd Edition, (1995).
- [8] M. Huhtinen and G.R Stevenson, Energy deposition, star densities and shielding requirements around the inner triplet of the high luminosity insertions of the LHC, CERN Divisional Report TIS-RP/IR/95-16 (1995), LHC Note 338.
- [9] M. Huhtinen and G.R Stevenson, Estimates of dose to Components in the LHC Tunnel close to the Quadrupoles of the High- luminosity Low- beta regions, LHC Project Note 22.



Radiation Induced Effects on the Hydrostatic Leveling System of the LHC Low Beta Quadrupoles

E. Dimovasilis[†], A. Herty[‡], H. Mainaud Durand[†], A. Marin[†], F. Ossart[†], T. Wijnands[†]

Introduction

The Large Hadron Collider (LHC) is a high energy proton accelerator presently under construction at CERN.

The Hydrostatic Leveling System (HLS) will be placed on reference points on the inner triplet magnets that will focus the LHC beams before they collide.

Proton losses and interaction of protons with residual gas molecules create a strong radiation field in these areas with dose rates up to 16,000 Gy/year.

The HLS shows a strong dependence on dose rate that is interpreted by the read-out electronics as an offset movement.

Operating Principles Of The HLS

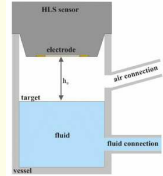


The HLS sensors perform hydrostatic leveling measurements with respect to a plane which is the free surface of a water network following the principle of communicating vessels.

- ✓ The continuous monitoring of the relative position is performed by the sensor's surface (electrode) and the water surface (the target).
- ✓ Capacitive measurements determine the distance to the target. The change ΔC in capacitance is directly related to the change in the distance between the electrode and the target level as:

$$\Delta C = \frac{\epsilon_0 \cdot \epsilon_r \cdot S}{\Delta h}$$

where ϵ_0 the absolute permittivity of free space (8.85×10^{-12} F/m),
 ϵ_r the relative permittivity (dielectric const.) of air,
 S the surface of the electrode and
 Δh the variation of the distance between the electrode and the target.



Experiments at CEA Scaly



PAGURE irradiator: ^{60}Co source (activity ~14 kCi)
 Dose rates: 30 Gy/hr to 1 kGy/hr (large volumes)
 30 Gy/hr to 20 kGy/hr (small volumes)

Radiation Induced Effects

Physical process inside the sensor similar to ionization chamber

Bragg Gray principle

$$I_m = \frac{D \cdot m \cdot S_e}{W \cdot S_c}$$

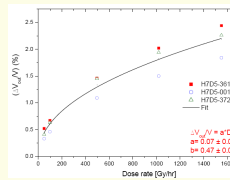
Ionizing radiation creates ions and electrons in the air cavity
 → Due to applied potential difference → ions and electrons move in opposite directions
 Charge deposited on the target plate changes the electric field and varies the excitation voltage

At low dose rates, low number of electron-ion pairs produced

At high dose rates, more recombination → HLS signal saturates

Results

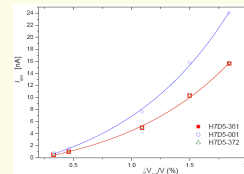
The measured voltage offset for all sensors and the average variation (in black)



The ionization current and the voltage decrease in a HLS sensor at various dose rates

Sensor	Dose rate [Gy/hr]	I_{ion}	$\Delta V_{out}/V$ (%) (meas)	$\Delta V_{out}/V$ (%) (calc)
H7D5-361	50	0.50	0.52	0.46
	100	1.00	0.67	0.60
	500	4.98	1.46	1.29
	1000	10.31	2.02	1.79
	1500	15.65	2.44	2.16

Ionization current versus output potential difference for all sensors. The lines are exponential growth fits of first order



Conclusions

- ✓ HLS signal modified when exposed to ionizing radiation
- ✓ HLS can be compared to a condenser type ionization chamber
- ✓ HLS do not show any signs of aging
- ✓ Radiation tolerance of HLS electronic readout is ~200 Gy Total Ionising Dose
- ✓ During LHC operation, HLS may show radiation induced offsets ~ a few microns
- ✓ The signal of the HLS can be corrected with the proposed model

[†] CERN
 European Laboratory for Particle Physics
 Geneva 23
 1211 Switzerland



[‡] FOGALE Nanotech
 Parc Kennedy, Bat-A3, 285 Rue Gilles Roberval
 F30915, Nîmes Cedex

C.3 Combined levelling systems for the vertical monitoring of a large physics experiment

Jean-Christophe Gayde, Andreas Herty, Hélène Mainaud Durand, Christian Lasseur

The European Organization for Nuclear Research (CERN) is building the largest particle accelerator in the world to find out about the fundamental elements. A 27 km long accelerator ring and four experiments will be part of the new LHC for which the end of installation is planned on 2007. One of these experiments, named ATLAS, is installed in a new huge cavern located 90 m deep below ground level, with a height of 35 m and a surface of 53 m x 35 m. One of the main problems that this experiment is facing is the ability to inspect and react to any movement in the floor level, relative to the LHC beam which is 12 m higher. In addition, the assembly of the ATLAS detector is done step by step and therefore the load to the supports and to the floor changes subsequently. In order to monitor continuously at better than 50 μm accuracy the relative movements of the bedplates which support the detector, a Hydrostatic Levelling System (HLS) composed of six sensors has been installed on them. Then, at regular intervals, the position of this system is measured relatively to the LHC beam line, using vertical distance measurements with optical levelling. This paper will describe the HLS system installed as well as the methods and instrumentation used for the positioning with respect to the LHC beam line, concluding with measurements and results over more than two years.

3rd IAG Symposium on Geodesy for Geotechnical and Structural Engineering and 12th FIG Symposium on Deformation Measurements, Baden, Austria, 2006

COMBINED LEVELLING SYSTEMS FOR THE VERTICAL MONITORING OF A LARGE PHYSICS EXPERIMENT

*Jean-Christophe Gayde, Andreas Herty, Hélène Mainaud Durand, Christian Lasseur
European Organization for Nuclear Research, CERN, TS/SU
Email: forename.surname@cern.ch*

Abstract: The European Organization for Nuclear Research (CERN) is building the largest particle accelerator in the world to find out about the fundamental elements. A 27 km long accelerator ring and four experiments will be part of the new LHC¹ for which the end of installation is planned on 2007. One of these experiments, named ATLAS², is installed in a new huge cavern located 90 m deep below ground level, with a height of 35 m and a surface of 53 m x 35 m. One of the main problems that this experiment is facing is the ability to inspect and react to any movement in the floor level, relative to the LHC beam which is 12m higher. In addition, the assembly of the ATLAS detector is done step by step and therefore the load to the supports and to the floor changes subsequently. In order to monitor continuously at better than 50 μm accuracy the relative movements of the bedplates which support the detector, a Hydrostatic Levelling System (HLS) composed of six sensors has been installed on them. Then, at regular intervals, the position of this system is measured relatively to the LHC beam line, using vertical distance measurements with optical levelling. This paper will describe the HLS system installed as well as the methods and instrumentation used for the positioning with respect to the LHC beam line, concluding with measurements and results over more than two years.

1. Introduction

The LHC is the new 27 km long particle accelerator project at CERN in Geneva, Switzerland which will come in operation in 2007.

Large physics detectors (ALICE³, ATLAS, CMS⁴, LHCb⁵) are being installed in huge caverns at the four interaction points. These detectors aim to study very high energy collisions of proton beams with the best precision possible and are being built from many separate pieces of structure, from central tracking units, to end caps closing the system.

The performance of these physics experiments depends on the intrinsic precision of sub-detectors and of their positioning on the Nominal Beam Line of the LHC machine.

One of the main problems that the ATLAS experiment is facing is the ability to inspect and to anticipate any movement in the floor level, relative to the LHC beam which is 12 m higher.

¹ LHC Large Hadron Collider

² ATLAS A Toroidal LHC ApparatuS

³ ALICE A Large Ion Collider Experiment

⁴ CMS Compact Muon Solenoid

⁵ LHCb Large Hadron Collider beauty experiment

The next chapters describe the ATLAS experiment, the Hydrostatic Levelling System (HLS), and methods which have been implemented to monitor the floor and supporting structure stability.

2. The ATLAS experiment monitoring system

The ATLAS experiment is being built step by step in a cavern of 53 m long, 35 m large, and 35 m high. It is made of physics detectors and of a magnet system assembled in a typical onion layout. The overall dimensions of the experiment are 25 m long, 20 m diameter and the total weight is near 7000 t.

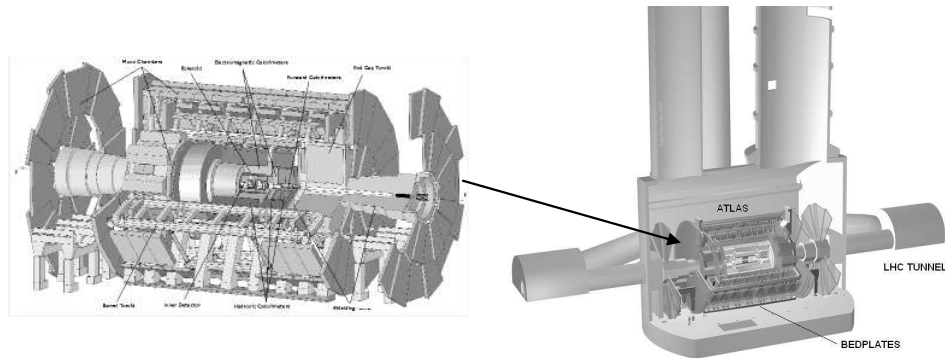


Figure 1: The ATLAS experiment

Except for the forward big wheels muon detectors fixed to the cavern walls ATLAS is supported by nine pairs of feet standing on 20 m long big stainless steel rails – the bedplates - fixed to the 5 m thick concrete floor.

According to the civil engineering simulations a long term 1mm per year heave of the floor is predicted for several years after the excavation phase due to hydrostatic pressure. In addition a short term settlement of 4 mm due to the weight of the experiment is expected.

Due to the mechanical conception of the detector, the adjustment will be very difficult. The aim of the floor stability monitoring is to confirm and refine these predictions. This allows anticipating the experiment movements during the assembly phase in order to have it aligned on the LHC beam line with the nominal luminosity on 2010 as requested by the physics collaboration.

To monitor the ATLAS movements with respect to the LHC beam line a combined method has been implemented. A HLS system has been installed on the ATLAS bedplates feet used as a remote, long term monitoring tool to measure the deformations during the construction of the detector and to provide real-time observations during the operation of the experiment. The stability of the cavern floor with respect to the LHC machine geometry is measured using optical precision levelling performed at regular intervals. The HLS observations and the optical levelling measurements can be analysed together in the same geodetic network.

3. Bedplates HLS – Principle and Examples

3.1. Hydrostatic Levelling System

The HLS sensors provide vertical distances with respect to the equipotential water surface of the hydraulic network, which is the reference height. This system works according to the principle of the communicating vessels.

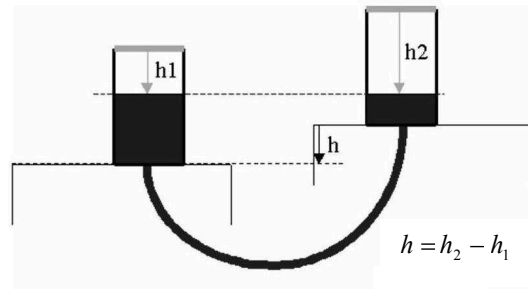


Figure 2: principle of communicating vessels

The water network is composed of vessels connected to each other by pipes, partially filled with water, allowing water and air to circulate freely. In order to eliminate the effects of the differential variations of atmospheric pressure, the whole pipe work system is only open to atmosphere at one point. To avoid salt deposition and the growth of flora and micro fauna, demineralised water is used with a biocide additive.

Sensors – associated to each vessel – determine the distance to the surface of the liquid. Several technologies are possible as for example optical, capacitive or ultrasonic measurements. [1]

At CERN, sensors based on capacitive technology are used. The measurements are based on the following principle: the sensor electrode and the target (in our case the water surface) create a capacitor. Measuring the capacitance C and knowing the permittivity and the electrode size, one can deduce the distance d from equation (1).

$$C = \frac{\epsilon_o \epsilon_r S}{d} \quad (1)$$

3.2. Bedplates HLS system

The installed HLS system was originally composed of six individual sensors, three on each side of the bedplates facing each other and linked as an H-shaped hydraulic network (see figure 3). Since November 2005, one additional sensor (REF) placed in a more stable zone of the cavern allows in real-time the determination of the bedplates deformation and their movement with respect to the floor. This zone is not affected by the additional load which is installed in the cavern.

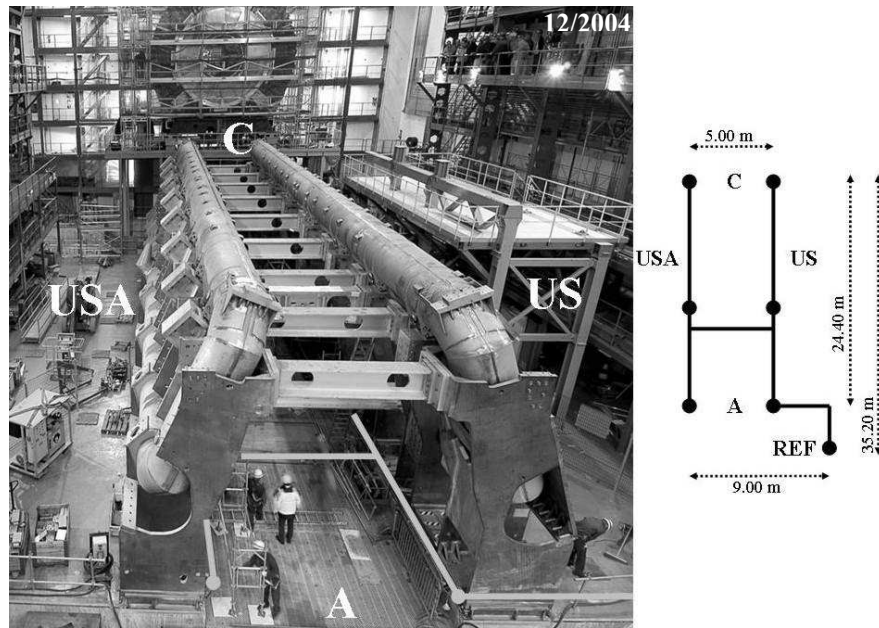


Figure 3: configuration of the bedplates HLS system

The sensors have a range of 5 mm with sub-micrometric resolution. Electronic components have been separated from the sensor due to the expected magnetic field of 800 Gauss and a radiation level of 100 Gy in the bedplates region and have been transferred to a remote electronics which can be located as far as 30 m away from the sensor itself. The electronics is expected to operate in an environment with a total radiation dose of up to 400 Gy and in a magnetic field of 300 Gauss [2]. As sensor, cable and remote electronic is one unit, they have been calibrated by the manufacturer and validated at reception.

A survey target ball interface on top of each sensor allows a three-dimensional link to classic geodetic networks as used for the floor stability monitoring. The height measurement of the sensor can therefore directly be linked via mechanical constants to other networks.

The free water surface network is made of a main hydraulic tube with an inner diameter of 50 mm, half filled with water and linked by separate water and air pipes to the sensor's vessel, named secondary hydraulic network. Each secondary hydraulic network is isolated from the main network by valves, which can be closed during the replacement of a sensor or the maintenance of the network.

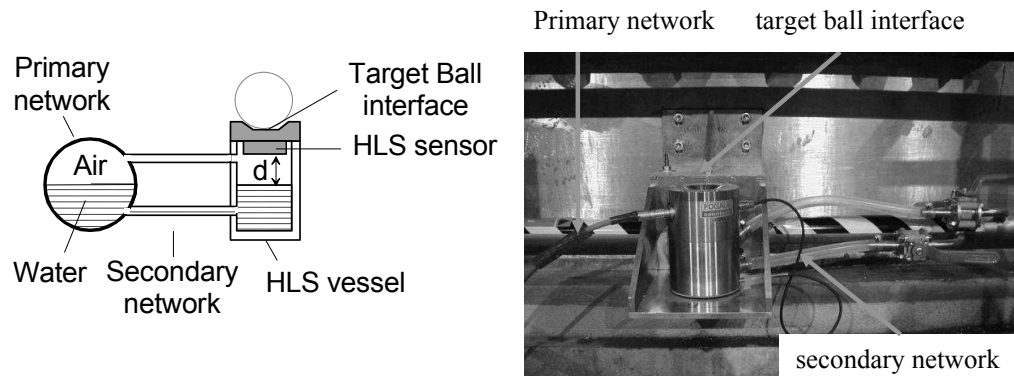


Figure 4: layout of the HLS

The sensors and their remote electronics are linked to a computer for data acquisition. Signals from the sensor's remote electronics are linked to an A/D converter, allowing the acquisition of data via RS485. The typical data acquisition interval is one minute.

3.3. HLS data and analysis

In the context of the installation phase of the ATLAS experiment, two main demands are defined:

- Online monitoring and visualisation of sensors readings
- Long-term deformation monitoring

As the system is operated in a local mode with the data acquisition on a computer, off-the-shelf software as provided by the manufacturer of the sensors can be used. For data acquisition and analysis during machine operation, a centrally hosted data base system will be implemented and analysis tools will be integrated into the central control system of the LHC.

The four main functions which can be fulfilled with the DAQ software are:

- Online visualization of the sensor's data as needed for installation tasks
- Internal correction of the measurements with temperature induced effects prior to storing in a ASCII file
- Corrected values (mm, °C) as well as uncorrected values (V) are stored in the file to allow further modelling
- Flexibility in the data acquisition intervals

The degree of analysis of the acquired data depends on the phenomena to be seen. Three types of treatments used for the analysis can be distinguished:

- **Screening** (see figure 5): in order to facilitate the visualization of the readings, a reference time t_0 is chosen. The readings of each sensor are calculated with respect to their own reference reading at t_0 . This "rough" treatment allows seeing how the sensors behave in time. This treatment does not prevent from seeing the evaporation

of water, which may not be considered as a drift of the sensors (see slight slope of the curves in figure 5).

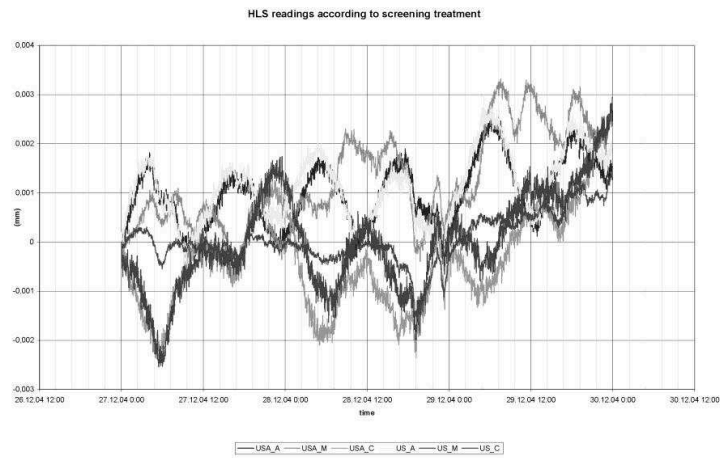


Figure 5: Screening treatment

- **Height difference** (see figure 6): Due to the principle of communicating vessels the height differences Δh_i between all sensors are continuously determined. This calculation is based on the choice of one of the sensors as reference, assumed to be the most stable and on the calculation of the height differences between this sensor and the others.

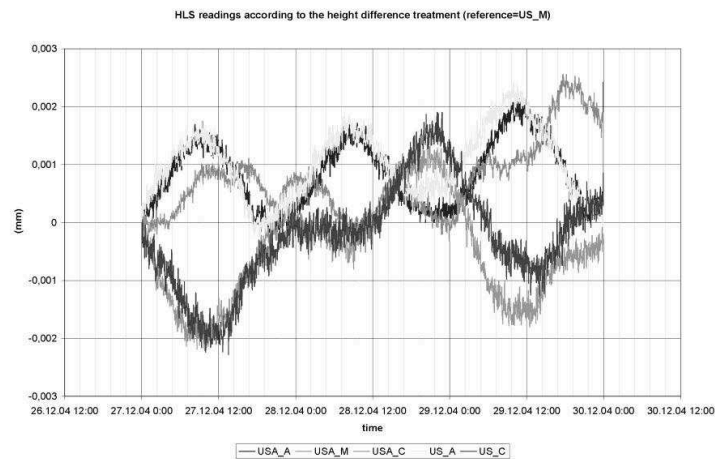


Figure 6: Height difference treatment

- **Mean plane** (see figure 7): The objective of this treatment is to calculate at each time, the mean plane of water, using the least squares compensation method, and to calculate the displacement of each sensor with respect to this plane. All problems linked to the water surface like e.g. the change of the water surface level due to external influences, evaporation or tidal effects can be hidden with this method. It is used to study long terms effects in a place with surrounding perturbations, but it does not reflect the real changes in height.

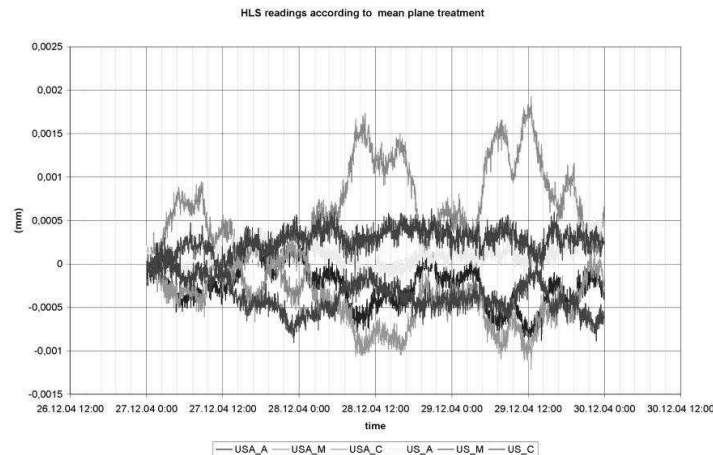


Figure 7: Mean plane treatment

The hydrostatic network can not be completely protected from influences of installation activities around. This leads to peak-to-peak waves in the system of several millimetres. During the installation of the detector, the HLS system has preferably to be used for short term observations as too many perturbations do not allow undisturbed measurements in the micrometre range. The full performance can only be maintained during periods of some days as for example during the installation of large elements as therefore the experimental area is partially evacuated. Long term observations over several weeks will be possible on a reliable base, once the machine will be in operation and installation activities have finished.

3.4. Example I: Barrel Toroid

The ATLAS experiment barrel toroid magnetic system is made of eight superconductive coils of approximately 100t each. They are as long as the experiment itself. As the load is brought into the cavern eccentric to the main detector axis, a roll effect of the bedplates was likely to occur.

Figure 8 shows the readings of the HLS sensors during the installation step of one coil. It shows a rotation of approximately $8 \mu\text{m}$ in the middle of the bedplates when the magnet is put into its final position (readings of the sensors USA_M and US_M which are symmetrical around the 0 axis of the curve) and a slight settlement on the A side. Small perturbations in the course of the measurement are due to positioning manoeuvres of the magnet, before fixing it. The first peak is caused by putting down the magnet on the central platform on the feet before tilting into its nominal position.

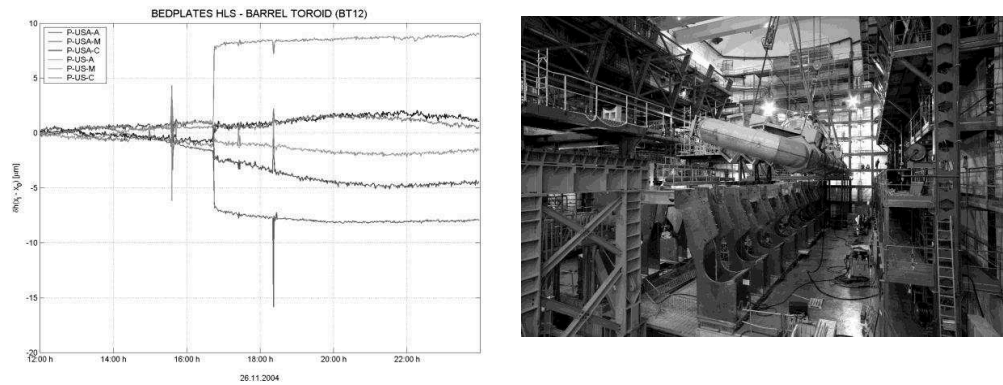


Figure 8: Barrel toroid

3.5. Example II: Tile Calorimeter

On November 2005 after the barrel toroid magnet was completed, the ATLAS Calorimeter Barrel detector, with the dimensions of 8 m in diameter and 8 m long, was brought into its final position, see figure 9. As the module has with 1.600 tons about 20 percent of the total weight of the experiment, significant deformations in the order of one millimetre were feared to occur.

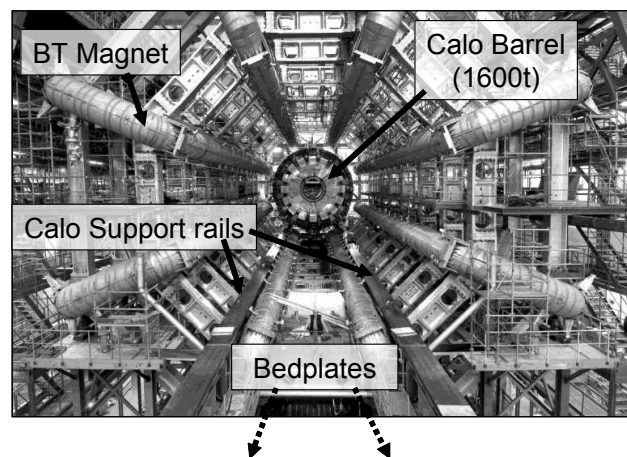


Figure 9: Calorimeter Barrel before insertion

It was asked for a measurement concept to monitor online the relative deformation at two different levels of the experiment – the rail on which the load was transported and the bedplates of the detector – in order to measure the deformation of the detector's mechanical support structure itself and of the ground where it is based on.

The HLS system was upgraded with one additional sensor in order to have a reference sensor in a zone which was likely not to be affected by the installation.

Figure 10 shows the relative deformation of the ATLAS bedplates during the installation of the tile calorimeter.

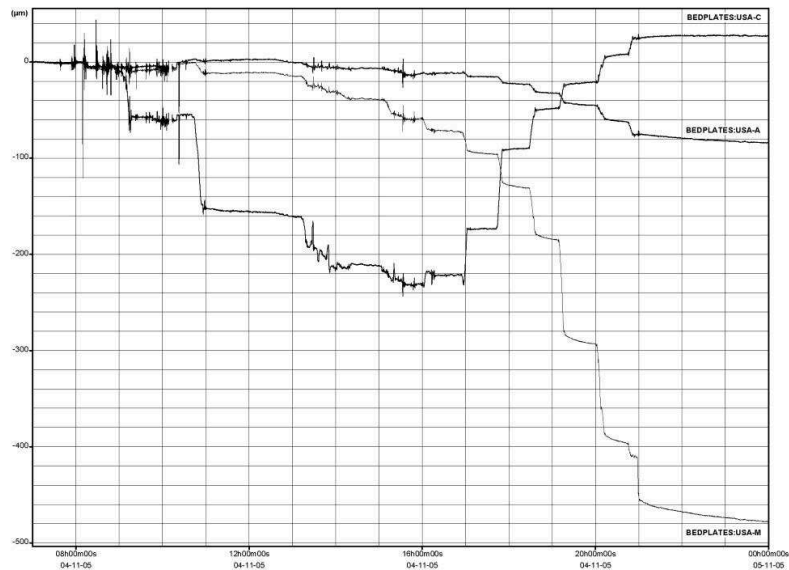


Figure 10: HLS monitoring during Calorimeter installation

A staircase-like effect can be seen for the three different sections of the bedplates as the load is transported in steps of one to two meters to the centre of the experiment (M position) starting from an outside position on the C side; see positions indicated in figure 13. The applied load causes a temporary deformation of 200 μm which is reduced to its original value after the transition of the load. The middle section is affected by 500 μm once the tile is in place.

3.6. Example III: Earthquakes

Sometimes, the HLS sensors monitor phenomena which were not expected. As shown in figure 11, the readings recorded by the sensors at the end of the year 2004 revealed two perturbations: one on December 23 starting at 15:45 UTC and the other on December 26 at 01:23 UTC. Seeing these unusual and punctual readings on December 26, we immediately wondered whether they were connected with the earthquake off the Indonesian coast. This hypothesis was confirmed by an expert from the Laboratory for studies on Geological Risks in Geneva.

The epicentre of the Sumatra quake was 9.700 km from CERN. The primary P waves, which are the fastest waves propagating at a speed of 6 to 8 km/s, took about 20 minutes to reach CERN, which is consistent with the first perturbations recorded by the sensors at 1:23 UTC. The earthquake occurred at 0:58 UTC [3].

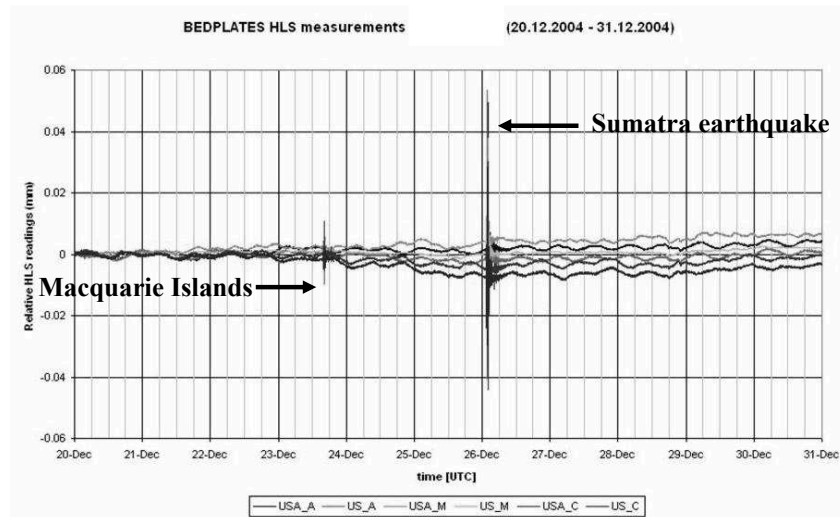


Figure 11: Tsunami earthquakes (Dec. 26, 2004)

The first perturbation, which occurred at 15:45 UTC on December 23, was also due to an earthquake, at 14:59 UTC near the Macquarie islands located between Australia and Antarctica, which measured 8.1 on the Richter scale.

The waves detected by the HLS system do not reflect the real displacement of the system. They show in fact the amplifying effect of the main hydraulic network as the water can easily loop up waves.

3.7. Combined levelling systems

The HLS measurements are an excellent tool to detect relative movements in the ATLAS bedplates. Even with the perturbing influences of installation activities in the cavern, the demanded 50 μm accuracy can be obtained. The combination of continuous measurements with the HLS system and discontinuous epoch-wise levelling measurements allows the integration of the relative HLS measurements into an absolute coordinate frame, e.g. with respect to the machine system.

Note that comparisons of the relative levelling between the HLS target ball interfaces obtained by optical and hydrostatic levelling are similar within 0.1 mm (comparison limited by the optical levelling precision).

The next chapter shows the methods used for the epoch-wise levelling and the positioning with respect to the LHC beam.

4. Cavern floor stability

4.1. Layout

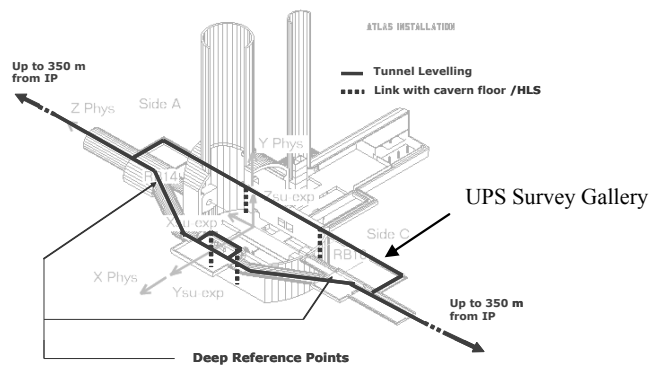


Figure 12: Optical Levelling path

The base points of the optical precise levelling – carried out using a precise Leica NA2 level and classical invar staff - are 2 deep references placed in the tunnel on both sides of the experiment and which are independent of the tunnel floor, see figure 12. The deep references consist in 16 m long invar bars fixed to the bed rock at their bottom part and sliding in a tube. A reference socket is placed at the top of each bar at the tunnel floor level in order to allow the measurement.

In order to inspect the tunnel stability around the cavern zone – some civil engineering works were also performed in this area – the levelling includes the tunnel reference points on a distance of 350 m on each side. These points are placed in the tunnel floor every approximately 40 m and they are used for the machine magnets installation.

The measurements are transferred to the cavern through two UPS survey galleries on one side and through communication doors on the other one. Another set of 20 reference points are distributed on the cavern floor along profiles near the experiment and also close to the walls. See figure 13.

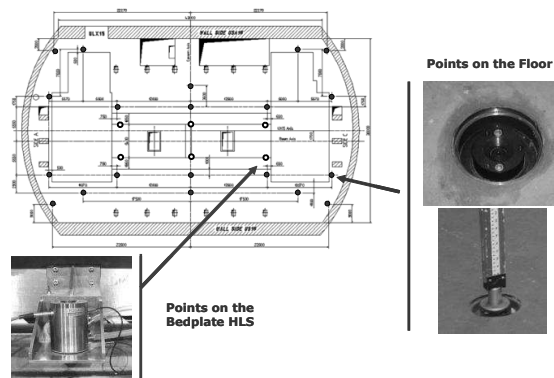


Figure 13: Reference points on the floor

These points and the HLS Bedplate sensors are linked to the tunnel geometry via 4 vertical paths in the corners of the cavern, see figure 12.

Special brackets are installed at top (tunnel level) and bottom (close to cavern floor level) of these paths. Vertical distances are measured between them - using a Leica TC2002 calibrated instrument - with a precision better than 0.2 mm. This measurement is made in a relative way in order to avoid systematic errors due to instrumental constant influence. These brackets are then included in the tunnel and cavern floor optical levelling.

According to the configuration and to the redundancy of the measurements, the level of the points after least square calculation is obtained with an accuracy of 0.2 mm (1 sigma) with respect to the tunnel geometry datum. Then the precision of the difference of level between two epochs is of 0.3 mm (1 sigma).

In small area such as the bedplates region the difference of level between points measured in the same epoch is 0.1 mm (1 sigma).

4.2. Stability measurements and results

From August 2003, nine stability measurements have been performed regularly and when special events occur such as the 1600 t Calorimeter Barrel installation.

From August 2003 to March 2005, a heave of the cavern floor was seen. The movement is not equally distributed on the floor surface, see figure 14. An average movement of +1.0 mm was measured on the central zone, near the experiment feet with a maximum at +1.2 mm. The outer points of the cavern floor moved up of +0.5 mm.

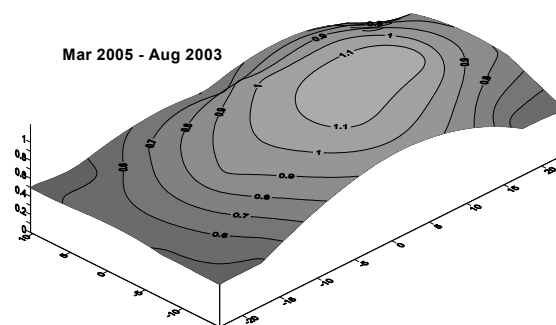


Figure 15: 3D view of the Cavern floor deformation from August 2003 to March 2005

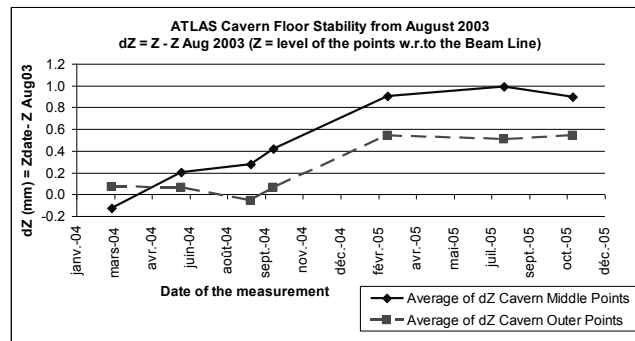


Figure 16: Cavern floor deformation from August 2003 to March 2005

From March 2005, the floor seems more stable, see figure 16. This corresponds to a period of heavy pieces installation, mainly the Barrel Toroid Magnet assembly and the Calorimeter Barrel insertion. During this period, the weight increased up to 50% of the total load.

5. Conclusion

The combined survey of the ATLAS stability using optical levelling and HLS Bedplate system is of importance in the help to the physics responsible persons in charge of the detector assembly. The obtained values are included in the detector alignment decisional process together with some other parameters such as the supporting structures behaviour and the sub-detectors internal deformations due to the working temperature (some detectors are working in cryogenic conditions).

The HLS system, designed and installed to follow the relative movements of the bedplates at better than 50 μm accuracy, has proved that it can monitor expected or unexpected deformations in the micrometer range, which is very promising for long term observations once the machine will be in operation.

References:

- [1] Mainaud Durand H., 2004. Micrometric alignment metrology: means, developments and applications, CERN Technical Note TS-Note-2004-038
<http://edms.cern.ch/file/473751/1/01-Mainaud.pdf>
- [2] Dimovasili E. et al., 2005. Radiation induced effects on the sensors of the Hydrostatic Levelling System for the LHC low beta quadrupoles, CERN Technical Note TS-Note-2005-52
[http://edms.cern.ch/file/629483/1/TS_Note_2005_052\(LEA\).pdf](http://edms.cern.ch/file/629483/1/TS_Note_2005_052(LEA).pdf)
- [3] The Asian earthquakes detected in the ATLAS cavern, CERN Bulletin 09/2005
<http://cdsweb.cern.ch/search.py?recid=824438&ln=en>

C.4 Radiation induced effects on hydrostatic levelling sensors

A. Herty, E. Dimovasili, H. Mainaud Durand, A. Marin, F. Ossart, T. Wijnands

In preparation for the permanent alignment system of the LHC low beta quadrupoles, several irradiation tests had been carried out since 2000 in order to validate the use of capacitive HLS sensors. The sensors will be located in areas where significant radiation doses are predicted. Tests have shown perturbing offsets in the sensors' signals as a function of the dose rate. Due to these observations, a theoretical study regarding the HLS sensors has been undertaken. This has shown that at high dose rates the ionization of the air inside the sensors causes charge recombination and this perturbs the position measurement. One correction model is proposed, and is compared to the sensors' signals monitored during the irradiation tests in 2005.

International Workshop on Accelerator Alignment (IWAA), Stanford, USA, 2006

Radiation Induced Effects on Hydrostatic Levelling Sensors

A. Herty, E. Dimovasili, H. Mainaud Durand, A. Marin, T. Wijnands
CERN, 1211 Geneva 23, Switzerland

F. Ossart
FOGALE nanotech, 30900 Nîmes, France

In preparation for the permanent alignment system of the LHC low beta quadrupoles, several irradiation tests had been carried out since 2000 in order to validate the use of capacitive HLS sensors. The sensors will be located in areas where significant radiation doses are predicted. Tests have shown perturbing offsets in the sensors' signals as a function of the dose rate. Due to these observations, a theoretical study regarding the HLS sensors has been undertaken. This has shown that at high dose rates the ionization of the air inside the sensors causes charge recombination and this perturbs the position measurement. One correction model is proposed, and is compared to the sensors' signals monitored during the irradiation tests in 2005.

1. PRECISE MEASUREMENTS AND RADIATION PROBLEMS

The installation of geodetic measurement equipment in a radiation environment, like that in particle accelerators, needs proof of radiation hardness and full functionality in the given conditions. The influences on the sensors can be of different types, ranging from perturbation of the measurements in a known and compensable way to non-compensable drift phenomena. Tight alignment tolerances of several microns as found in the final focussing magnet regions, require any influence on the sensor due to radiation to be determined.

According to the CERN policy, all electronic components have to be qualified as radiation hard before being installed in the experiments and the accelerator. For the Large Hadron Collider (LHC) project, a test facility in TCC2 was set up in 1999 to study the influence of radiation on instrumentation which is going to be installed in the tunnel. Particle beams similar to those that will be circulating in the LHC are available in this test facility at CERN [2].

The Large Scale Metrology group (TS/SU) took advantage of this setup from 2000 to 2003 in order to test the sensors which will be used for the alignment of the LHC final focus magnets. These magnets, situated within 50 m of the experiment's interaction points, will be strongly affected by radiation dose rates of up to 16,000 Gy/year. In 2004 and 2005, additional tests at the irradiation facility CEA in Saclay (France) were carried out to complete the test series and study some phenomena in more detail.

2. RADIATION TESTS

For equipment validation in radiation environments many different aspects can be taken into account. Finding answers to two basic questions was the main goal of the tests on the low beta magnet monitoring sensors. First, do the sensors withstand the high radiation doses that are expected during 20 years operation of the LHC [6]? Second, can influences on the sensors be observed and if so, can they be modelled?

2.1. Test Facilities

2.1.1. TCC2

This irradiation test facility operated by CERN allows the exposure of equipment to LHC-like radiation types in an area of 10 m². In a radiation-safe control room on the upper floor, data acquisition systems can be installed for the read out of the sensors during the tests. Modifications to the data acquisition or real-time analysis is possible. A dose rate exposure of about 3 Gy per hour can be achieved in this facility. Over a period of 15 weeks per test series, a total dose between 700 Gy and 2,000 Gy has been accumulated.

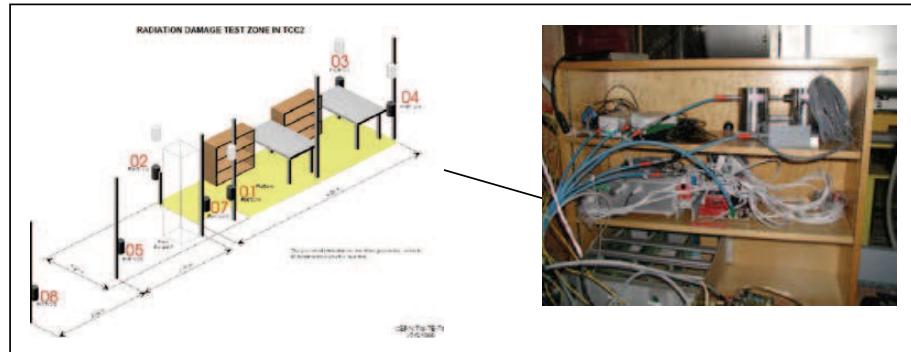


Figure 1: radiation damage test zone in TCC2

These irradiation tests have been designed to provide radiation hardness qualification of commercial off-the-shelf electronics for the LHC tunnel. As a part of these tests, the identification of radiation sensitive components and their replacement with radiation hard items had to be studied. Complete systems had to be validated and the equipment life-time had to be evaluated.

The life-time evaluation for the sensors installed in the highly radiation affected region of the inner triplet was difficult at the low dose rates provided at TCC2.

2.1.2. CEA Saclay

Two irradiators – Pagure and Poseidon – operated by CIS bio international at CEA in Saclay (France) have been used for tests at higher dose rates. The Pagure irradiator can host large volumes of several cubic meters. For small volumes dose rates of up to 20 kGy per hour can be achieved. The Poseidon irradiator can provide dose rates of up to 5 kGy per hour. Both can be operated 24 h a day, seven days per week. They use ⁶⁰Co gamma ray sources, which do not cause any activation of the tested material. Therefore it is possible to return them immediately to the home institute for further tests.

2.2. Test methods

A **Total Ionisation Dose (TID)** test exposes the sensor to a desired quantity of radiation which is achieved by keeping them in a radiation environment at a known dose rate over a certain amount of time. Total Ionisation Dose tests

characterize the materials and components used in the sensor. This test is essential for the sensor's qualification, as it provides fundamental information on whether the sensor can stand the radiation dose or not. Measurements on the degradation of the signal during the exposure have been carried out in parallel. For example this can happen due to the drift of components in the sensor. In case changes in the measurement data are observed, they are likely to be non-reversible for this type of test.

Dose rate dependence (DRD) tests are used to determine the influence on a certain radiation dose to the sensor. Offsets at 'beam on' or 'beam off', which might be caused by ionisation inside the sensor, can be quantified in these tests. These effects are generally reversible and can be directly correlated with the dose rate applied, empirical corrections and models which can be derived from such tests.

2.3. Sensors

The tests focussed on HLS sensors of different types, manufactured by FOGALE Nanotech. During this five year test series, modifications were necessary to achieve the best possible design of the sensor and its components, in regards to their radiation hardness. Tests were initially carried out with HLS sensors, which had integrated electronics and a ceramic housing of the electrode (2nd generation as used in LEP). Later developments lead to a stainless steel housing and remote electronics with connecting cable lengths of up to 30 m.

Table I: HLS sensor generations

generation	HLS sensor	
	body	electrode
2 nd	ceramic	on ceramic
3 rd	glass	protected behind glass
4 th	stainless steel	on circuit print board in body



Figure 2: HLS sensor 4th generation with remote electronic, temperature sensor and cable

During the development of the sensors, major problems occurred with a glass type HLS and therefore this type of HLS sensor was abandoned. The cables to the remote electronics needed some expertise as well, because a radiation hard cable with good shielding qualities was not easy to find. The cable type is important as the transport of the primary, capacitive signal is done via this cable to the electronics.

2.4. Test Series

In the test series between 2000 and 2004, only prototype sensors with remote electronics were used. They were either based on the 2nd and 3rd generation off-the-self sensors or on the prototypes of the 4th generation of HLS sensors. Hardware costs to test several sensors of the same type during one test series are immense; therefore only one sensor per stage of expansion has been tested. In consequence, no statistical results could be drawn from the measurements and the different HLS sensor types. In 2005, sets of three sensors were used in their final LHC design for each test; therefore comparisons of the different measurements are possible.

In contrast to previous tests where the dosimetry was achieved by few dosimeters for the whole setup, the 2005 test's dosimetry determination has been done with radiophoto luminescent (RPL) glass dosimeters and Alanine dosimeters attached to every sensor. This was essential for the statistical evaluation of the dose rate dependence tests.

2.4.1. Tests 2000 – 2004

Tests were carried out on HLS sensors with integrated and remote electronics. The sensors were installed on a fix target to avoid additional effects of a water network. The sensors as well as the electronics were exposed at the same time to radiation during these tests. The measurements in 2000 showed a drift of the sensors right from the beginning, which has been detected as a mechanical instability in the setup.

In 2001, short cable lengths for remote electronics were used, as the electronics were supposed to be hosted under the magnets. The sensors, as well as the electronics and cables were irradiated at the same time. Due to failure of the electronics after approximately 800 Gy during the TID test, Marin (2004) concluded, that the use of remote electronics is only possible in a place with less than 10 Gy per year. This prompted on further investigation into an extension of the cable length to 30 m. Prototype development of sensors with remote electronics, as well as of generation four of the HLS sensors were carried out in consequence.

During tests in 2004 only the sensor was exposed to radiation. The electronic was placed outside because it was likely to fail at lower dose rates. In this configuration, a stable signal of the sensors has been obtained for a total dose of 67,000 Gy. This result was obtained for 2nd generation as well as for 4th generation HLS with remote electronics.

While sensors were exposed to radiation, an offset of the signal was observed and lead to further investigation of a possible dose rate dependence. Investigations lead to the idea that ionisation in the HLS vessel might be the cause of this effect, as previously proposed by Coosemans et al. (1999, 2000) [4, 5].

2.4.2. Tests 2005

The tests in 2005 were carried out in order to complete the information obtained from the tests in previous years, but with at least three sensors per test to allow for statistical comparison. These tests were carried out in cooperation with FOGALE Nanotech. The final HLS design for the LHC had to be validated in the TID test. The dose rate dependence tests at different dose rates were necessary as well to conclude on the phenomenon seen in 2004.

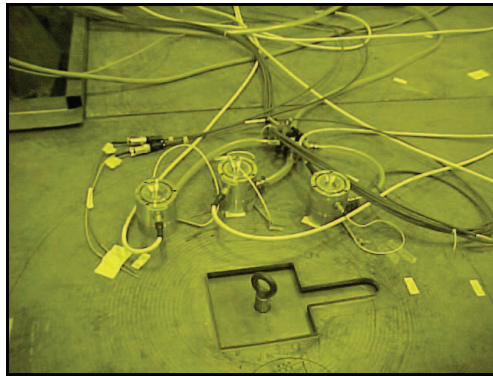


Figure 3: setup of sensors around the radiation source (2005)

Sensor TID test

Two HLS sensors already used in the 2004 test series have been installed in a hydrostatic levelling network to test their performance under real environmental conditions, e.g. to investigate influence of humidity during irradiation. One of the HLS was a second generation sensor; the other was a fourth generation one. Both remote electronics were situated outside the test bunker. The dose rate was supposed to simulate 10 years of LHC operation with an annual dose rate of 16,000 Gy as the worst case scenario; therefore the HLS were exposed to dose rates of 2,200 Gy/h during 72 hours.

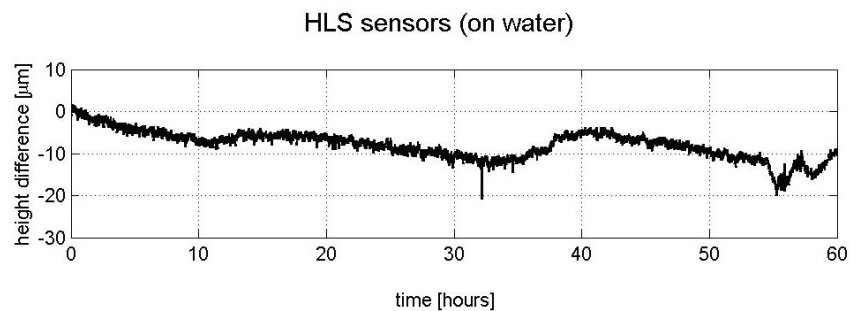


Figure 4: Δh between two HLS measuring on water during TID test

Both prototype sensors succeeded the test and were able to resist a total dose of 225,500 Gy cumulated in 2004. In parallel, two HLS sensors of the fourth generation were tested in the same irradiation conditions, measuring on a target. The sensor exposed to the radiation showed reliable results at a total dose of 158,500 Gy.

One sensor of the 4th generation was exposed in the DRD test to another 21,500 Gy, which makes a total of 180,000 Gy for this sensor without any signs of degradation.

Electronic TID test

As the electronics were the sensitive part in previous tests, a TID test at a high dose rates would be inappropriate. Therefore they have been exposed to different dose rates. From the set of three electronics, two failed at total dose rate of about 700 Gy, the other one at 1200 Gy (figure 5).

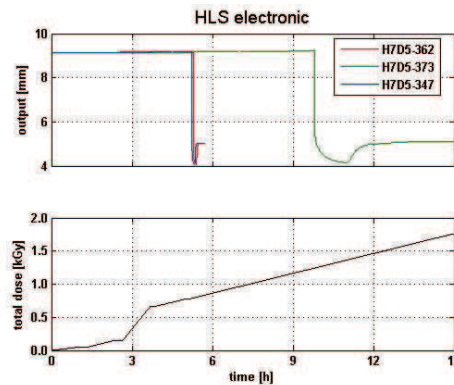


Figure 5: electronics break down

The necessity for remote electronics has been confirmed during this test. The installation of the remote electronics has to be done in places where dose rates of a maximum of 10 Gy per year can be expected (Marin, 2004). For example, this is the case in the survey galleries dedicated to the radial link of the ATLAS and CMS experiment, or behind the shielding in a service tunnel for the LHCb and ALICE experiment [7].

Though the electronics failed during the test, it was not a permanent failure of any of the components inside. The problem was caused by a sort of saturation of the electronics. Heating the electronics for one week at 50 °C made them return to normal operating conditions.

Sensor DRD test

For the dose rate dependence test, a series of measurements of one hour each were planned. The sensors were exposed to a dose rate of 50 Gy, 100 Gy, 500 Gy and 1,000 Gy before having a dose of 1,500 Gy per hour for a period of 12 hours. Finally the one hour measurements at lower dose rate were repeated in inverse order.

Figure 6 shows the steps observed at the different dose rates. The red and green curve are sensors of the 4th generation, the blue curve is from a sensor with a ceramic support of the electrode. All curves show an echelon form when the sensors are exposed to radiation and the quantity of the offset is strongly correlated to the applied dose rate. Peaks in the curves are caused by a vacuum pump which allowed the evacuation of the air inside the HLS vessel. The pumping was an essential part of these tests and was introduced due to the assumptions made after the 2004 test. With an ionisation phenomenon of the air inside the vessel, one was able to show, that the influence could be minimized by evacuating the vessel. This is clearly visible with the ceramic sensor (blue curve). The 4th generation sensors have too much mechanical stress on the electrode caused by the vacuum, that the deformation of the electrode is more important than the reduction of the signal due to evacuation of the vessel.

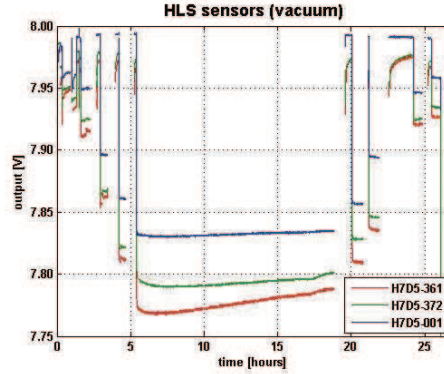


Figure 6: offset radiation

3. THEORY AND MODEL OF DOSE RATE DEPENDANCY

Tests on HLS sensors in 2004 showed an offset when the sensors were exposed to radiation. As the electronics were situated outside the irradiation chamber, the offset must be due to radiation effects acting on the sensor. Similar observations have already been made by Coosemans et al. (1999) during tests at the LEP spectrometer [4].

Dimovasili et al. (2005) made the assumption that the enclosed air volume in the vessel of a HLS system can be assumed to act like an ionization chamber and therefore similar physical processes can be observed inside the vessel. The model derived from the radiation tests in 2005 is based on the Bragg Gray principle [1].

This hypothesis has been evaluated with a series of tests on three HLS sensors. Figure 3 shows the setup around the radiation source. The source itself is not shown in the figure. The sensors were exposed to doses of 50 Gy/h, 100 Gy/h, 500 Gy/h, 1000 Gy/h and 1500 Gy/h.

The derivation of the following model is special to the capacitive sensors used for non-contact measurements. With this technology a change in the capacitance ΔC observed by the sensor is directly linked to a change in the distance between the electrode of the sensor and the target

$$\Delta C = \frac{\epsilon_o \cdot \epsilon_r \cdot S}{\Delta h} \quad (1)$$

with ϵ_o as the absolute permittivity in vacuum, ϵ_r the dielectric constant of air, S the surface of the electrode and Δh the variation of the distance between the electrode and the target. This can also be described by an output voltage

$$V_{out} = (V_{offset} + \frac{1}{C_e} \cdot V_e \cdot C_{ref}) \cdot G \quad (2)$$

where as C_e is the measured capacitance, C_{ref} is the reference capacitance, V_e is the voltage applied between the plates of the capacitor and G is the scaling factor (gain) of the electronic.

By the assumption, that a HLS sensor acts like a condenser ionisation chamber a hypothesis was established. It was supposed to be confirmed by the empirically determined values of the measurement. The link between HLS and

condenser chamber is the fact that they are built as a capacitor. As the Bragg-Gray conditions are met with this assumption, one can calculate the ionization current by the following equation:

$$I_{ion} = \frac{D \cdot m \cdot S_g}{W \cdot S_w} \quad (3)$$

where I_{ion} is the induced ionization current and D is the dose rate in the air inside the vessel. The mass of the air inside the vessel is describe with m , W is a constant that depends on the gas used and the ratio S_g/S_w is the mass stopping power of the gas.

Relating the dose rate and therefore also the ionisation current (3) to the voltage output of the sensor shows a non-linear, proportional offset and is according to Dimovasili [1], the proof of recombination in the HLS vessel.

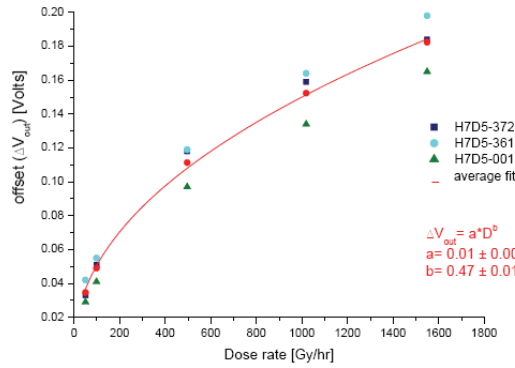


Figure 7: measured voltage offset for all sensors and average curve (red)

The influence of radiation on the HLS sensors leads to the question whether corrections can be applied for the measurements.

As shown in figure 7, the voltage output changes in dependence of the dose rate. The ionisation of the air inside the HLS vessel causes a change to the measurements as the voltage V_e applied to the capacitor to maintain a stable electric field is in consequence reduced by the electronic. This is misinterpreted by the electronic as a change of capacitance C_e . The result is a decrease in the output voltage V_{out} , which could be misinterpreted as a change of height (2).

The corrected height calculation for a HLS is done with the parameters of a polynomial providing the calibration curve $f(V_{out}, c_0, \dots, c_x)$ with c_0 to c_x as coefficients of the polynomial. Additionally, a function $f(V_{out}, D)$ has to be applied where as V_{out} is the output voltage measured and D is the radiation dose applied to the sensor. This defines the transformation of voltage measurement data to height information via the equation:

$$h = f(V_{out}, c_0, \dots, c_x) + f(V_{out}, D) \quad (4)$$

To validate the results obtained for radiation influence compensation, a comparison between the theoretical parameter calculation from equation 2 and the experimental setup test was carried out. The results in table II show a theoretical variation of Δh . Since the nominal distance between electrode and target is known, a hypothetical offset due to radiation

can be determined from the measurements. The results agree within one percent. Therefore the method can be seen as valid for the compensation of radiation induced effects on HLS sensors.

Table II: comparison between theoretical determination and experimental values

Dose rate Gy/h	Δh (theoretical) μm	Δh (experimental) μm	Difference %
50	21.10	21.06	0.21
100	27.34	27.29	0.21
500	59.18	59.06	0.20
1000	81.79	81.64	0.19
1500	98.96	98.79	0.18

4. CONCLUSION

Irradiation test for HLS sensor validation were carried out at different facilities at CERN and at CEA. Modifications on the sensor design have been done in order to get radiation hard equipment for the LHC. Remote electronics, cable lengths of 30 m for the transport of the primary signal and new electrode design were introduced. Ionisation of the air inside the vessel at high dose rates lead to investigations on a compensation model.

Three major conclusions can be drawn from the tests in the last five years. First, the modification of the sensors and the development of remote electronics were necessary with respect to the dose rates of the LHC. The sensors can provide reliable measurements within some microns if the electronics are installed in a radiation safe environment. Second, the second and fourth generation of hydrostatic levelling sensors have passed the total ionization dose test. The simulated test period was ten years of LHC operation. Third, ionization in the air between sensor and water surface occurs and can be compensated with a model that has been determined.

These extensive tests were essential to prepare the survey group for the online monitoring and alignment of the LHC final focusing magnets. Modifications on HLS alignment sensors had been done to customise them to the high radiation doses expected in this and future particle accelerators.

References

- [1] E. Dimovasili et al., "Radiation induced effects on the sensors of the Hydrostatic Leveling System for the LHC low beta quadrupoles", CERN Technical Note TS-2005-052, Geneva (Switzerland), August 2005.
- [2] R. Rausch et al., "Qualification of electronic components and systems in a LHC tunnel radiation environment", EPAC conference, Paris (France), June 2002
- [3] A. Marin, W. Coosemans, "Radiation tolerance of positioning sensors and their conditioners used for the LHC low beta magnets", poster presentation, International Workshop on Accelerator Alignment, Geneva (Switzerland), October 2004
- [4] W. Coosemans et al., "Performance of wire position sensors in a radiation environment", International Workshop on Accelerator Alignment, Grenoble (France), October 1999
- [5] W. Coosemans et al., "Determination of accuracy of Wire Position Sensors", CERN Note CERN-SL-2000-029, Geneva (Switzerland), July 2000

- [6] LHC Design Report, Volumes I-III, CERN
- [7] A. Herty et al., “Status of the alignment of the LHC low beta quadrupoles”, International Workshop on Accelerator Alignment, CERN (Switzerland), October 2004

RADIATION INDUCED EFFECTS ON HYDROSTATIC LEVELLING SENSORS



ABSTRACT

In preparation of the permanent alignment system of the LHC low beta quadrupoles, several irradiation tests had been carried out since 2000, in order to validate the use of capacitive HLS sensors. The sensors will be located in areas where significant radiation doses are predicted. Tests have shown perturbing offsets on the sensors' signals as a function of the dose rate. Due to these observations, a theoretical study regarding the HLS sensors has been undertaken, showing that at high dose rates, ionization of the air inside the sensors causes charge recombination and this perturbs the position measurement. One model of correction is proposed, and is compared to the sensors' signals monitored during the irradiation tests performed in 2005.

TEST FACILITIES

The TCC2 irradiation test facility has been operated at CERN from 2000 to 2004. It allowed the exposure of equipment to LHC-like radiation types. A radiation exposure of 3 Gy per hour can be achieved with this facility. Over test periods of 15 weeks, total doses between 700 Gy and 2.000 Gy have been cumulated.

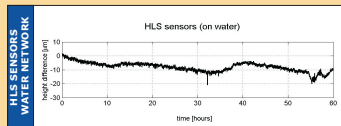


As the LHC low beta magnets will face annual total dose rates of up to 16 kGy, a more powerful test facility was chosen to complete tests. The CEA in Saclay (France) provides such a facility, where dose rates of up to 20 kGy per hour can be achieved. The use of ⁶⁰Co gamma ray sources does not cause any activation of the tested material. This allows the sensors to be returned to CERN immediately after the tests.

TOTAL IONISATION DOSE

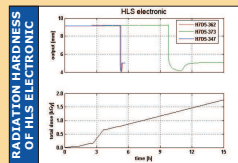
Already first tests in the TCC2 facility showed drifts when electronics and sensors were irradiated at the same time. Perturbation of the signal at the relatively low dose rates made a separation of the sensor and the electronic necessary.

Different test series cumulated total doses of up to 180.000 Gy per sensor. The sensors were measuring on fixed targets. The targets were chosen to avoid possible influences of water to the measurements. With the electronics situated outside the irradiation chamber, no degradation of the signal has been observed during constant radiation; the sensors are classified as radiation hard for the LHC. A variation of the signal at the beginning and at the end of those tests will be explained in the chapter dose rate dependence.



In 2005, one of the tests was set up as a total ionisation dose test with two sensors linked by a hydrostatic levelling network. These already previously irradiated sensors did not show any influence due to the water and can be considered to be stable during irradiation, as shown in the figure above.

Electronics are more sensitive to radiation influences. They broke typically down at a total ionisation dose of approximately 800 Gy. They have to be protected in places with low dose rates, like for example the survey galleries in the experimental area.



DOSE RATE DEPENDENCE

Tests in 2004 at high dose rates showed a possible influence of the radiation dose on the measurements. Similar observations were made in 1999 during measurements on the LEP spectrometer.

An additional HLS test series in 2005 with dose rates between 50 Gy/h and 1.500 Gy/h confirmed this hypothesis and a model for compensation of this influence has been derived.

The sensor interprets a change in the capacitance ΔC as a change in the distance between the electrode of the sensor and the target

$$\Delta C = \frac{\epsilon_0 \cdot \epsilon_r \cdot S}{\Delta h} \quad (1)$$

with ϵ_0 as the absolute permittivity in vacuum, ϵ_r the dielectric constant of air, S

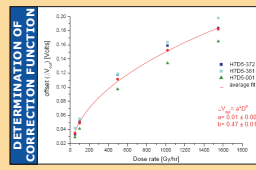
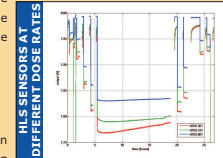
the surface of the electrode and Δh the variation of the distance between the electrode and the target. This change occurs during irradiation when ionisation in the HLS sensor is created.

$$V_{out} = (V_{offset} + \frac{1}{C_e} \cdot V_e \cdot C_{ref}) \cdot G \quad (2)$$

$$I_{ion} = \frac{D \cdot m \cdot S_e}{W \cdot S_v} \quad (3)$$

Equation 2 describes the corresponding change in the output voltage with the main parameters C_e as the measured capacitance and V_{out} as the output voltage.

The link between HLS and condenser chamber is the fact that they are built as capacitors. As the Bragg-Gray conditions are met with this assumption, one can calculate the ionization current by equation 3, with the main parameters I_{ion} as the induced ionization current and D as the dose rate in the air inside the vessel.



The hypothesis and model were confirmed and influences on measurements in a radiation environment can now be corrected. The influence during LHC runs will be much less as dose rates are not that high as during irradiation tests.

CONCLUSIONS

Irradiation test for HLS sensor validation were carried out at different facilities at CERN and at CEA. Modifications on the sensor design have been carried out in order to get radiation hard equipment for the LHC. Remote electronics, cable lengths of 30 m for the transport of the primary signal and a new electrode design were introduced. Ionisation of the air inside the vessel at high dose rates lead to investigations on a compensation model.

Three major conclusions can be drawn from the tests in the last five years. First, the modification of the sensors and the development of remote electronics were necessary with respect to the dose rates of the LHC. The sensors can provide reliable measurements within some microns if the electronics are installed in a radiation safe environment. Second, the 2nd (ceramic) and 4th (stainless steel) generation of hydrostatic levelling sensors have passed the total ionisation dose test. The simulated test period was ten years of LHC operation. Third, ionization in the air between sensor and water surface occurs and can be compensated with a model that has been determined.

These extensive tests were essential to prepare the survey group for the online monitoring and alignment of the LHC final focusing magnets. Modifications on HLS alignment sensors had been done to customise them to the high radiation doses expected in this and future particle accelerators.



C.5 The remote positioning of the LHC Inner Triplet

H. Mainaud Durand, A. Herty, M. Acar, J. Boerez, A. Marin

On account of stringent alignment tolerances and severe environment (high radiation fluxes and magnetic fields), the LHC inner triplets are equipped with permanent instrumentation (a combination of WPS and HLS) and are supported by motorized jacks, allowing their remote positioning thanks to the sensors' readings. This paper describes the alignment systems and motorized jacks from the technical choices to the installation and commissioning in the LHC tunnel. It also details the associated databases, analysis software and supervision tools implemented for this remote positioning.

International Workshop on Accelerator Alignment (IWAA), 2008

THE REMOTE POSITIONING OF THE LHC INNER TRIPLET

H. Mainaud Durand, A. Herty, M. Acar, J. Boerez, A. Marin, CERN, Geneva, Switzerland.

Abstract

On account of stringent alignment tolerances and severe environment (high radiation fluxes and magnetic fields), the LHC inner triplets are equipped with permanent instrumentation (a combination of WPS and HLS) and are supported by motorized jacks, allowing their remote positioning thanks to the sensors' readings. This paper describes the alignment systems and motorized jacks from the technical choices to the installation and commissioning in the LHC tunnel. It also details the associated databases, analysis software and supervision tools implemented for this remote positioning.

Introduction

For the first time at CERN, the low beta quadrupoles will be repositioned remotely according to the readings of the alignment sensors attached to them. Motorized jacks located under the magnets cryostats will allow this remote positioning. More than 7 years were needed to decide, integrate, carry out, install and then commission the alignment systems and the motorized jacks involved, not counting the energy needed in order to justify such a repositioning system and to obtain the infrastructure and necessary budgets.

This paper describes successively the alignment systems and the motorized jacks, detailing their configuration, the associated technical choices, the installation steps and the commissioning. Then, the global strategy concerning the remote positioning is introduced, as well as the associated databases, analysis software and supervision tools.

THE LOW BETA ALIGNMENT SYSTEMS

The sensors configuration

The position of each of the 3 low beta quadrupoles is determined according to 5 degrees of freedom, thanks to a combination of two alignment systems: the Wire Positioning System (WPS) and the Hydrostatic Levelling System (HLS). The longitudinal position of the magnet is not monitored because it is less stringent than the other degrees of freedom. The sensors configuration allows some redundancy and is described in [1]; this paper will not deal with the link between two triplets.

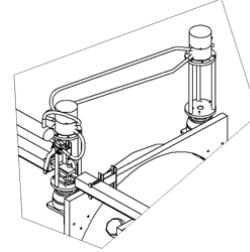
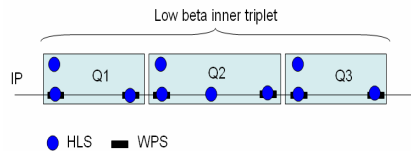


Fig. 1: The sensors configuration.

The alignment and monitoring sensors are located on fiducials which have been defined using laser tracker measurements [2].

The main technical choices

Due to the high radiations level expected in the low beta quadrupoles areas (around 16 kGy / year), the electronics of the sensors are remote in a safer place and the cables linking each sensor to its electronics are radiation hard. Radiation tests have been carried out showing that the sensors can tolerate total doses greater than 300 kGy with no damage [3].

Also, due to the delay in the installation of the equipments, some more elaborate reception tests were carried out on the sensors, showing that the HLS and WPS sensors are not calibrated to be interchangeable better than 100 microns [4]. So, dedicated procedures and benches were implemented in order to improve this determination.

As far as the acquisition of the sensors is concerned, it was decided to use the WorldFIP field bus for data transmission. This implied the development of a new acquisition device allowing the powering and A/D for the sensors, named Survey Acquisition System (SAS) [5].

Concerning the hydraulic network associated to the HLS sensors, two technical choices were considered:

- The hydraulic network is independent from the magnets to be aligned. It is supported by pillars screwed on the tunnel ground, and the HLS sensors are connected to the main common air/water network (\varnothing 50 mm), by means of 2 separate air and water tubes.
- For a fast stabilization of the network requested in the tilt HLS readings, a separate air and water network links the two sensors on each magnet.

Concerning the wire, the emphasis was laid on its protection: the carbon peek wire is entirely hidden in an assembly of 2 metallic U-shaped profiles, and the 15 kg weight for the tension of the wire is surrounded by a special mechanism preventing it from falling on the ground in case of wire cut.

The storage of information

100 HLS sensors, 64 WPS sensors, 24 dimensional sensors, and more than 60 temperature probes are being installed in the LHC tunnel. The calibration parameters of each sensor shall be managed. In addition, as 2 or more sensors are installed on the same fiducials and as they are not exchangeable, the management of their localization is absolutely necessary. The fact that the LHC tunnel has a slope adds another difficulty: the wire follows the slope, and the hydraulic network follows the geoid. Thus, on each support, the distance between the WPS, HLS sensors and the fiducial on which they are located is different, and must be determined precisely if the sensors readings are to be compensated to the fiducial level.

In order to facilitate the management of the sensors and the recovery of their data and that of their support, the official database of CERN named MTF (Manufacturing and Test Folder of a Component) is used. It ensures close follow-up and control of all equipment installed in the LHC tunnel.

The installation sequence

Two conditions are needed concerning the installation of the alignment systems:

- Because of the risk of breaking the wire due to co-activities, the interconnections between magnets must be closed,
- The triplet shall have been pre-aligned with respect to the geodetic network, and smoothed with respect to the Long Straight Section magnets and the triplet on the other side of the collision point.

Before the installation, the sensors supports are assembled, the parameters are measured. The sensors, their associated cables and electronics need also to be checked [6].

After the correct adjustment of the fiducials with respect to the local vertical, the installation of the alignment systems and their supporting parts can start. The HLS system is always the first to be installed and validated, as it is located above the wire and it is less fragile.



Fig. 2: Sensors and motors installed on a low beta quadrupole

The commissioning

The HLS system is commissioned thanks to the filling and purging of its hydraulic network: the difference in height seen by each sensor must be the same within a few microns.

The WPS system is commissioned thanks to the displacement of the wire on one extremity: each sensor shall be able to detect a displacement of the cryostat proportional to its position along the wire, within a few microns [7].

Then, the measurement chain must be controlled from the output of the sensor to the supervision, to be sure that the good measurements are stored at their right place.

In addition, as these quadrupoles have been pre-aligned with standard tools (stretched wires, optical levelling, and LTD measurements) during a previous stage, the position given by the alignment sensors has also to be coherent.

The first results

Five triplets out of eight triplets are now equipped with their alignment systems. Each installation on a triplet takes between 2 and 3 weeks, depending on the level of preparation and on the problems encountered during the installation (mainly interference problems with other equipment).

Despite a lot of co-activities around the stretched wire, the protection implemented was rigid enough to prevent the wire from breaking.

The design of the hydraulic network answers the requirements for the repositioning. The stabilization between the two tilt HLS takes about 100 seconds (stabilization better than one micron), and 10 minutes are needed for the stabilization along the whole hydraulic network.

One major problem still needs to be solved: it has been found that Electro-Magnetic Interferences (EMI) disturb the sensors readings, with effects that are not negligible (up to 0.1 mm for sub-micrometric sensors). Some studies

concerning the sensors have been undertaken, while some investigation to identify the equipment responsible for these EMI effects is under way.

THE MOTORIZED JACKS

The motorized jacks configuration

Q1 and Q3, weighing 15 t, which are ~ 10 m long, are considered totally rigid, while Q2, weighing 18 t, which is 14 m long, needs a control of its vertical sag between support points with a central jack. The configuration of the jacks and their axes of displacement is the following.

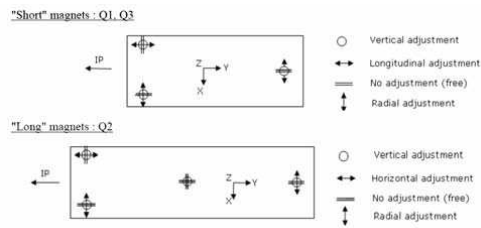


Fig. 3: The jacks' axes of displacement

Only 5 degrees of freedom are motorized: the longitudinal position of the magnet being less stringent than the others.

The main technical choices

In order to carry out the remote displacements, it has been decided to motorize the standard LHC cryo-magnet jacks and to use them for the low beta magnets. Some modifications were needed to meet the specific requirements of the inner triplets: a minimum effective displacement of 0.01 mm and a motor plugging/unplugging time inferior to 15 minutes. The major modifications were the enhancement of the jack stiffness (75 kN/m) and the incorporation of the necessary features for their motorization [6].

A mechanical interface, an adaptor, was designed through a collaboration frame with the Center of Advanced Technology (CAT) in India, allowing the plugging of a motor assembly on the jack axis. Two types of adaptors were carried out:

- 48 transverse adaptors, providing motion in roughly "horizontal direction", through an Oldham coupling, chosen for its high torsional stiffness between the pentagon socket of the jack and the gear head output shaft.
- 80 vertical adaptors dedicated to the vertical axis, using a polyurethane block as hydraulic fluid.

Once the design of these adaptors was determined, the characteristics of the motorization needed were defined: a 120 Nm output torque, a 25 Nm/arc-minute overall torsion stiffness, a 230 mm maximum length and a 10 t radial force capability. Then, the technical specification concerning the motorization was written and sent to the

industry. The Slovak firm ZTS vvu KOSICE A.S. delivered the 128 motors needed.

The adaptor and motor were both tested individually according to a given procedure. Then the assembly of these two devices, the "motor assembly", was tested and pre-adjusted under a spare 15 t magnet. Each motor assembly includes a mechanical gear, one stepper motor, an angular encoder, 3 mechanical switches (two ends and a median one), and 2 external connectors. It provides a ± 2 mm range of displacement on each jack axis, once installed, within a few microns resolution.

The storage of information

All information related to the motor and adaptor (type, serial number, reception report) is attached to each jack position in the MTF database, and contrary to the sensors, no particular parameters concerning the motor assembly is needed for the repositioning.

The installation sequence

Before the installation of the motor assembly, two conditions must be fulfilled:

- The alignment systems are installed and validated.
- The sensors data are accessible through Ethernet and can be displayed locally, close to the jacks to be equipped.

The motor assemblies are installed quadrupole per quadrupole, in no particular order. The sensors data are recorded just before the installation: as a matter of fact, during the installation of the assembly, a small displacement, smaller than 0.1 mm may occur, monitored by the sensors. Then, the sensors are brought back to their initial values using the motors through local command, and this position is considered as the medium range position of the motor assembly: the 2 safety end switches and the medium one are adjusted consequently.



Fig. 4: Motor assemblies plugged on jacks

The commissioning

The local command of the motor assemblies is tested during the installation process when the motors are

adjusted with respect to the sensors reference readings, using the same service command tool for all motor assemblies.

These installation parameters are then transferred to the dedicated command racks, and the control of the commands can be performed from the racks.

The next step will be the commissioning of the quadrupole repositioning in a remote mode. This will be done first according to the displacements given by the sensors, then at the level of beam.

REMOTE REPOSITIONING

The repositioning of the quadrupoles will not be closed loop, e.g. that there will be no displacements as soon as the sensors readings leave their set point. The moment for the repositioning will be chosen by the physicists. They will have a continuous access to the positions of the two ends of the magnets. When these positions are no longer acceptable for the quality of the beam, the parameters for better positions are calculated. First, these values will be translated in relative displacements to be done at the level of the magnet fiducials. Secondly, the data will be translated into displacements to be performed by the motor assemblies. Once these displacements have been carried out, the new position of the magnet is computed, thanks to the new sensors readings.

Such a strategy implies a large number of information stored in databases (concerning the position of the sensors, the association of their calibration polynomials), calculations and corrections to be carried out. In particular, mean least squares method will be used as far as the redundancy of the measurements is concerned, and corrections as the geoid effect, the earth and water tides or the temperature effects on the sensors readings shall be applied. Thus, a complete structure has been implemented.

The repositioning sequence

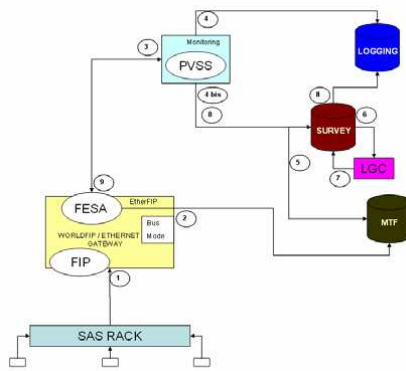


Fig. 5: The repositioning sequence

The data recovery

The sensors readings (0-10 V) are transmitted through WorldFIP field bus to a Gateway WorldFIP/Ethernet (1), where they are converted into millimetres or degrees Celsius, taking into account the calibration parameters stored in the MTF database (2). The raw and converted sensors readings are then transferred to the PVSS supervision via the FESA (Front End Software Architecture) protocol. (3)

PVSS (Prozeß-Visualisierungs und Steuerungs System) is a Supervisory Control and Data Acquisition system. It is used to connect to hardware or software devices, acquire the data they produce, monitor their behaviour and operate them.

Under PVSS, three different visualizations will be accessible:

- An “expert” visualization, dedicated to persons responsible for the maintenance, showing only raw and converted sensors readings.
- A “client” visualization, dedicated to physicists, showing the calculated position of the magnets. This visualization implies the correction of the sensors readings: wire catenary, earth and water tides, temperature, inertial forces and radiations, as well as an adjustment of the redundant information by the least squares method, and the knowledge of the theoretical position of the magnet.
- A repositioning visualization, showing the 3 types of sensors readings: before the repositioning, during the repositioning and the values to be obtained after repositioning according to the calculations, as well as all the motors commands sent.

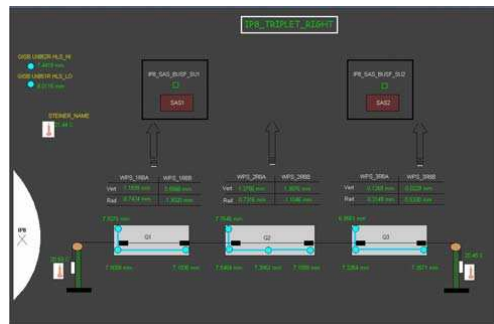


Fig.6: The expert visualization

After visualization under PVSS, all the raw and converted data are stored into the LHC measurements database named LOGGING (4). This allows an a-posteriori analysis thanks to a consultation interface: TIMBER.

The data processing

In order to implement data in the “client” visualization, the Survey database plays a major part. Indeed “SURVEY” is the database of the Large Scale Metrology group at CERN, where all the theoretical positions and

offsets to these positioning of the fiducials and beam elements extremities of all the CERN machines are stored.

First, the SURVEY database will allow to generate an input file for the least squares adjustment software named LGC (Logiciel Général de Compensation), compiling the converted data from PVSS (4b), and all the mechanical information stored in MTF (5). This input file is transferred to LGC (6). After calculations, LGC sends back to the SURVEY database an output file containing the offsets of the theoretical position of the magnet beam Start/End. (7) Then these values are recovered by PVSS in order to be displayed (8). For a displacement to be processed, the motors commands are sent to the Gateway (9) through FESA protocol, up to the WorldFIP bus of the motors assemblies' drivers.

The repositioning strategy

There is a sequence of repositioning to follow in order to position the magnet within few microns:

- To adjust the tilt
- To carry out the radial displacements
- To control the tilt and re-adjust the tilt
- To carry out the vertical displacements, knowing that the same displacements must be applied on the tilt jacks in order to keep the tilt adjusted.

The repositioning will be performed within several iterations. The backlash on the jack being important (about 8°), the displacement must always be carried out keeping the same direction.

The first results

At the present time, the repositioning of a triplet can only be carried out on a "local" mode, e.g. the motors commands are sent from the assemblies' drivers and the sensors readings to be obtained are calculated independently from the algorithms and the SURVEY database.

The first tests carried out confirmed that a repositioning within a few microns is possible.

After a few seconds, HLS and WPS readings located on the same fiducial show a very good correlation, though the HLS system has a longer stabilization time.

CONCLUSION

The installation of the alignment and repositioning systems started at the end of 2006 on the low beta triplets. Unfortunately, some technical problems on these magnets forced us to dismount all the alignment systems and the motor assemblies. Now, these problems are solved and five triplets out of eight are equipped with alignment and repositioning systems. Apart from EMI effects on the readings of the sensors, both systems seem to meet their requirements. The last pieces of the puzzle are actually being placed in situation, before the circulation of the first beam in the LHC, foreseen this summer.

REFERENCES

- [1] W. Coosemans and al., The alignment of the LHC low beta triplets: review of instrumentation and methods, IWAA 2002, Spring-8, 2002.
- [2] L. Bottura, D. Missiaen, Definitions of Survey and magnetic data systems at IR1, 2, 5 and 8, LHC-LQX-ES-007, CERN, 2004.
- [3] A. Herty and al., Radiation induced effects on the HLS sensors, IWAA 2006, SLAC, 2006
- [4] A. Herty and al., Test and calibration facility for HLS and WPS sensors, IWAA 2004, CERN, 2004.
- [5] H. Mainaud Durand and al., Status of the alignment of the LHC low beta quadrupoles, IWAA 2004, CERN, 2004
- [6] H. Mainaud Durand, Commissioning of the low beta alignment and repositioning systems, LHC-GI-TP-0001, CERN, 2006
- [7] M. Acar and al., The motorized alignment jacks for the LHC low beta quadrupoles, IWAA 2006, SLAC, 2006.

C.6 Alignment of the low-beta magnets and the experiments in the LHC

A. Herty, D. Mergelkuhl

For the LHC project the demands on alignment and positioning have been increased with respect to previous projects; this concerns the experiments as well as the accelerator.

Alignment and continuous monitoring of the low-beta magnets in combination with new methods have become necessary. The layout of the measurement system provides a permanent follow up of the magnets, the possibility of remote alignment and has interfaces to the alignment reference network in the experimental area.

The low-beta magnets define the Nominal Beam Line which is the reference for the experiments. The installation of the experiments started up to five years before the low-beta magnets arrived in the tunnel. The influence of deformation on the cavern had to be taken into account. This problem had to be considered for assembly and positioning work of the numerous detector parts.

CERN Technical Note TS-2008-036, CERN, 2008



EUROPEAN ORGANIZATION FOR NUCLEAR RESEARCH
ORGANISATION EUROPÉENNE POUR LA RECHERCHE NUCLÉAIRE

CERN - TS Department

EDMS Nr: 936560
Group reference: TS-SU-EM

TS-Note-2008-036
29 May 2008

ALIGNMENT OF THE LOW-BETA MAGNETS AND THE EXPERIMENTS IN THE LHC

A. Herty, D. Mergelkuhl

Abstract

For the LHC project the demands on alignment and positioning have been increased with respect to previous projects; this concerns the experiments as well as the accelerator.

Alignment and continuous monitoring of the low-beta magnets in combination with new methods have become necessary. The layout of the measurement system provides a permanent follow up of the magnets, the possibility of remote alignment and has interfaces to the alignment reference network in the experimental area.

The low-beta magnets define the Nominal Beam Line which is the reference for the experiments. The installation of the experiments started up to five years before the low-beta magnets arrived in the tunnel. The influence of deformation on the cavern had to be taken into account. This problem had to be considered for assembly and positioning work of the numerous detector parts.

1 INTRODUCTION

The low-beta magnets represent one of the most delicate regions in the LHC to be aligned, as they have to be positioned relative to each other and relative to the experiment. The demanded tolerances and special alignment methods make a permanent monitoring for the triplets necessary – see figure 1.

For each experiment the reference system datum, called ‘nominal beam line’ is defined as the final best fit position of the low-beta magnets relative to each other and relative to each triplet on either side of the experiment.

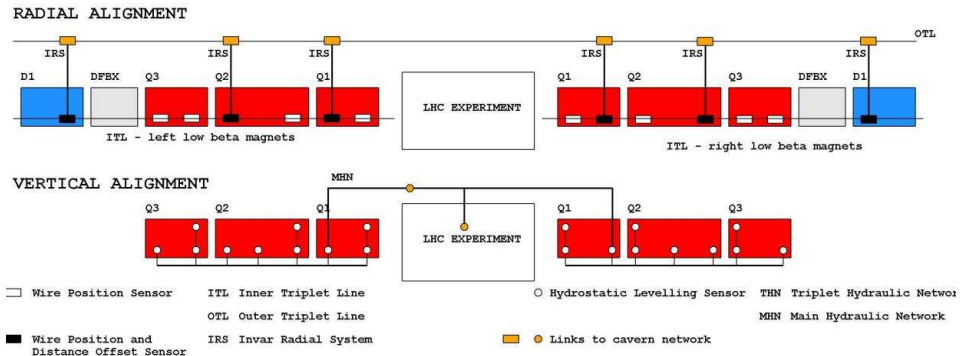


Figure 1: alignment concept of the LHC low-beta magnets

2 EXPERIMENTS

2.1 Determination of the experiment reference survey network

As the detector assemblies started more than four years before the final low-betas alignment, a preliminary datum has been defined from the reference sockets in the tunnel (‘GGPSO geometry’) [1] from which all the machine elements, triplets included, have been installed within an expected uncertainty to 0.5 mm at one sigma.

The reference networks for the experiments comprise up to 130 points per experiment on walls and structures. These networks surround the experiments and have been established by standard survey within the same uncertainty.

2.2 Stability of the floor and reference networks in ATLAS and CMS

Civil engineering calculations predicted vertical floor movements in UX15 [2] of:

- - 5.5 mm sag, due to the total weight of ATLAS;
- - 2.0 mm sag, due to the concrete contraction;
- + 1.0 mm per year heave, due to the hydrostatic pressure.

20 reference marks embedded in the UX15 cavern floor have been regularly monitored since August 2003 and referred to the machine reference points and the deep reference rods in the tunnel.

A rise of the floor up to 1.2 mm was recorded in the central part of the cavern [3] during the first 20 months after the completion of the civil engineering (08/2003 – 03/2005). 85% of the total charge has been loaded in the following time up to 02/2008. An absolute accuracy between two epochs of 0.3 mm one sigma has been achieved and the cavern shows a global stability with respect to the deep references in the tunnel within this accuracy.

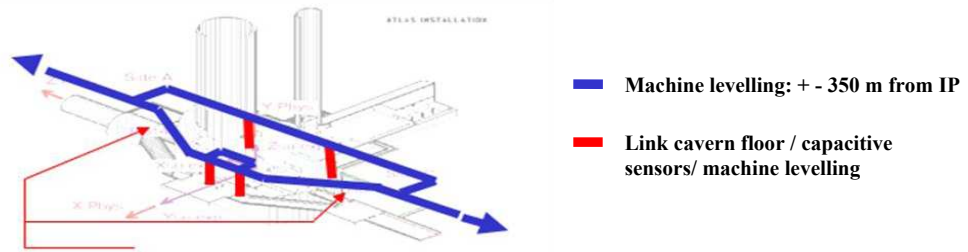


Figure 2: Scheme for stability measurements for ATLAS

The reference brackets on the lateral walls in ATLAS have been monitored over the last four years regularly and linked to the machine geometry: altogether shrinkage up to 8 mm in the central part, the extremities being more stable, has been recorded - see figure 3.

Due to the bigger weight than ATLAS, five deep reference rods have been implemented in the CMS cavern foundations and linked to the machine geometry within an accuracy of 0.3 mm. These points are the leveling datum for all the detectors in UX55. No significant movements have been recorded up to the full loading of the cavern.

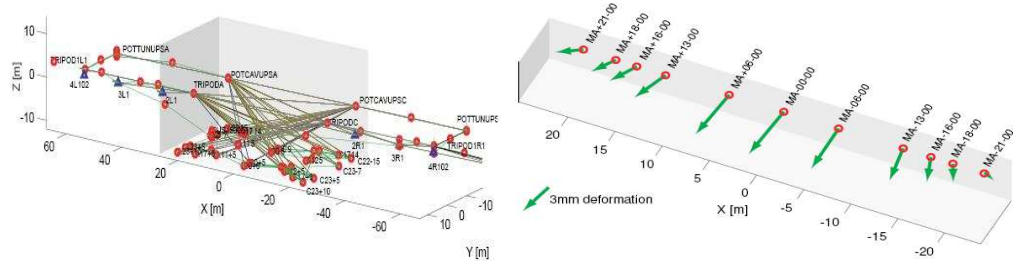


Figure 3: Scheme of link measurements machine - radial movements over 3 years (ATLAS)

2.3 As-built metrology, envelope, axis of detectors and precise positioning

Specifically ATLAS and CMS are complex assemblies. There are containers and contents with some either mechanical or geometrical possible out of tolerances. Therefore the question of the determination of the ‘best’ as-built object has been raised before any precise positioning. Forms and dimensions of some critical elements of which the envelopes were very tight with respect to the surrounding elements have been measured by standard survey or digital photogrammetry in factory or at CERN [4].

Pre-assemblies of modular objects have been controlled also at manufacturing premises or in-site surface halls in order to cross-check the expected deformations under construction and loading and determine the final mean axis for the subsequent elements. See figure 4 for the form of the assembled ATLAS Tile Barrel with respect to theoretical data.

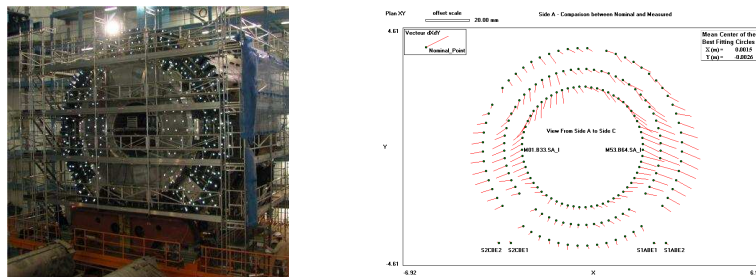


Figure 4: Assembly of the 64 ATLAS tile barrel modules: as-built differences and deformations

The precise detector positioning in the caverns with respect to the best known reference network determined at the assembly time for a given element began with the accurate adjustments of the supporting structures. Those have been accorded with the measured envelopes and deformations so that no a priori theoretical values could be applied and several iterations have been needed.

Once released from their assembly tooling and after their axis have been positioned with respect to the reference network, a complete geometry measurement of the critical elements has been performed so that the best possible accurate and spatial coordinates of fiducial points can be delivered in accordance to their final forms and dimensions. Some regular deformation measurements have been also carried out even once in place to monitor the deformation due to the charge of additional detectors.

2.4 Monitoring and future closures of the detectors



Installed BCAMs (Brandeis Cameras Angle Monitor) enable to inspect three alignment control lines joining the Atlas central and extended calorimeters, the JD (see figure 5) up to the end cap toroids and similar systems are implemented in four devoted corridors surrounding the YBs and the YEs in CMS [5]. All the camera plates have been referred to the experiment grid and then linked to the machine geometry within an overall accuracy of one mm at one sigma. Permanent positions will be visualized via an expert and client mode and will be logged in the ATLAS and CMS data base. The system can be used as independent, online monitoring system for future closures of the experiments.

Figure 5: Bottom BCAM on ATLAS JD

3 LOW BETA MAGNETS

The low beta magnets, which have been installed and aligned in the last 18 months, have to fit into alignment of the installations previously present: other machine components and the experiments.

3.1 Alignment concept, sensors and systems

The first positioning of the magnets is done with total station measurements for the initial 3D positioning with respect to the CERN underground, geodetic reference network. In a second step, called smoothing, the magnets are positioned with respect to their neighboring magnets in the long straight section (LSS) [1]. This is done with inclinometer measurements for the tilt, optical leveling for the height and a stretched wire for radial positioning.

The requested alignment tolerance for the magnets is described in the LHC design report by the alignment functions that demand 0.3 mm for the alignment of one triplet with respect to the other triplet and the same tolerance for the magnets with respect to the tunnel at 3σ . More crucial is the demanded short term stability in the triplet to some μm . The interface network points to the experiments – see figure 5 – are provided within the same tolerances.

These tight demands need a permanent monitoring and repositioning system of the low-beta magnets in order to fulfil the demands. The alignment concept of the triplet is based on stretched wire and hydrostatic levelling measurements.

The monitoring of one triplet in radial position is carried out with respect to a stretched wire that is positioned independently from the magnets. Wire position sensors (WPS) on the fiducials are used to monitor the position. Those 2D sensors also carry out a vertical measurement on the magnet at the same time and allow redundant measurements for the vertical in combination with the hydrostatic levelling system (HLS).

A permanent radial link between the two triplets is established in ATLAS and CMS. The survey galleries (UPS) allow a stretched wire over 140 m in combination with three invar rods and distance offset measurement sensors (DOMS) on each triplet to have a link between the two stretched wires [6]. The HLS is also fixed on the fiducials and allows with the principle of communicating vessels the determination of changes in height as well as, in combination of several sensors, the determination of the tilt angle of the magnet. A hydrostatic network crosses the caverns to have both sides linked as well as to provide intermediate points in the cavern. In CMS additionally one sensor is installed on the YB0 magnet itself.

In total 260 sensors have been tested before their installation in the LHC [7]. In order to carry out these tests, procedures and test benches have been developed [8]. The use of these sensors in this high radiation area of the LHC made it necessary to design remote electronics with cable lengths between sensor and electronic of up to 30 m [7]. Influences of radiation on the measurements have been detected and compensation methods have been developed [9, 10]. The jacks for the low-beta magnets are equipped with stepper motors that allow the remote positioning of the magnets to the accuracy of some micron [11].

3.2 Interfaces for monitoring and alignment

Two types of interfaces have to be taken into account when looking at interfaces for this alignment system. On one hand, visualization tools have been developed that provide the possibility to see and analyze the measurement online or in post-processing. On the other hand, mechanical interfaces have to be provided in order to allow links to the experiments or other points in the geodetic network of the LHC.

Visualization. The measurements are recovered in real-time via the field bus system WorldFIP and transferred to the supervisory control and data acquisition system PVSS. The conversion of the raw measurements to SI units is done during this step. For analysis of the measurements with geodetic compensation methods, a long term availability of the data has to be provided. The database LOGGING provides this context. With data from the SURVEY database and information about the sensors and support stored in MTF, a compensation calculation can be carried out. Two types of visualization interfaces are provided: expert and client mode [11].

Geodetic Interface. All HLS sensors and the WPS sensor supports in the UPS galleries provide a mechanical, geodetically referenced interface between the sensor measurement and classical survey methods. This interface is important, as it allows these points to be integrated in the geodetic network of the experiment and in consequence to fulfill the alignment demands with respect to the experiment. The supports in the cavern or the UPS galleries can be accessed directly. No additional transfer measurements from the tunnel are necessary as the position in radial or vertical is available directly with the sensor readings.

3.3 Perspectives

Such a complex alignment system provides new possibilities for the alignment of the machine with respect to the experiment. The permanent and direct link the alignment between the machine system and the experiment system are new for the LHC.

During LEP, SPS and ISR, measurements of the final focus magnets have been carried out with standard survey methods, like the determination of distances and angles in order to calculate the shape of the machine around the experiment. The alignment methods used in the LEP were hardly redundant and the desired precision was not obtained [12]. Monitoring of the LEP final focus magnets with hydrostatic leveling systems started in the mid 1990's. Automated wire measurements were used on the magnets under the excavation site of the roof of the ATLAS cavern, while the LEP was still running [13]. Both measurements showed that the sensors were reliable in the radiation and magnetic field environment. This led to the proposal of a permanent monitoring in radial and vertical position of the LHC based on the same principles.

The installation of the alignment system is based on the fiducials of the magnets. The magnets are equipped with two sets of fiducials: one dedicated to the use of the alignment system and the other

for classical survey methods to allow adjustment measurements with respect to adjacent magnets. All fiducials are determined with respect to the cold mass inside the magnet [1]. The parameters of the inner geometric and magnetic shape of the magnet were provided by FermiLab, but for optimization of the alignment the measurements were discarded. A re-fiducialisation was carried out for all low beta magnets at CERN [14].

Once the connection between two adjacent magnets is closed, the relation between the cold mass inside the cryostat and the fiducials can no longer be monitored. The inside of the magnet becomes a black box. As the low-beta magnets showed some problems with the cold mass during pressure tests and transport [15], there are concerns how stable is the cold mass inside.

The visualization and calculation interface 'PVSS client' will be available for physicists in order to calculate the position of the triplet and to draw conclusions from the measurements and data analysis provided. The remote alignment in combination with the monitoring system provides the optimization to protect personnel and to respect the ALARA principle [16].

4 CONCLUSION

The final focus magnet alignment system is designed for the high alignment demands of the LHC combined with the experience of previous accelerators. A permanent real-time monitoring and remote alignment will allow an optimization of the beam position and reduces the presence time of personnel in the tunnel. Reference points in the cavern and on the experiments allow a direct link between the machine and the experiments. Analysis of the alignment sensors measurement, comparison to standard alignment methods for the LHC and the calculation of the triplet shapes with respect to the experiments show converging results.

REFERENCES

- [1] J.-P. Quesnel (2004). LHC Design Report (Vol. II – Cha. 11), CERN, Geneva, Switzerland
http://edms.cern.ch/file/445932/5/Vol_2_Chapter_11_v6.pdf
- [2] D. Lissauer. Alignment of ATLAS experiment, EDMS: ATC-T-ER-0004
<https://edms.cern.ch/document/320043/1>
- [3] A. Lippitsch (2007). A deformation analysis method for the metrological ATLAS cavern network at CERN, Shaker Verlag
- [4] C. Lasseur. Placement strategy and survey in Atlas, Atlas note: ATL-COM-TECH-2008-003
<http://cdsweb.cern.ch/record/1094576>
- [5] J. Bensinger et al (2006). High Precision Optical Instrumentation for Large Structures Position Monitoring: The BCAM System Applied to the CMS Magnet. IWAA 2006, SLAC, Stanford
<http://www.slac.stanford.edu/econf/C06092511/papers/TH009.PDF>
- [6] W. Coosemans et al (2002). The alignment of the LHC low beta triplets: review of instrumentation and methods. International Workshop on Accelerator Alignment, SPring-8, Japan
- [7] H. Mainaud Durand et al (2004). Status of the alignment of the LHC Low Beta quadrupoles. International Workshop on Accelerator Alignment, CERN
<http://www.slac.stanford.edu/econf/C04100411/papers/014.PDF>
- [8] A. Herty, A. Marin, H. Mainaud Durand (2004). Test and Calibration Facility for HLS and WPS sensors. International Workshop on Accelerator Alignment, CERN
- [9] E. Dimovasili et al (2005). Radiation induced effects on the sensors of the Hydrostatic Leveling System for the LHC low beta quadrupoles. CERN Technical Note CERN-TS-2005-052
[https://edms.cern.ch/file/629483/1/TS_Note_2005_052\(LEA\).pdf](https://edms.cern.ch/file/629483/1/TS_Note_2005_052(LEA).pdf)
- [10] A. Herty et al (2006). Radiation induced effects on the Hydrostatic Leveling Sensors. IWAA 2006, SLAC, Stanford
<http://www.slac.stanford.edu/econf/C06092511/papers/WEPO16.PDF>
- [11] H. Mainaud Durand et al (2008). The remote positioning of the LHC inner triplet. International Workshop on Accelerator Alignment, KEK, Japan

- [12] J. P. Quesnel (1996). Presentation at TCC meeting. CERN, Switzerland
- [13] W. Coosemans and H. Mainaud (1997). Pre-alignment of CLIC using the double-wire method, IWAA 1997, Argonne, Chicago
<http://www.aps.anl.gov/News/Conferences/1997/iwaa/papers/cooseman.pdf>
- [14] P. Bestmann (2006). Final geo-magnetic fiducialization of the LHC Short Straight Sections.
<https://edms.cern.ch/document/790018/1>
- [15] H. Mainaud Durand (2008). Alignment of the new triplets. LHC Insertions Upgrade Meeting.
- [16] CERN (2006). Radiation Protection and Radiation Safety Manual. CERN, Switzerland
https://edms.cern.ch/file/335729/LAST_RELEASED/F_E_1996.pdf